Julius-Maximilians-Universität Würzburg

Fakultät für Biologie

Design onkolytischer Viren zur Bildgebung und Therapie von Krebserkrankungen: Das Vaccinia-Konstrukt GLV-1h153 als Träger des menschlichen Natriumjodid Symporters

Design of oncolytic viruses for the imaging and treatment of cancer: The vaccinia construct GLV-1h153 carrying the human sodium iodide symporter

Dissertation

zur Erlangung des naturwissenschaftlichen Doktorgrades der

Julius-Maximilians-Universität Würzburg

vorgelegt von Dana Haddad

aus Kuwait City

Würzburg, March 2011

Eingereicht am: _____

Mitglieder der Promotionskommission:

Vorsitzender: _____
Prof. Dr. T. Dandekar

Erstgutachter : _____
Prof. Dr. A. A. Szalay

Zweitgutachter: _____
Prof. Dr. Georg Krohne

Tag des Promotionskolloquiums: _____

Doktorurkunde ausgehändigt am: _____

Eidesstattliche Erklärung

Hiermit versichere ich, dass ich die vorliegende Dissertation selbstständig und nur mit den angegebenen Hilfsmitteln und Quellen angefertigt habe.

Ich erkläre weiterhin, dass diese Dissertation weder in gleicher noch in anderer Form bereits in einem anderen Prüfungsverfahren vorgelegt wurde.

Neben dem akademischen Grad „**Bachelor of Human Biology**“ und „**Dr. med, The University of Auckland**“ habe ich keine weiteren akademischen Grade erworben oder zu erwerben versucht.

Würzburg, den _____ _____

Signature

For my sister, Rasha.

Thank you for being my companion in life.

TABLE OF CONTENTS

ABBREVIATIONS

ATCC	American Type Culture Collection
(c)DNA	(Complementary) Deoxyribonucleic acid
CPM	Counts per minute
DMEM	Dulbecco's modified Eagle's medium
dpvi	Days post virus injection
FDR	False discovery rate
FOV	Field of view
GFP	Green fluorescent protein
gusA	β-glucuronidase
GM-CSF	Granulocyte macrophage colony stimulating factor
hrpi	Hours post radiotracer injection
hNIS	Human sodium iodide symporter
hNET	Human norepinephrin transporter
hSSTR2	Human somatostatin receptor
HSV1-tk	Herpes simplex virus 1 - thymidine kinase
^{124}I	Iodine-124
^{125}I	Iodine-125
^{131}I	Iodine-131
IFN	Interferon
IL	Interleukin
IP	Intraperitoneal
IT(ly)	IT(ly)
IV(ly)	IV(ly)
kDa	KiloDalton
LacZ	β-galactosidase
LDH	Lactate dehydrogenase
LIVP	Lister vaccine strain
MIBG	Meta-iodobenzylguanidine
MOI	Multiplicity of infection
(m)RNA	(Messenger) Ribonucleic acid
$NaClO_4$	Sodium perchlorate
OV(s)	Oncolytic virus(es)
PBS	Phosphate buffer serum
PCR	Polymerase chain reaction
PET	Positron emission tomography
$^{99m}TcO_4$	99m-technecium pertechtenate
SPECT	Single photon emission computer tomography
VACV	Vaccinia virus
WR	Western Reserve vaccinia strain

SUMMARY

Replication-competent oncolytic viral therapies have shown great promise preclinically and in clinical trials for the treatment of various cancers, with the possible advantages of stronger treatment efficacy compared to conventional therapy due to higher tumor selectivity as well as lessening side effects. They are able to preferentially and selectively propagate in cancer cells, consequently destroying tumor tissue via cell lysis, while leaving noncancerous tissues unharmed.

Oncolytic vaccinia virus (VACV) strains have been of particular interest due to several advantages. VACV's large 192-kb genome enables a large amount of foreign DNA to be incorporated without significantly reducing replication efficiency of the virus. It has fast and efficient replication, and cytoplasmic replication of the virus lessens the chance of recombination or integration of viral DNA into the genome of host cells. Perhaps most importantly, its safety profile after its use as a live vaccine in the World Health Organization's smallpox vaccination program in over 200 million people makes it particularly attractive as an oncolytic agent and vector for the delivery of heterologous proteins.

Currently, biopsy is the gold standard for monitoring of viral tumor colonization and oncolysis. This may be feasible in preclinical or early clinical trials; however, a noninvasive method facilitating ongoing monitoring of viral therapy is needed for human studies. The tracking of viral delivery could give clinicians the ability to assess the biodistribution of oncolytic viruses to ensure safety and correlation with treatment efficacy. Furthermore, a more sensitive and specific diagnostic technique to detect tumor origin and, more importantly, presence of metastases may be possible.

This work centers on the construction and testing of a VACV strain, GLV-1h153, carrying the human sodium iodide symporter (*hNIS*) as a marker gene for non-invasive tracking of virus by imaging. This virus strain was derived from GLV-1h68, which has already been shown to be a simultaneously diagnostic and therapeutic agent in several human tumor models including breast tumors, mesothelioma, pancreatic cancers, anaplastic thyroid cancers, melanoma, and squamous cell carcinoma. Further, GLV-1h68 is currently undergoing clinical trials. Thus, this project aimed to help develop imaging techniques for use in clinical trials of oncolytic viral therapy. Further, the feasibility and effectiveness of virally induced targeted radiotherapy as an anti-cancer strategy was also investigated.

hNIS is an intrinsic plasma membrane protein which mediates the active transport and concentration of iodide in the thyroid gland and some extra-thyroidal tissues. It is also one of several human genes currently being used as reporters in preclinical studies and has already been used in clinical studies for imaging viral replication in prostate cancer. hNIS gene transfer via viral vector may allow infected tumor cells to concentrate several carrier-free radionuclide probes such as Iodide-124 (^{124}I), Iodide-131 (^{131}I), and 99m-Technecium Pertechtenate ($^{99m}TcO_4$), which have long been approved for human use. hNIS also has the advantage of being of human origin thus minimizing immunogenicity, and its transporter based system allows intracellular signal amplification.

GLV-1h153 was tested in pancreatic adenocarcinoma cell line PANC-1. GLV-1h153 infected, replicated within, and killed PANC-1 cells in cell culture as efficiently as GLV-1h68 and provided dose-dependent levels of *hNIS* transgene expression in infected cells. Immunofluorescence detected successful transport of the protein to the cell membrane prior to cell lysis, which enhanced dose and time-dependent intracellular uptake of ^{131}I. *In vivo*, GLV-1h153 was as safe and effective as GLV-1h68 in regressing pancreatic cancer xenografts. In animal models, biodistribution profiles revealed persistence of virus in tumors 5 weeks post injection, with the virus mainly cleared from all other major organs. Tumor infection by virus was confirmed via optical imaging and histology.

GLV-1h153 further facilitated deep tissue imaging of virus replication in tumors via Iodide-^{124}I positron emission tomography (PET) as well as $^{99m}TcO_4$-mediated gamma scintigraphy. This was possible with both intratumoral and intravenous injection of the virus with radiouptake retained as long as 24 and 48 hours after radiotracer injection. PET image quantitation of radiouptake in tumors was found to correlate well with tissue radiouptake counts. Repeated radiotracer injection revealed optimal radiotracer uptake around 1-2 weeks post virus treatment, with decreasing signals after around 3 weeks. The decrease in signal correlated with tumor growth retardation, eventual regression from initial volume at baseline, and necrosis on histologic analysis by 5 weeks post treatment. Autoradiography of GLV-1h153-infected tumors revealed a need for presence of virus (visualized with green fluorescent protein expression), viable tissue, and adequate blood flow to enhance radiouptake in tumors. Dosimetric analysis of uptake in infected tumors displayed potential for therapeutic doses of radiotherapy to be delivered systemically to tumors. When GLV-1h153 was combined with ^{131}I for treatment, a modest additive effect was seen as compared to GLV-1h153 alone.

Therefore, Insertion of the *hNIS* gene does not hinder replication capability of GLV-1h153 and induced the functional production and transportation of the hNIS protein to the cell membrane. GLV-1h153 was also a safe oncolytic agent against pancreatic cancer with a promising biosafety profile. GLV-1h153 facilitated time, dose-dependent and hNIS-specific intracellular radiouptake both in cell culture and *in vivo*, facilitating deep tissue imaging via PET and gamma scintigraphy with ^{124}I and $^{99m}TcO_4$, respectively. Radiouptake required a combination of viable tissue, blood flow, and presence of virus, and was adequately retained at potentially therapeutic levels. GLV-1h153 is thus a promising new candidate for treating pancreatic cancer and noninvasively imaging viral therapy. These findings warrant further investigation into possible long term monitoring of viral therapy, as well as synergistic or additive effects of radioiodine combined with this novel treatment and imaging modality.

ZUSAMMENFASSUNG

Therapien mittels replikations-kompetenter onkolytischer Viren zeigten bereits vielversprechende Erfolge in klinischen Studien zur Bekämpfung verschiedener Krebserkrankungen, wobei der Vorteil der erhöhten Behandlungseffizienz im Vergleich zu konventionellen Therapien in der hohen Tumorselektivität und den damit verbundenen verringerten Nebenwirkungen zu suchen ist. Die Viren sind in der Lage, sich präferentiell und selektiv in Krebszellen zu vermehren, wodurch das Tumorgewebe durch Zelllyse zerstört, das gesunde Gewebe jedoch nicht geschädigt wird.

Onkolytische Vaccinia Virus (VACV) Stämme sind aufgrund einiger besonderer Eigenschaften von besonderem Interesse. Das 192-kb große Genom der VACV macht es möglich, große Stücke fremder DNA in einzufügen, ohne, die Replikationseffizienz der Viren wesentlich zu beeinflussen. Die schnelle und effiziente zytoplasmatische Replikation der Viren erniedrigt die Chance der Rekombination oder Integration viraler Erbinformation in die DNA der Wirtszellen. Möglicherweise am wichtigsten jedoch, ist das bekannte Sicherheitsprofil als Lebend-Impfstoff in der von der WHO (World Health Organization) initiierten, erfolgreichen Ausrottung der Pocken, welches die VACV als attraktives onkolytisches Agens und Vektor für heterologe Proteine erscheinen lässt.

Biopsien sind zurzeit der Gold-Standard zur Überwachung onkolytischer Virus Therapien. In der präklinischen und frühen klinischen Phasen ist dies auch durchführbar, doch für weitere Studien am Menschen werden Methoden benötigt, die eine nicht-invasive Überwachung der Therapie ermöglichen. Das Nachverfolgen der Viren könnte Klinikern die Möglichkeit geben, die Verteilung der Viren im Körper nachzuverfolgen, die Effizienz und therapeutische Effekte zu korrelieren bzw. die mögliche virale Toxizität zu überwachen. Weiterhin könnten so möglicherweise die Sensitivität und Spezifität erhöht werden, wenn es darum geht den Ursprung des Tumors, oder noch wichtiger, das Vorhandensein von Metastasen, zu detektieren.

Im Fokus dieser Arbeit stand die Konstruktion und das Austesten des VACV Stamms GLV-1h153, welches das Gen für den humanen Natrium-Iodid-Symporter (*hNIS*) kodiert, das als Reportergen für nicht-invasive bildgebende Nachverfolgung der Viren diente. Der Virusstamm leitete sich aus dem bereits beschriebenen Stamm GLV-1h68 ab, welcher bereits in einigen Tumor-Modellen (Brust-, Mesothelioma-, Pankreas-, anaplastischen Schilddrüsen-, Melanoma- und Plattenepithelkarzinom-Modellen) erfolgreich sowohl als

diagnostisches, wie auch therapeutisches Agens eingesetzt wurde, und sich zur Zeit in klinischen Studien befindet. Demzufolge diente das hier vorgestellte Projekt der Entwicklung von Bildgebungsverfahren, die in der onkolytischen Virustherapie eingesetzt werden können. Weiterhin sollte als weitere Strategie zur Krebsbekämpfung die Möglichkeit untersucht werden, mit Unterstützung der Viren eine gezielte Radiotherapie durchzuführen.

Bei dem Natrium-Iodid-Symporter handelt es sich um ein intrinsisches Membranprotein welches den aktiven Transport und die Anreicherung von Iodid in Schilddrüsenzellen und einigen anderen Geweben vermittelt. Zudem wird das Gen, neben einigen anderen humanen Genen, bereits in präklinischen Studien als Reportergen verwendet und wurde in klinischen Studien bereits zur Darstellung von Viren in Prostata-Krebspatienten benutzt. Der Transfer des hNIS-kodierenden Gens mittels viraler Vektoren könnte es ermöglichen, dass infizierte Tumorzellen Träger-freie Radionuklidproben wie z.B. Iodid-124 (^{124}I), Iodid-131 (^{131}I), und 99m-Technecium Pertechtenate ($^{99m}TcO_4$), anreichern, welche schon lange für die Verwendung am Menschen zugelassen sind. Weitere Vorteile bei der Verwendung von *hNIS* als Reportergen humanen Ursprungs sind zum einen seine minimale Immunogenität und zum anderen die intrazelluläre Signalamplifikation durch die Transportfunktion des Systems.

Der Stamm GLV1h153 wurde in der Pankreas-Adenokarzinom Zelllinie PANC-1 getestet. GLV-1h153 konnte diese Zellen infizieren, sich in ihnen replizieren und sie in Zellkultur schließlich ebenso effizient abtöten wie GLV-1h68. Zudem wurde eine Dosis-abhängige Expression von hNIS in infizierten Zellen nachgewiesen. Immunfluoreszenzanalysen bestätigten den erfolgreichen Transport des Proteins an die Zellmembran bevor die Zelllyse stattfand, was die Zeit- und Dosis-abhängigen Aufnahme von ^{131}I verstärkte. *In vivo* war GLV-1h153, ebenso wie GLV-1h68, sicher und führte zu einer effektiven Regression der Pankreasxenograft Tumoren. Biodistribitionsstudien 5 Wochen nach Injektion, zeigten ein Vorhandensein von Viren in Tumoren. In anderen Organen war kein oder kaum Virus nachweisbar. Die Infektion des Tumors wurde weiterhin durch optische Bildgebung und histologische Untersuchungen bestätigt.

GLV-1h153 ermöglichte weiterhin die Bildgebung von Viren in Tumoren mittels ^{124}I-abhängiger Positronen-Emissions-Tomographie (PET) sowie 99m-Technecium Pertechnat-abhängiger (^{99m}TcO4) Gamma Szintigraphie. Die Darstellung konnte sowohl mit intratumoral, wie auch mit intravenös applizierten Viren erfolgen, war quantitativ, und die Radiotracer konnten bis zu 24 bzw. sogar 48 h nach deren Injektion nachgewiesen werden. Die quantitative Analyse der Radionuklidaufnahme aus PET-Bildgebungsdaten korrelierte mit den Daten der Bioverteilungsdaten aus isolierten Gewebn. Wiederholte Injektionen des

Radiotracers zeigten, dass 1-2 Wochen nach Virus-Injektion die Aufnahme des Tracers in den Tumor am höchsten war. Die Signalintensität begann dann 3 Wochen nach Injektion der Viren abzufallen, was mit dem Rückgang des Tumors und der letztendlichen Regression und der Nekrose in histologischen Untersuchungen 5 Wochen nach Behandlung korrelierte. Autoradiographische Untersuchungen von GLV-1h153 infizierten Tumoren zeigten, dass das Vorhandensein von Viren (visualisiert durch die viral vermittelte GFP Expression), lebendes Gewebe und ausreichender Blutfluss benötigt werden, um die Aufnahme des Radiotracers in den Tumor zu erhöhen. Dosimetrische Analysen infizierter Tumoren zeigten das Potential für eine systemisch applizierte Radiotherapie des Tumors auf. So führte eine Kombination aus GLV-1h153 mit ^{131}I-Behandlung zu geringfügig besseren therapeutischen Erfolgen, als eine alleinige Therapie mit GLV-1h153.

Zusammengefasst, hindert die Insertion von *hNIS* die Replikation von GLV-1h153 nicht und resultiert in der Produktion, dem Transport und dem Einbau funktionellen hNIS in die Zellmembran. Zudem konnte gezeigt werden, dass GLV-1h153 ein sicheres onkolytisches Agens gegen Pankreaskrebs ist, das eine vielversprechende Bioverteilung aufweist. GLV-1h153 vermittelte Zeit- und Dosis-abhängige sowie hNIS-spezifische intrazelluläre Radiotracer-Aufnahme sowohl in Zellkultur wie auch in vivo, was eine Bildgebung tieferer Gewebsschichten mittels PET und Gamma Szintigraphie mit ^{124}I bzw. ^{99m}TcO4 ermöglichte. Die Aufnahme der Radioaktivität setzte eine Kombination lebenden Gewebes, Blutfluss und dem Vorhandensein von Viren voraus und sie konnte in therapeutsich aktvien Dosen zurückgehalten werden. GLV-1h153 ist demnach ein vielversprechender Kandidat zur Behandlung von Bauchspeicheldrüsenkrebs und zur nichtinvasiven Bildgebung der viralen Therapie. Die Ergebnisse untermauern die Notwendigkeit weiterer Untersuchungen und Entwicklungen in der Langzeitverfolgung viraler Therapien sowie synergistischer Effekte einer Radioiod-Kombinationstherapie mit dieser neuen therapeutischen und bildgebenden Substanzklasse.

1.0 ONCOLYTIC VIRAL THERAPY

12 million people worldwide will be diagnosed with cancer this year, and 7 million people will die from cancer-related causes[1]. In the United States alone, the figures are estimated at 1,479,350 new cases and 562,340 deaths in 2009[2]. In Germany, an estimated 340,000 new cancer cases are diagnosed annually, and 210,000 lives are lost to cancer related causes, making cancer the second leading cause of death in Germany after diseases associated with the circulatory system[3]. Unless dramatic breakthroughs in treatments are achieved, cancer will be leading cause of death in Germany within 15 to 20 years. Adding to the overwhelming loss of life and decline in quality of life for both patient and family, the economic costs associated with a diagnosis of cancer is an immense burden on society estimated at $228.1 billion dollars in 2008 in the United States alone[2].

Despite advances in conventional therapy, the formidable challenge of treating cancer, especially if progressed, still remains. Even with aggressive chemo- and radiation therapy, the commonest forms of cancer have not seen improvements in survival rates[4]. Furthermore, despite a prominent increase in cost, anti-cancer drugs approved in 1995 – 2000 do not show increased efficacy in providing cures from cancer[5].

Pancreatic cancer in particular is the fourth leading cause of cancer death in the United States[6], and objective response to single agent or combination chemotherapies occurs in less than 20% of patients which is never curative[7]. These results explain the active investigation underway seeking novel therapeutic strategies for this disease. Developing novel therapies, which may also work synergistically in combination with conventional treatment options, is vital.

It is well established that combining several treatment modalities appears to be the strongest chance of fighting this disease[8]. Treatments such as surgery, radiation therapy, and chemotherapy are often used together to treat multiple different cancer origins. Oncolytic viral therapies have also made their mark on the cancer research world as another novel, potential therapeutic option, with the possible advantage of lessening side effects as well as higher treatment efficacy due to higher tumor selectivity[8, 9]. In fact, results have been so promising that oncolytic viral treatments have now been approved for clinical trials in several countries, and the first oncolytic viral therapy has now been marketed as a treatment for head and neck cancers in China [10].

1.1 What are Oncolytic Viruses?

Oncolytic viruses (OVs) refer to those that are able to preferentially and selectively propagate in cancer cells, and consequently destroy tumor tissue leaving non-cancerous tissues unharmed[11]. For a virus to be truly *oncolytic*, it must possess these qualities. Examples of oncolytic viruses studied to date include Newcastle disease virus, adenovirus, herpes simplex virus (HSV), vesicular stomatitis virus (VSV), and vaccinia virus, among others. The ultimate goal of replication-competent anti-cancerous viral therapy is to produce a safe and effective therapeutic index with minimal toxicity and side effects [12].

This chapter presents a summary of the literature available on replication-competent oncolytic viruses and will focus on the development of oncolytic vaccinia virus strains.

1.1.1 History of Oncolytic Viruses.

The idea that viruses may be able to treat cancer was born almost by chance, when in the early 20th century patients with malignancies who experienced viral infection or received rabies vaccinations were noted to experience transient remissions[13, 14]. Dock, who was the first to describe this phenomenon in 1904 when he reported of a patient who underwent significant remission of leukemia after experiencing an influenza infection [15]. NG De Pace described a case of a woman with uterine cancer experiencing remission after a rabies vaccination, presenting his findings in 1910 at the International Congress in Paris [16, 17]. Levaditi *et al*. then demonstrated that vaccinia virus inhibited various mouse and rat tumors in 1922, and described this phenomenon as “le tumeur fait function d’eponge”[18].

These early discoveries led to several viruses being tested in both pre-clinical and clinical settings during the late 1940s, 50s and 60s[8]. In the late 1940s, G.T.Pack inoculated live attenuated rabies vaccines into human melanoma tumors and reported the first remissions at Memorial Sloan-Kettering Cancer Center[19-21]. Alice Moore laboratory at Memorial Sloan-Kettering also became a prominent force in the field of oncolytic virotherapy[22-24]. Working with Russian Far East encephalitis virus, complete regression was achieved in some cases of mouse sarcoma 180 – the first animal model to demonstrate full regression through viral oncolysis[22]. Hoster *et al*. published the first clinical trial assessing the impact of viral oncolysis on cancer. Twenty-one volunteers with Hodgkin’s disease were inoculated with

samples of tissue and sera from other patients noted to have developed viral hepatitis. Development of viral hepatitis in the volunteers was defined at the time of jaundice onset. Although there were obviously many significant side effects, some patients did show clinical improvement and decreased tumor size after manifesting classic signs and symptoms of viral hepatitis [25]. In 1956, the National Cancer Institute (NCI) conducted the first large-scale clinical study, administering wild-type adenoviruses to 30 patients with cervical cancer and achieving varying degrees of localized tumor necrosis but no significant tumor regressions or remissions [26].

While these early studies and trials were considered groundbreaking, interest in viruses as potential anti-neoplastic therapies was abandoned due to unimpressive and short-lived success, as well as unacceptable side-effects that eventually ended trials[17]. These viruses thus failed to infect only malignant cells, failed to replicate only in cancer cells, and were unable to circumvent detection and clearance by the immune system. Limited virology, molecular biology, immunology, and genetics knowledge, as well as primitive biotechniques, likely contributed to this [8].

It is only recently that the fervor of viruses as a strategy against cancer has been reignited with the advancement in scientific knowledge and technology. We now possess tools that enable us to develop more targeted and effective viruses[12]. The adenovirus gene deletion mutant ONYX-015, which was deleted for the E1B-55K gene and hypothesized to target p53-deficient tumor cells, was the first replication-competent modified virus that displayed anti-cancer effects in humans[27]. China is now the first country in the world to market an adenoviral therapy for head and neck cancers[10].

1.1.2 Why Oncolytic Viruses?

Oncolytic viruses (OVs) have the potential to fulfill many criteria for the ideal cancer therapeutic (modified from Breitbach *et al.*)[28]:

1. Cancer therapeutics should be cytotoxic rather than cytostatic;
2. The new therapeutic must have novel, multi-pronged mechanisms of action in order to decrease the onset of resistance;
3. Novel therapeutics should target or exploit validated genetic pathways and should also possess a broad spectrum of efficacy in order to allow for development for various markets;

4. Beyond having a cytotoxic effect, anticancer agents should ideally cause acute tumor debulking, as this facilitates the evaluation of tumor responses, leading to faster, lower-cost development. Acute debulking approaches are also complimentary to combination therapy with standard (cytostatic) treatments.
5. The agent's route of administration should be flexible, e.g. both IV and IT administration should be feasible in order to facilitate systemic tumor targeting as well as local boosts of therapeutic to cause tumor debulking;
6. Novel therapeutics should be a part of a broad product class, with room for development of improved next generation products.

With regards to oncolytic viruses:

1. OVs can directly infect and lyse cancer cells, thereby acting as cytotoxic agents.
2. OVs can trigger vascular disruption and loss of tumor perfusion shortly following OV therapy. An acute inflammatory response was shown to cause vascular shutdown and apoptosis of uninfected tumor cells[29]. In addition, the association of immunostimulatory products and antigens from the virus with tumor antigens within the tumor microenvironment may 'tip the balance' to rejection of the tumor by the host immune response (reviewed in section 2.5 and 2.6).
3. Advances in genetic engineering have allowed for improved OV targeting and potency; many opportunities exist for the development of next generation products. Since OVs currently in development exploit validated genetic pathways known to be dysregulated in many cancer types (e.g. EGFR/Ras[30]), OVs may have a broad spectrum of efficacy.
4. Furthermore, evidence of acute tumor debulking in patients was also reported in clinical trials. A reduction of tumor perfusion was observed in patients with advanced HCC treated with an oncolytic vaccinia virus (JX-594, Jennerex Inc.) within 6 days of therapy[31].
5. OVs are replicating therapeutics with unique pharmacokinetics; they are quickly cleared from systemic circulation but can rapidly and selectively amplify within tumors and may re-emerge systemically (consistent with waves of replication) [31]. Therefore, OV therapeutics are amenable to both to IV infusion as well as local IT boosts.
6. Finally, advances in genetic engineering have allowed for improved OV targeting and potency; many opportunities exist for the development of next generation products.

1.1.3 An 'Ideal' Replication-Competent Oncolytic Virus.

There are several versions in the literature of what characteristics an ideal replication-competent oncolytic virus should incorporate. These characteristics may be combined and summarized as follows [12, 32, 33]:

1. Effective, direct, and preferably complete destruction of tumor cells via lysis;
2. Preferential or exclusive and rapid infection of tumor cells, ideally also in nondividing tumor cells;
3. Initial evasion of immune system in order to effectively infect and distribute to neighbouring cancer cells and cause exponential destruction;
4. Subsequent autologous anti-tumor response elicited;
5. Normal tissues are unharmed;
6. Mild, limited, or no side effects caused, especially in immunocompromized patients;
7. Treatments are known and available if needed to control or cease replication;
8. No safety concerns for medical personnel, contacts of the infected individual, or public safety;
9. Stable genetic make-up, especially if virus is modified;
10. No risk of integration of viral genome into the genome in non-cancerous cells. No cells with viral genome contents in host cell genome should survive;
11. Sufficient genomic carrying capacity;
12. Unlikely recombination with other organisms; and
13. Able to be manufactured and distributed for widespread clinical use according to 'Good Manufacturing Practices' (GMP) guidelines.

An 'ideal' virus has yet to be identified. However, the vaccinia appears to be one of the most promising.

1.2 Vaccinia Viruses

In order to develop safer and more efficacious vaccinia viral therapies, it is important to understand the history, taxonomy, morphology, and replication of the therapy agent. Moreover, an understanding on immune responses of oncolytic viral therapies is also needed.

1.2.1 History of Vaccinia Viruses as Oncolytic Virotherapies.

Levatidi's laboratory were the first to discover vaccinia viruses (VACVs) were naturally oncolytic[34]. Cassel and Garrett followed by successfully treated murine ascites carcinoma[35]. At M.D. Anderson, a patient was witnessed to have remission of Chronic Lymphocytic Leukemia after being inadvertently vaccinated with vaccinia virus[36], and another patient although becoming significantly ill from vaccinia vaccination requiring immunoglobulin had remission of his CLL for over 3 years[37]. Another patient with multiple myeloma had a partial response after IV administration of vaccinia virus[38]. In patients with metastatic renal or pulmonary carcinomas also experienced partial remissions[38, 39]. This lead to several clinical trials including treating melanoma with a potent vaccinia virus encoding GM-CSF[40, 41], the use of thymidine kinase deleted JX-594 encoding the granulocyte macrophage colony stimulating factor (GM-CSF) for various cancers[42], as well as the parent vaccinia virus discussed in this thesis[43]. Ongoing clinical trials are discussed in section 4.0.

1.2.2 Taxonomy.

Vaccinia virus is a member of the Poxviridae family[44, 45]. Viruses of this family are split into two subfamilies, *Chordopoxvirinae*, which infect vertebrates and *Entomopoxvirinae* which infect solely insects. The subfamily of *Chordopoxvirinae* is subdivided into eight different genera, similar in morphology and host tropism. VACV belongs to the genus Orthopoxviridae of the *Chordopoxvirinae* subfamily*,* whose members are the causative agents of smallpox. Following a massive worldwide effort in the 1970s, the World Health Organisation (WHO) declared smallpox to be eradicated in 1980[46]. This effort was due in part to the availability of a stable and effective vaccine based on vaccinia virus with sufficient antigenic cross reactivity to provide protection to other orthopox viruses. The origins of modern vaccinia virus are obscure, and although now known to be distinct from the cowpox virus used in 1798 by Edward Jenner as a vaccine for smallpox[47], it is closely related. Historically the two are often considered to be one and the same [46].

1.2.3 Morphology.

VACV belongs to the group of double-stranded DNA viruses and is one of the largest known viruses. Vaccinia virus particles are approximately 300 x 240 x 120 nm in size and possess an oval, brick-shaped structure with a lipoprotein shell surrounding a complex core structure [45]. The core structure contains a linear, dsDNA genome of approximately 192kb, encoding for some 200, non-overlapping genes. The double-strand DNA is associated with a number of virus-encoded proteins necessary for early transcription of RNA polymerase and enzymes for RNA capping, methylation and polyadenylation[48]. Approximately half of the VV genome is transcribed before DNA replication (early class viral genes)[49, 50]. Minimal interaction with host proteins allows VACV to replicate in many different cell types and to avoid host defence mechanisms.

At least four distinct types of vaccinia virus particles are produced during productive infection: mature virus, also referred to as intracellular mature virus (IMV), intracellular enveloped virus (IEV), and two forms of extracellular virus, cell-associated enveloped virus (CEV) and extracellular enveloped virus (EEV)[45, 51]. The IMV particle is surrounded by one membrane, and the EEV particle comprises an IMV particle enclosed within a second lipid membrane containing several viral antigens[52].

1.2.4 Replication.

VACV is unique among most DNA viruses in that its replication occurs in the host cell cytoplasm for the duration of the infectious cycle. The first step in infection is the fusion of enveloped virus and cell membrane or the membrane of an endocytotic vesicle[53]. The mode of entry is dependent on the particle form. CEVs, EEVs and IMVs use different and yet partly unsolved mechanisms and receptors for entry [54].

After fusion of the viral and cellular membranes, the viral core is released into the cytoplasm and transported further into the cell along microtubules to the cytoplasmic side of the endoplasmatic reticulum (ER). Upon entry into the cytoplasm, the core partially uncoats to synthesize early viral mRNAs which resemble host cell mRNAs. The cellular translational apparatus is recruited for translation of these mRNAs that encode for proteins involved in viral DNA synthesis. Other early proteins serve to modify the host cell (recruitment of the

transcriptional and translational apparatus) to the advantage of the virus and aid virus escape from the host innate immune response[52]. After DNA replication has begun in so-called mini-nuclei, which are surrounded by rough ER membranes, immediate genes and late genes are transcribed[55]. Immediate genes serve mostly for the transcription of late genes which are involved in packaging of the new viral particles and for essential proteins that initiate early gene transcription in a newly infected cell (Figure 1).

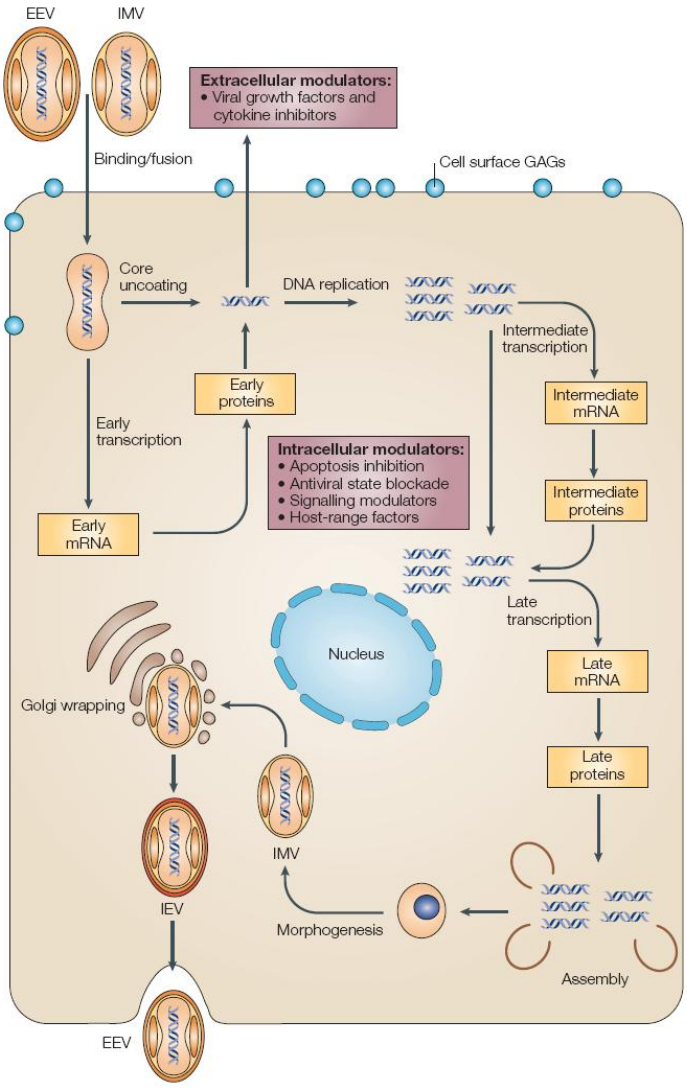

Figure 1. Poxvirus replication cycle. Poxviruses replicate in the cytoplasm. Two distinct infectious virus particles, the intracellular mature virus (IMV) and the extracellular enveloped virus (EEV), can initiate infection. The IMV and EEV virions differ in their surface glycoproteins and in the number of wrapping membranes. Fully permissive viral replication is characterized by three waves of viral mRNA and protein synthesis (early, intermediate and late), which are followed by morphogenesis of infectious particles. The initial intracellular mature virus (IMV) is transported via microtubules and is wrapped with Golgi-derived membrane, after which it is referred to as an intracellular enveloped virus (IEV). The IEV fuses to the cell surface membrane to form cell-associated enveloped virus (CEV; not shown), which is either extruded away from the cell by actin-tail polymerization or is released to form free EEV. EEV might also form by direct budding of IMV, therefore bypassing the IEV form. *McFaden. Poxvirus tropism. 2005.*

After synthesis of all the necessary proteins, assembly of progeny virus particles begins[56]. Assembly starts with the formation of crescent-shaped membranes and spherical immature virions (IVs) that appear at the sites of DNA replication around 5 hours post infection. These IVs still lack the genome and once they take up DNA, they mature into the brick-shaped IMV, the first infectious form of the virus[57]. IMVs will either be released upon cell lysis or alternatively move away from DNA sites by binding to microtubules of the host cell, where they can obtain a second double membrane from a trans-Golgi or early endosomal compartment to form IEVs[56]. The IEV particles use microtubules and kinesin to propel towards and fuse with the cell membrane forming CEVs. CEVs can then recruit actin from the cytoplasm to be transported to adjacent cells or dissociate from the cell membrane to become EEVs. The latter form has evolved for rapid systemic spread within the host and for evasion of immune-mediated clearance.

1.2.5 Host Immune Response to VACV Infection.

In order to develop strategies to combat cancer with oncolytic viruses, it is important to have an understanding of the immune response to viruses and virus-colonized tumors. The immune system has the capability to hinder or enhance oncolytic viral therapy and anti-tumor effects, especially in immunocompetent patients. Furthermore, combining immunotherapy and oncolytic viral therapy may result in more potent, effective, and successful treatment outcomes. By further understanding the pathways and mechanisms of the immune response, we may be able to develop more safe, potent, and efficacious treatments.

Mammalian host cells are able to initiate immune responses against viruses in order to limit viral replication and clear infection [58]. They do this through several processes of viral recognition and innate defence signaling, inducing immune responses against the viruses. Of particular importance are IFNs, especially the type I IFNs, IFN-α and IFN-β. These cytokines, and the genes they stimulate, are essential for immune defences against viruses. Innate sensing of viruses and induction of IFNs induce three main innate immune responses via activation of: 1) the complement cascade; 2) further mediators of inflammation including cytokines; and 3) innate immune effector cells such as macrophages and dendritic cells[59]. If pre-existing immunity is present, viruses can also be directly neutralized by circulating antibodies[60]. The innate immune system then orchestrates the lysis of virions and virus-infected cells, inducing either necrosis or apoptosis, as well as providing a link to adaptive

immunity[59]. Research into the role of innate defences in dampening the oncolytic effects of oncolytic viruses has only recently begun, and the importance of this knowledge lies in finding avenues to modulate such initial innate responses, in order to allow for efficient viral delivery, replication, dissemination, and increased oncolysis of tumors while minimizing host toxicity.

Immediately after VACV invasion, antiviral mechanisms involving induction of innate immune system complement and productions of interferons (IFNs) and cytokines, are activated and serve as the first-line host defence. Recent studies have revealed that vaccinia activates innate immunity through a TLR2/MyD88-dependent pathway, resulting in the production of pro-inflammatory cytokines and a TLR-independent pathway, leading to the induction of antiviral IFN-β production[61, 62]. Subsequently, adaptive immune responses that are mediated by cytotoxic and helper T cells assume importance in defence[63]. Several studies have demonstrated that both the T helper 1 (Th1) and cell-mediated immune responses play a critical role in host defence against VACV infection[64-67]. In addition, neutralizing antibodies could also be involved in preventing subsequent VACV infections.

Furthermore, it was demonstrated that antivirus neutralizing antibodies (Abs) were more important in clearing VACV than cytotoxic T-lymphocytes (CTLs) following acute infection, while in the absence of Abs, CTLs contribute to protection against VACV infection[68]. However, there is still only limited knowledge about the protective immune responses against VACV infection.

A number of studies have established the multiple factors encoded by VACV that actively suppress innate immunity and the Th1 immune response. Vaccinia virus immunomodulators can act either inside or outside infected cells. Intracellular VACV proteins regulate host gene transcription (shut off of DNA, RNA, and protein synthesis of cellular origin), the antiviral activity of IFNs, innate immune signalling, and apoptosis, whilst extracellular VACV proteins inhibit the action of complement, cytokines, and chemokines [for reviews see [48, 69]]. Taken together, these viral-encoded proteins allow VACV to infect and replicate with remarkable efficiency in its host.

1.2.6 Host Immune Responses to Tumors Colonized With VACV.

Several studies have been emerging recently specifically looking at the immune response to tumors colonized with oncolytic vaccinia viruses. Patients treated with vaccinia expressing GM-CSF delivered directly to cutaneous melanoma, for example, demonstrated regression of not only the treated lesions but also metastases. The metastases showed no signs of vaccinia infection, but did show T cell infiltration[70]. Therefore, in these experimental settings vaccinia was not only able to induce CTL responses against itself, but also against tumor cells. Furthermore, studies in immunocompetent mice found that animals cleared of a tumor by vaccinia treatment were subsequently resistant to rechallenge by cells of the same tumor type, possibly due to the development of immune memory[71].

In addition, transcriptional profiling of regressing GI-101A subcutaneous breast xenografts in mice treated with the VACV GLV-1h68 based on a mouse-specific platform also revealed gene expression signatures consistent with immune defence activation, inclusive of IFN-stimulated genes (STAT-1 and IRF-7), cytokines, chemokines, and innate immune effector function. These findings, the authors concluded, suggested immune activation may combine with viral oncolysis to induce tumor eradication in this model, providing a novel perspective for the design of oncolytic viral therapies for human cancers[43]. This was further validated in pancreatic and prostate xenograft models, where profiling of immune proteins revealed a significant proinflammatory response and marked activation of innate immunity in virus-colonized tumors[72, 73].

Further transcriptional analysis of responding vs. non-responding xenografts infected with GLV-1h68 revealed that tumor rejection was associated *in vivo* with activation of IFN-stimulated genes and again innate immune host's effector functions correlating with VACV colonization of the xenografts. Interestingly, tumors resistant to VACV showed combined activation of Th1 and Th2 with a deviation toward Th2 and humoral immune responses that failed to achieve rejection, which is possibly explained by a lack of target antigen. Moreover, the tumor tolerance model instead displayed immune suppression pathways through activation of regulatory mechanisms that included in particular the overexpression of interleukin-10 (IL-10), IL-10 receptor, and suppressor of cytokine signaling SOCS-1 and SOCS-3[74]. These immune signatures reproduced those observed in humans during immune-mediated tissue-specific destruction that causes tumor or allograft rejection, autoimmunity or clearance of pathogens[75]. The authors suggested that there may be common pathways in a universal mechanism associated with tumor rejection [76].

1.2.7 Why Vaccinia Viruses as Oncolytic Agents.

The advantages of using vaccinia virus as a vector for oncolytic viral therapy are several. Vaccinia's large genome enables a large amount of foreign DNA to be incorporated without reducing the replication efficiency of the virus, which has been shown to be the case with some adenoviruses[77]. It has fast and efficient replication, unlike, for example adenovirus ONYX-015. Cytoplasmic replication of the virus lessens the chance of recombination or integration viral DNA into cells. Its DNA-based genome also makes it more stable than RNA-based viruses. It has been shown to be capable of immune evasion, and capable of infecting a wide variety of cells. Perhaps most importantly, its safety profile after its use as a live vaccine in the WHO's smallpox vaccination makes it particularly attractive as an oncolytic agent and gene vector[46]. In addition, a vaccinia immunoglobulin and antiviral drugs are available if needed[78].

Mechanisms of vaccinia viral oncogenesis remain speculative and unproven. It has been shown that oncolytic viruses target cancers that overexpress proteins such as ribonucleotide reductase, DNA repair enzymes, and proteins rendering them resistant to apoptosis, characteristics that tend to make tumor cells resistant to chemotherapy and radiation therapy[79]. Recently it was discovered that both R1 and R2 subunits of ribonucleotide reductase are needed for vaccinia viruses to replicate [80]. Although both subunits are already encoded in most VACV strains, it suggests that vaccinia viruses may prefer environments high in ribonucleotide reductase which may explain vaccinia's natural attraction to cancer cells. More investigation is needed to elucidate the exact mechanisms rendering vaccinia viruses highly selctive and oncogenic in tumors.

1.3 Vaccinia Virus in Oncolytic Tumor Therapy

Due to the advantages of vaccinia viruses, several preclinical trials have been performed in a variety of cancer origins. Success of these studies has also lead to several clinical trials with novel oncolytic viral strains.

1.3.1 Preclinical Data.

The successful use of vaccinia virus as an oncolytic agent has been so far published in around 50 tumor models (Table 1). This clearly demonstrates the potential of vaccinia virus strains to be applicable as tumoricidal agent in a wide variety of cancers. Moreover, as the primary tumor is usually not the cause of death, it is important to note that vaccinia virus injection has the potential to reduce metastatic burden when, seen with the aggressive PC-3 prostate cancer model[73] or in rabbits bearing VX2 liver tumors[81, 82].

Table 1. Vaccinia virotherapy in tumor models.

Tumor model	origin	host	VV background	References
Prostate				
PC-3	human	mouse	LIVP	[73, 75]
DU-145	human	mouse	LIVP	[73, 75, 83]
Renal				
786-O	human	mouse	WR	[84]
ACHN	human	mouse	WR	[84]
769P	human	mouse	WR	[84]
Renca	mouse	mouse	WR	[84]
Pancreatic				
Mia-Paca2	human	mouse	LIVP	[72, 75, 83, 85]
PANC-1	human	mouse	LIVP	[72, 75, 86]
Suit-2	human	mouse	LIVP	[87]
Lung				
A549	human	mouse	LIVP	[75, 83]
TC-1	mouse	mouse	Not reported	[88]
CMT-64	mouse	mouse	IHD-J	[89]
Breast				
GI-101A	human	mouse	LIVP	[43, 75]
ZMTH3	dog	mouse	LIVP	[90]
MTH52c	dog	mouse	LIVP	[91]
4T1	mouse	mouse	WR	[92]
JC	mouse	mouse	WR(WI)	[81, 89]
Brain				
C6	rat	mouse	WR(vvDD)	[93]

U87MG	human	mouse	WR(vvDD)	[93]
U118	human	mouse	WR(vvDD)	[93]
RG2	rat	rat	WR(vvDD)	[93]
F98	rat	rat	WR(vvDD)	[93]
NXS2	mouse	mouse	VSC20	[94]
Squamous cell carcinoma				
MSKQLL2	human	mouse	LIVP	[95]
Mesothelioma				
MSTO-211H	human	mouse	LIVP	[96]
Thyroid				
8505C	human	mouse	LIVP	[97]
DRO90-1	human	mouse	LIVP	[97]
Multiple myeloma				
My5	human	mouse	WR	[98]
RPMI8226	human	mouse	WR	[98]
Liver				
VX2	rabbit	rabbit	Wyeth	[82]
VX2	rabbit	rabbit	WR	[81, 99]
spontaneous	rat	rat	Wyeth	[82]
TIB-75	mouse	mouse	WR	[81]
Colorectal				
MC38	mouse	mouse	WR	[81, 100-103]
LoVo	human	mouse	Copenhagen	[104]
HCT116	human	mouse	WR	[101, 105]
CMT-93	mouse	mouse	WR	[92, 105]
HT29	human	mouse	WR	[81]
Ovarian				
OVCAR-3	human	mouse	LIVP	[75]
UCI-101	human	mouse	WR	[92]
SKOV-3	human	mouse	WR	[92]
A2780	human	mouse	WR	[103, 106]
ES2	human	mouse	LIVP	[107]
MOSEC(-luc)	mouse	mouse	WR, LIVP	[103, 106, 108]
Defb29 Vegf-luc	mouse	mouse	LIVP	[107]

Melanoma				
1858-MEL	human	mouse	LIVP	[75]
888-MEL	human	mouse	LIVP	[75]
B16F10	mouse	mouse	Wyeth Not reported	[109] [88]

The use of different oncolytic vaccinia virus strains (WR, LIVP, Wyeth, Copenhagen), revealed that WR-derived strains were able to colonize tumors in human xenografts in nude as well as syngeneic tumors in immunocompetent wild-type animals, and virus strains producing higher amounts of EEV were shown to be better suited to colonize distant metastasis and result in faster tumor regression[89, 110]. LIVP-derived strains, on the other hand, are not as well suited to colonize murine tumors but showed a better safety profile in a study comparing WR- and LIVP-derived tumor selective strains[43]. In addition, a LIVP-mutant which does produce higher amounts of EEV did not show improved therapeutic potential[111]. Therefore, although different vaccinia virus strains are able to show therapeutic effects in a number of tumor models, properties of each strain may be better suited in particular patients or tumor origins.

1.3.2 Development of New VACV Generations.

Enhanced understanding and advancements in molecular biology has enabled a generation of oncolytic viruses engineered for safer and more efficacious treatments. Several strategies have been investigated with regards to vaccinia viruses.

1.3.2.1 VACVs Armed With Cytokines / Immunostimulatory Molecules.

One of these strategies relates to the combination of viral therapy with cytokines, which may harness the host's own immunity to assist tumor rejection and destruction.

As mentioned, thymidine kinase(-) vaccinia virus strains encoding human GM-CSF, JX-549 and JX-963, were developed[81, 82]. Both viral strains resulted in enhanced antitumor immunity due to the expression of the GM-CSF transgene in situ. Direct oncolysis plus GM-CSF expression stimulated shutdown of tumor vasculature and antitumoral immunity, significantly reducing tumor burden and increasing median survival. Tumor-specific virus replication and

gene expression, systemically detectable levels of GM-CSF, and tumor-infiltrating CTLs as well as significant increases in neutrophil, monocyte and basophil concentrations in the peripheral blood were also demonstrated.

Expression of T-cell costimulatory molecule 4-1BBL by an oncolytic vaccinia virus resulted in modest tumor regression in a poorly immunogenic murine melanoma model[109]. In a setting when lymphodepletion was employed, the expression of 4-1BBL resulted in promoted MHC class I expression. At the same time the authors showed reduced antiviral antibody titers, enhanced viral persistence, and rescued effector memory CD8+ T cells. This significantly improved the therapeutic effectiveness of the oncolytic vector.

Vaccinia expressing co-stimulator cytokines has even been shown to help overcome the tumor microenvironment's immune suppressive characteristics. The melanoma microenvironment in particular has been shown to possibly lead to local T cell tolerance in part through downregulation of costimulatory molecules, such as B7.1 (CD80). A 2-dose-escalation phase I clinical trial was conducted with 12 patients using a recombinant vaccinia virus expressing B7.1 (rV-B7.1) for monthly IT vaccination of accessible melanoma lesions. The approach was well tolerated with only low-grade fever, myalgias, and fatigue reported, with 2 patients experiencing vitiligo[112]. An objective partial response was observed in 1 patient and disease stabilization in 2 patients, 1 of who was alive without disease 59 months following vaccination. All patients demonstrated an increase in post vaccination antibody and T cell responses against vaccinia virus. Local and systemic immunity was evaluated in patients demonstrated an increased frequency of gp100 and T cells specific to melanoma antigen recognized by T cells 1 (MART-1), and tumor regression was associated with increased expression of CD8 and IFN-γ.

Continuing this work, the effects of a vaccinia virus expressing three costimulatory molecules, B7.1, ICAM-1, and LFA-3 (rV-TRICOM) was evaluated in patients with metastatic melanoma in a dose escalation phase I trial[113]. Of the twelve patients followed up, there was a 30.7% objective clinical response, with one patient achieving a complete response for more than 22 months. An inverse association was detected between anti-vaccinia antibody and anti-vaccinia T cell responses, and patients who received high dose IL-2 but failed to respond to vaccination had a trend toward improved survival. These studies confirm the safety profile and feasibility of direct injection of vaccinia virus expressing multiple costimulatory cytokines and molecules in patients with established tumors in order to stimulate anti-tumor immunity.

Cytokines have even been utilized in order to increase tumor selectivity. Kirn *et al*. developed a vaccinia virus strain expressing the cytokine IFN-β, JX-795, which is incapable of responding to this cytokine in order to have the dual benefits as a cancer therapeutic with increased anticancer effects and enhanced virus inactivation in normal tissues[105]. The virus was based on a vaccinia B18R deletion mutant backbone for IFN-β expression, as the B18R gene product neutralizes secreted type-I IFNs. JX-795 had superior tumor selectivity and systemic efficacy when compared with the TK-/B18R- control or wild-type vaccinia in preclinical models. The authors concluded that by combining IFN-dependent cancer selectivity with IFN-β expression to optimize both anticancer effects and normal tissue antiviral effects, tumor-specific replication, IFN-β gene expression, and treatment efficacy was achieved following systemic delivery in preclinical models.

1.3.2.2 VACV Delivering Anti-Angiogenic Agents.

Further improvement of the oncolytic potential could recently be achieved in three independent studies in which the authors tried to inhibit the tumor vasculature by expression of an endostatin/angiostatin fusion gene[87] or, as in two of the studies, targeting the vasculature endothelial growth factor (VEGF)[83, 84]. VEGF binds to specific receptors on epithelial cells and is a major player in tumor angiogenesis. Inhibition of VEGF has been extensively studied in several cancer models[84, 114-117], with Avastin being one of the most successful immunotherapeutic proteins to date. This drug has been approved by the US Food and Drug Administration for use in combination with chemotherapy for treatment of metastatic colorectal cancer and most forms of metastatic non-small cell lung cancer[118, 119]. Vaccinia-mediated blocking of VEGF was achieved by either fusing the VEGF receptor 1 to the Fc tail of human IgG antibody (VEGFR-1-Ig) or by secretion of a single-chain antibody (GLAF-1) to VEGF. In both cases, VEGF was bound and thus prevented interaction to its natural receptors on endothelial cells resulting in lower blood vessel densities within the tumor tissue. The reduced tumor vascularity was accompanied by faster regression of tumors, although in one study, this depended on the dose of virus injected[84]. In the same study the VEGFR-1-Ig encoding vaccinia virus strain was found to be more lethal to mice than the parental strain. For the GLAF-1 encoding virus strains no changes in toxicity were described.

1.3.2.3 Use of VACVs in Gene Directed Enzyme Prodrug Therapy.

Another approach to enhance the oncolytic effects caused by vaccinia virus strains is the so called gene directed enzyme prodrug therapy (GDEPT). Here, a relatively non-toxic prodrug

is enzymatically converted to toxic drugs which result in killing of the enzyme producing tumor cells. Moreover, the so called bystander effect caused by diffusion of the drug into neighboring cells results in killing of cells in close proximity to the enzyme-producing cell even if they were not made to express the prodrug converting protein.

The most prominent enzyme type in vaccinia virus-mediated GDEPT certainly is cytosine deaminase which is absent in mammalian cells and used in combination with 5-fluorocytosine[104, 106, 120-122]. This prodrug is converted to 5-fluorouracil whereby the efficiencies depend on the specific cytosine deaminase (e.g. bacterial, fungal) and the presence of uracil phosphoribosyltransferase[123, 124]. When using this system in combination with oncolytic vaccinia virus strains, the reported results indicate better therapeutic effects when compared to the oncolytic virus alone. However, the therapeutic benefit was expected to be higher as recently discussed by Chalikonda *et al*[106]. In other studies, similar results were found when using a β-galactosidase expressing vaccinia virus strain in combination with an inducible prodrug seco-analog of duocarmycin SA[125]. Several reasons might be responsible for these observations: first, the rapid kinetics of oncolytic vaccinia virus replication might functionally overlap with the used prodrug system; and second, the administration of prodrug may have inhibited the viral replication, thus reducing the antitumoral cytotoxicity induced by the oncolytic virus itself. This effect has already been reported by McCart *et al* [126] but was not observed in all prodrug systems [125]. Different dosing schemes or other GDEPT systems should still be considered and might cause stronger synergistic effects between the oncolytic virus strain and prodrug therapy.

1.3.2.4 Combination Therapies with VACVs.

Although the therapeutic effect of vaccinia virus shows promise, combining conventional therapies may also be used to enhance oncolytic viral treatment and help circumvent the immune system for optimal delivery of viruses to tumors.

Combination of oncolytic vaccinia virus with classical chemotherapeutic agents such as gemcitabine and cisplatin led to accelerated tumor size reduction compared to monotherapy using VACV alone [72]. At the same time each of the chemotherapeutics could only slow down tumor growth but did not result in complete tumor regression. Furthermore, immunosuppressive chemotherapeutic agents like rapamycin and cyclophosphamide did also have beneficial effects in the oncolytic treatment of malignant gliomas in rats[93]. Injection of the immunosuppressive agents resulted in enhanced viral replication and spreading which ultimatively led to further prolonged survival of the immunocompetent rats.

Combination with other chemotherapeutic agents in future studies will provide useful data as to which combination therapies are best suited for each type of cancer.

Radiation therapy has also been explored as a possible strategy against malignancies to be used in combination with oncolytic viral therapy[127-129]. Radiotherapy can either be local in the form of external beam radiation therapy (EBRT), or systemically administered. Although many oncolytic viral therapies have been combined with radiation therapies including adenoviruses, herpes, and vesicular stomatitis viruses (VSV), no studies are present in the literautre exploring oncolytic vaccinia viruses in this context. OVs may act as radiosensitizers by affecting pathways that render tumors resistant to treatment. Further, the selective cytotxicity of viruses to tumors may enable more targeted radiotherapeutic strategies especially with systemically administered radiotherapies. This will be discussed in further detail in chapter 2.

Further strategies included the use of carrier cells to deliver viruses undetected to tumors. An example of such therapy was the development of a cytokine induced killer (CIK) cell that expressed non-MHC restricted NKT cell markers and proteins that adhered to abnormal vasculature and NKG2D ligands, and which contained vaccinia virus[92]. The virus was found to have a prolonged eclipse period of 48–72 h after infection; and preliminary data indicated that virus can be delivered even if faced with an anti-viral immune response. Via whole body imaging, the CIK cells was shown to traffick to tumor cells effectively before releasing virus throughout the tumor, producing impressive anti-tumor effects. Even previously resistant tumors were sensitized to subsequent CIK cell targeting and destruction.

In another innovative strategy complementary oncolytic VSV was combined with oncolytic vaccinia virus to improve therapeutic outcome[130]. The two recombinant viral strains synergistically enhanced each other, resulting in a "ping pong" effect which lead to better tumor tissue penetration prolonged survival of tumor bearing mice. The synergistic effect was on the one hand dependent on the VACV B18R gene product which locally antagonizes the innate cellular, antiviral response initiated by type I IFNs[131-133] and therefore supports VSV growth. On the other hand, recombinant expression of the fusion-associated small-transmembrane by VSV resulted in enhanced spreading of the VACV.

1.4 Vaccinia Viruses in Clinical Trials

Due to the success of vaccinia viruses in preclinical models, there are several ongoing clinical phase I and II-studies for human cancer therapy following treatment with oncolytic vaccinia virus strains (Table 2).

Table 2. Clinical trials with oncolytic vaccinia viruses. Source: www.clinicaltrials.gov

Condition	Intervention	Phase	Sponsor
Advanced Solid Organ Cancers	Biological: Vaccinia virus (GL-ONC1)	Phase I	Genelux Corporation
Solid Cancers	Biological: Vaccinia virus (vvDD-CDSR)	Phase I	University of Pittsburgh
Unspecified Adult Solid Tumor	Biological: recombinant vaccinia-CEA(6D)-TRICOM vaccine	Phase I	National Cancer Institute (NCI)
Carcinoma, Hepatocellular	Genetic: JX-594: Recombinant vaccinia virus (TK-deletion plus GM-CSF)	Phase II	Jennerex Biotherapeutics

For example, seven patients with metastatic melanoma were then recruited for a phase I trial utilizing IT injection of JX-594[42, 119]. Response of both injected tumors (in 5 of 7 patients) and response of at least one non-injected tumor (in 4 of 7 patients) was demonstrated, including two patients who achieved a partial response (> 6 months) and a complete response (> 4 months) to JX-594 treatment. Moreover, efficacy and gene expression occurred despite pre-treatment vaccination and, therefore, pre-existing anti-vaccinia immunity in all patients.

In another phase I trial using JX-594 in patients with hepatic carcinoma, three of ten evaluable patients had a partial response and six had stable disease[31]. Patients received one of four doses of IT JX-594 (10^8 plaque-forming units (PFU), $3x10^8$ PFU, 10^9 PFU, or $3x10^9$ PFU) every 3 weeks. The primary goals were to determine the maximum-tolerated dose (MTD) and safety of JX-594 treatment. IT injection of JX-594 into primary or metastatic liver tumors was generally well-tolerated, with grade I-III flu-like symptoms reported by all patients, and four patients experiencing transient grade I-III dose-related thrombocytopenia. Grade III hyperbilirubinaemia was dose-limiting in both patients at the highest dose, and thus the MTD was calculated at 10^9 PFU. JX-594 replication-dependent dissemination in blood was shown, with resultant infection of non-injected tumor sites. Safety was therefore acceptable in the context of JX-594 replication, GM-CSF expression, and systemic

dissemination, which led to a phase II trial in patients with unresectable primary hepatocellular carcinoma, completed in March 2010[119].

Therefore, vaccinia viruses have been shown to be safe and promising in these early clinical trials. However, in order to monitor virotherapy, efficacy, and potential toxicity, a non-invasive imaging modality is needed. This will be discussed in chapter 2.

2.0 THE HUMAN SODIUM IODIDE SYMPORTER

As outlined in the previous chapter, oncolytic vaccinia virotherapy has shown success in preclinical trials and much promise in completed and ongoing human clinical trials. However, as discussed in a review by Breitbach *et al*.[28], a rational clinical development plan is key to the development of any novel therapeutic. This involves the following factors: (1) identifying an unmet need in medical oncology; (2) identifying a clinically important endpoint that can be reached in a reasonable time frame; (3) targeting patient populations that can be enrolled efficiently, and finally; (4) identifying a genetic marker to predict tumor response.

Oncolytic viral therapy has addressed most of the key points above. However, regarding predicting tumor response, biopsy is the current gold standard for monitoring the therapeutic effects of viral oncolysis[134]. This may be feasible in pre-clinical trials, or early clinical trials, however, a non-invasive test facilitating ongoing monitoring of therapy is needed for human studies[8]. This will enable assessment of the biodistribution of oncolytic viruses to ensure safety and correlation with treatment efficacy, as well as the potential for a more sensitive and specific diagnostic technique to detect tumor origin and, more importantly, presence of metastases[135].

2.1 Imaging Viral Therapy

Therefore, several noninvasive imaging methods have been developed using 'reporter genes', including optical methods using fluorescence and bioluminescence, as well as deep tissue imaging modalities utilizing instrumentation such as positron-emission-tomography (PET) and single photon emission computer tomography (SPECT) alongside cellular transporters.

2.1.1 Optical Imaging.

Optical detection methods such as fluorescence and bioluminescence have the advantage of short acquisition times (for fluorescence imaging few milliseconds to several seconds, for bioluminescence a few seconds to several minutes) and high spatial resolution. The major disadvantage of optical imaging is the inability to perform deep tissue imaging due to

autofluorescence, light scattering and the opacity of tissues to light below 600 nm due to absorbance by hemoglobin. Nevertheless, optical imaging in small animals has been and still is a very important tool to follow the distribution of oncolytic vaccinia viruses equipped with genes for luciferases [81, 87, 89, 90, 92, 107, 108, 110, 130] or fluorescent proteins such as green fluorescent proteins (GFP)[43, 72, 73, 90, 92, 93, 96, 98, 110, 130]. Moreover, a GFP-encoding vaccinia virus strain (GLV-1h68) currently is in clinical phase I trials in which this fluorescent protein can be used to monitor the colonization of near-surface tumors and metastases[119, 136].

The discovery of new fluorescent proteins in the near infrared spectrum will probably result in the ability to detect oncolytic viruses in somewhat deeper tissues[137]. In addition, the indirect labelling using fluorescent compounds with emission in the near infrared that bind to or are activated by virus encoded proteins may also be developed.

2.1.2 Deep Tissue Imaging.

In contrast to optical imaging, deep tissue imaging modalities such as PET and SPECT (also referred to as gamma (γ) scinitgraphy) can be used for non-invasive deep tissue imaging utlizing radiotracers with differing properties.

2.1.2.1 Introduction to PET, SPECT, and PET-CT.

Radiotracer imaging technologies are able to measure the distribution of radiotracers in the human body[138]. They are widely available and have a wide range of clinical and research applications. Two classes of clinical nuclear imaging systems exist, those designed to image single gamma–emitting radionuclides such as 99m-Technecium Pertechtenate ($^{99m}TcO_4$) and Iodine-131 (^{131}I), and those designed to image positron-emitting radionuclides such as fluorine-18, carbon-11, and Iodine-124 (^{124}I). The single gamma-emitting imaging system is referred to as single photon imaging or, when performed tomographically, single photon emission computed tomography (SPECT). The positron-emitting imaging system is known as positron-emission tomography (PET). PET has greater spatial resolution, higher sensitivity and is easier to quantify than SPECT, and is why it was primarily chosen to test GLV-1h153's ability to facilitate deep tissue imaging.

The potential power of using PET reporter genes in animal research, together with technological innovations, has led to the development of dedicated animal PET scanners by

a number of research centers in the past 5 years, such as the microPET system[139]. The microPET scanner (Figure 2) has a reconstructed image resolution of 1.8 mm in all three axes and has been shown to be fully quantitative[140]. Further, the volumetric resolution is more than an order of magnitude better than state-of-the-art clinical PET systems[138].

Figure 2. Focus microPet 120. Dedicated small animal PET scanner, Concorde Microsystems Inc, Knoxville, TN.

The use of PET reporter genes can play critical roles in developing gene therapies by allowing researchers to determine the location, duration, and expression level of transgenes and, specifically, 1) develop vector modifications to improve delivery, 2) control expression levels, and 3) improve treatments to control duration of expression[138]. The repeatability, quantifiability, and high sensitivity of PET reporter gene systems may lead to rapid advancements in our understanding of oncolytic virotherapy.

PET is based on the following principle, reviewed by Chatziioannou AF[141]. A usually cyclotron produced isotope, such as ^{124}I, decays with the emission of a positron. This positron travels a small distance in tissue depending on both the tissue density and the kinetic energy of the emitted positron. After a series of collisions with atomic electrons from the tissues, during which the positron loses its energy and slows down, it annihilates with a nearby electron and produces two high-energy photons emitted in opposite directions. The simultaneous detection of these photons is the basis of PET imaging. For the most commonly used positron emitters, this average distance is on the order of 0.5 mm or less. At the point of annihilation, two photons with equal energy of 511 keV are emitted traveling at opposite directions conserving the total energy and momentum. These photons travel with the speed of light toward the detectors positioned around the subject, where they interact and are absorbed, producing an electrical signal. The detector signals are further processed by specialized coincidence circuitry and, if the difference in the time of arrival of these photons is smaller than a predetermined value (typically ~ 10 ns), the two detectors then

define a line of response. Stored events and data are subsequently fed into mathematical algorithms, which through a process called “image reconstruction”, create the spatial distribution of the concentration of the positron emitter in the field of view (FOV). Consequently, the concentration of the labeled molecule in tissues can be determined in absolute units of mCi/cc.

PET reporter genes encode receptors that bind positron-emitting ligand probes or enzymes that modify the positron-emitting substrate probes to produce sequestered positron-emitting products[138]. Cells expressing the PET reporter gene will sequester the radiolabel of the PET reporter probe 1) as a ligand bound to the PET reporter receptor or 2) as a “trapped” product of the enzymatic reaction of the PET reporter enzyme. Ideally, those cells not expressing the PET reporter genes will not retain the PET reporter probe. Since positron-emitting radionuclides result in the creation of high-energy gamma rays (511 keV) by positron–electron annihilation as discussed above, the animal is largely transparent to the wavelength of the radiation produced, and visualization of radiolabeled probe/ligand accumulation is readily obtained in even deep and visually opaque tissues. Emission computed tomography then allows quantitative imaging of the accumulation of the PET reporter probe and, in turn, the expression levels of the PET reporter gene. Since PET imaging does not require obtaining tissue samples from the subject, this system is noninvasive and can be used to repetitively measure reporter gene expression *in vivo*.

One of the most basic considerations is whether the reporter gene is endogenous or exogenous for the organism under scrutiny[138]. Endogenous genes have the advantage of not inducing an immune response thus allowing for repeated studies, however, a high background or erroneous signal due to its inherent expression may be a complication. Exogenous genes have the disadvantage of possibly inciting an immune response that might limit their repeated application. An ideal reporter gene for longitudinal studies should therefore produce no immune response and not be normally expressed in the organ under consideration.

It is also important to note that radionuclide-based methods offer significant advantages over optical-based approaches for imaging reporter gene expression[142, 143]. Radionuclide-based methods offer the highest level of sensitivity for imaging relatively low levels of reporter gene expression—as low as 10^{-12} mol/L of radiolabeled substrate[144]. This high degree of sensitivity may allow the use of relatively weak promoters and the imaging of relatively low levels of gene expression

2.2 Oncolytic Viruses and Deep Tissue Reporter Genes

Advantages of using replication-selective oncolytic viruses for transgene delivery are several[145]. In addition to their oncolytic capabilities, replicating viruses can deliver therapeutic transgenes to image and enhance the probability of tumor eradication through multiple avenues. Replication-selective viral systems can employ endogenous viral gene expression control signals (promoter/enhancer, polyadenylation, and splice signals) for transgene expression. Eliminating the need for exogenous promoters often needed in replication deficient systems and polyadenylation signals is an economical use of the often limited transgene capacity afforded a replicating viral agent. Using endogenous viral promoters may also allow more predictable and controlled transgene expression. Further, in contrast to foreign or exogenous promoters, the promoters of the replicating agent are optimized for expression in the infected cell.

Viral gene expression during the lytic phase of the viral life cycle of vaccinia virus is highly regulated and, as discussed in chapter 1, can be broadly classified into three serially activated phases: immediate-early (IE), early (E), and late (L)[55]. Based on the expression of endogenous viral genes, it may be possible to predict the expression kinetics (timing and expression levels) of the transgene(s) carried by the replicating agent. Furthermore, when multiple transgenes are inserted into a single virus, their expression may be orchestrated to occur simultaneously or serially, at levels that will maximize their therapeutic benefit. Expressing transgenes serially at different times in the viral lytic cycle is of greatest value early in treatment when the infection may be more synchronized. As a viral infection spreads and encounters a heterogeneous tumor cell mass, it will likely become asynchronous, although the relative expression of different transgenes may still be maintained.

Consequently, novel oncolytic vaccinia virus strains have been generated that express proteins, such as thymidine kinase (TK), the human serotonin receptor (hSSTR2) or the human norepinephrin transporter hNET, which selectively bind radiotracers and therefore should also be detectable in deep tissues of humans[86, 120]. These viruses will not necessarily be used as diagnostic tools, but the possibility to track virus-mediated gene expression will help to monitor therapeutic effects, such as control of successful tumor colonization, and may help to predict therapeutic effects and potential toxicity. The latter may be significantly helpful, as time is needed for oncolytic viruses to regress tumor volume and thus will aid in identifying non- or poor-responders for additional therapies.

2.2.1 Thymidine Kinase (TK).

Thymidine Kinase (TK) has been used for years in cell culture and animal studies to assess cell proliferation. One approach has been use of radiolabeled thymidine or thymidine analogues, which are rapidly incorporated into newly synthesized DNA[146]. Herpes simplex virus 1 derived TK (HSV1-TK) has relaxed substrate specificity and so phosphorylates thymidine analogues (e.g., 5-iodo-29-fluoro-29deoxy-1-b-D-arabino-furanosyl-uracil [FIAU]) as well as acycloguanosine analogues such as acyclovir, ganciclovir (GCV), and penciclovir (PCV)[147]. Cellular enzymes then convert acycloguanosine monophosphates and the monophosphate of FIAU to di- and triphosphates, which have been shown to kill cells by incorporation as chain-terminating derivatives and/or by inhibition of DNA polymerase[148]. The study by Fong and colleagues was the first to show the successful dose- and time-dependent monitoring of oncolytic HSV-1 replication in colorectal xenografts[149].

However, thymidine analogue tracers are investigational drugs and add a level of regulatory complexity that has prevented their clinical usage. Furthermore, the non-human origin of HSV1-TK also raises concerns over their potential immunogenicity[138].

2.2.2 Human Somatostatin Receptor 2 (hSSRT2).

Other groups have attempted the insertion of the human somatostatin receptor type 2 (SSTR2) into oncolytic vaccinia viruses for non-invasive imaging. The SSTR2 is targeted by the high-affinity synthetic peptide pentetreotide, which is commonly used for receptor imaging after being radiolabeled with indium-111[150]. This receptor is normally expressed in human kidney cells and neuroendocrine tumors and gene therapy approaches to deliver the SSTR2 to tumors has also been attempted using adenoviral vectors [150, 151].

McCart *et al*. infected cells with an SSTR2-expressing VACV or controls, and incubated them with the somatostatin analog ^{111}In-pentetreotide with or without an excess of nonradiolabeled pentetreotide. The SSTR2-infected cells bound ^{111}In-pentetreotide sixfold more efficiently than control virus-infected cells and this binding was specifically blocked by nonradiolabeled pentetreotide. Further, nude mice bearing subcutaneous murine colon CA xenografts were injected intraperitoneally with the SSTR2-expressing VACV or control VACV and imaged 6 days later with ^{111}In-pentetreotide-mediated SPECT. Tumors infected with the

SSTR2-expressing VACV accumulated higher concentrations of radioactivity compared to tumors in animals receiving the control virus. Further, SSTR2-infected tumors were visible on imaging 6 days after VACV injection and could be visualized for up to 3 weeks post viral injection using repeat radiotracer injections[120].

More recently, it was shown that the same VACV encoding the gene for SSTR2 combined with the radiotherapeutic ^{111}In-DOTATOC was more effective than either alone at decreasing the growth rate of human embryonic kidney HEK-293 cells or colorectal MC-38 cells in monolayer[152]. However, ^{111}In- or 177Lu-DOTATOC combined with parental VACV provided equivalent growth inhibition of HEK-293 or MC-38 cells as spheroids, suggesting a bystander effect from ^{111}In-DOTATOC.

Nevertheless, radiotracers for SSRT2 require prior radiolabelling for accumulation of radioprobes. Further, most radiotracers used with this SSRT2 are able to be imaged with SPECT, and it is only recently that newer radioprobes are being developed for higher resolution PET imaging[153, 154]. Furthermore, unlike transporters such as the human norepinephrin transporter (hNET) and the human sodium iodide symporter (hNIS), SSTR2 is a receptor which usually has a 1:1 binding relationship with radiolabeled ligands and is therefore not capable of providing significant amplification through transport-mediated *concentrative* intracellular accumulation of substrate. It is therefore not surprising that accumulation of radiotracer was only at around 1.5% ID/gm tissue even 6 days post injection of the SSTR2 encoding VACV discussed above[120].

2.2.3 Human Norepinephrin Transporter (hNET).

Another deep tissue reporter gene investigated in oncolytic viral strains is the human norepinephrin transporter (hNET). hNET is a cell surface human protein belonging to a family of Na+/Cl-dependent transporters that contain multiple transmembrane domains, mediating the transport of norepinephrine, dopamine, and epinephrine across the cell membrane. It can be imaged by SPECT or PET using the radiotracer meta-iodobenzylguanidine (MIBG)[155, 156]. The use of the hNET-MIBG reporter imaging is attractive since it is of human origin and will unlikely induce an immune response, as well as its limited expression in the central and peripheral sympathetic nervous systems[157]. Moreover, MIBG is a standard radiopharmaceutical approved by the U.S. Food and Drug Administration.

Previously, attempts to image gene transfer therapy by PET using hNET-MIBG reporter imaging were successful in transduced cells and xenografts[155]. The feasibility of using hNET for imaging has also been demonstrated in adenoviral vectors[158].

Chen *et al*. was the first to report on an oncolytic vaccinia virus carrying hNET, GLV-1h99[86]. Like GLV-1h153, this virus is also a derivative of VACV GLV-1h68. The hNET protein was expressed at high levels on the membranes of cells infected with GLV-1h99, and expression of the hNET protein did not negatively affect virus replication in cell culture or *in vivo* virotherapeutic efficacy. GLV-1h99-mediated expression of the hNET protein in infected cells resulted in specific uptake of the radiotracer [^{131}I]-MIBG. In mice, GLV-1h99-infected pancreatic tumors were readily imaged by [^{124}I]-MIBG-PET. This virus was further investigated by Brader *et al*. for the imaging of an orthotopic mouse model of human malignant mesothelioma using both ^{123}I-MIBG mediated SPECT imaging and ^{124}I-MIBG mediated PET imaging[159].

A limitation of the hNET symporter is MIBG's requirement for radiotracer labeling. The question then remained: is there a potential deep tissue imaging reporter gene of human origin, which facilitates concentrative intracellular uptake of carrier free radioprobes, able to be imaged by high resolution PET imaging? This led to the interest in the human sodium iodide symporter (hNIS).

2.3 The Human Sodium iodide Symporter (*hNIS*) Reporter Gene

Limitations of available reporter genes prompted the testing and discovery of other novel reporter genes that may overcome them. This lead to the consideration of the human sodium iodide symporter (*hNIS*), an intrinsic plasma membrane protein which mediates the active transport and concentration of iodide in the thyroid gland cells and some extra thyroidal tissues, in particular, the lactating mammary gland, as well as in the stomach, salivary glands, skin, brain, spleen, small intestine, ovaries, prostate, and testes[160].

2.3.1 Biology, Physiology, and Tissue Distribution.

In 1896, Baumann was the first to discover that the thyroid gland concentrates iodide by a factor of 20–40 times with respect to plasma under physiological conditions[161]. Discovery

and cloning of the rat *NIS* by Carrasco and colleagues[162] and of the human NIS by Jhiang and colleagues[163] mediating this uptake opened an exciting and extensive new field of research, including exploring the pathophysiological implications of *NIS* in thyroid disease, the therapeutic potential of the gene, and its imaging and diagnostic potential.

hNIS is a glycoprotein with a currently proposed secondary structure of 13 transmembrane domains and an estimated molecular mass of around 70–90 KiloDalton (kDa) depending on the status of glycosylation (Figure 2)[164-167]. Glycosylation is not necessary for the function of NIS, its stability, or its targeting[168]. It is located on chromosome 19p13 – 13·2, and is composed of 643 amino acids, an extracellular amino-terminus, and an intracellular carboxyl-terminus. The coding region has 15 exons interrupted by 14 introns, and codes for a 3.9 kb mRNA. The symporter belongs to the sodium/solute symporter family (SSF, TC No. 2.A.21 (according to the Transporter Classification system)) or solute carrier family 5 (SCL5A, according to the Online Mendelian Inheritance in Man (OMIM) classification, www.ncbi.nlm. nih.gov/Omim/). This family includes more than 60 members of both prokaryotic and eukaryotic origin, many of which exhibit a high degree of similarity of sequence and function[166].

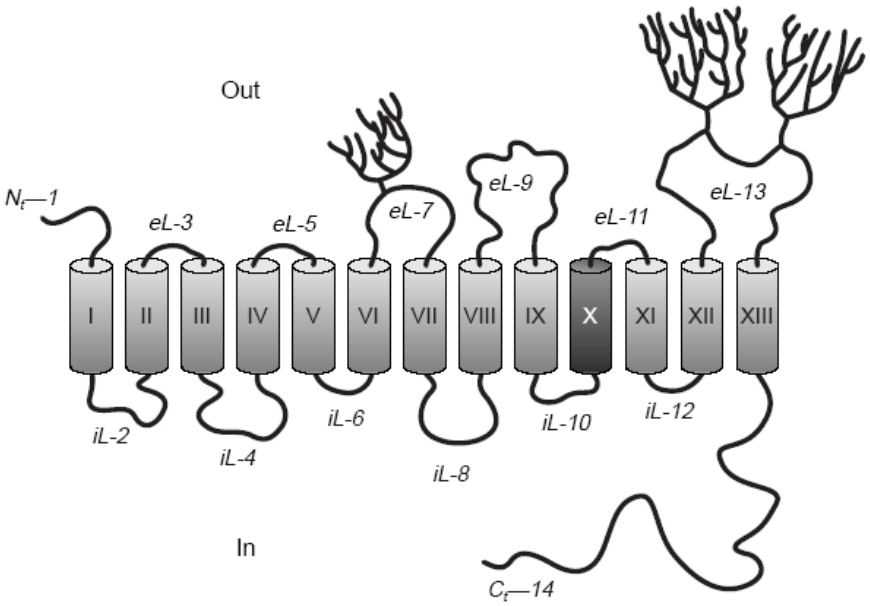

Figure 3. Proposed structure of the human sodium iodide symporter. hNIS has 13 transmembrane domains, an intracellular C terminus, and an extracellular N terminus. All three N-linked glycosylation consensus sequences are indicated: positions 225 (eL-7), 485 and 497 (eL-13). Amino acid residues 389–410 form a transmembrane segment X. Abbreviations: Ct, C terminus; eL, extracellular loop; iL, intracellular loop; Nt, N-terminus. *De La Vieja et al. Molecular analysis of the sodium/iodide symporter: Impact on thyroid and extrathyroid pathophysiology. 2000.*

Transcriptional activity of thyroidal NIS is primarily regulated by thyroid stimulating hormone (TSH), via the cyclic adenosine monophosphate (cAMP) pathway[169]. Multiple cAMP pathways, both protein kinase A (PKA)-dependent and -independent, may be involved in the regulation of NIS expression and function. The phosphatidyl-inositol 3-kinase (PI3-K) and TGF-β/Smad pathways have been shown to have an inhibitory effect on NIS transcription[170, 171].

Levy *et al*. [172] studied the biogenesis and post-transcriptional regulation of NIS. They showed that NIS is initially synthesized as a precursor protein that is immediately core glycosylated in the endoplasmic reticulum[168]. Further studies have shown that the precursor protein is a 56 kDa polypeptide whose maturation into full length 87 kDa polypeptide is first observed at about 1 hour and is completed at 3 hours after initial TSH stimulation[173]. Interestingly, NIS protein has an unusually long half-life and remains detectable 10 days after TSH deprivation. For active iodide transport to occur, NIS must be expressed, targeted and retained in the appropriate plasma membrane surface in polarized epithelial thyroid cells[174].

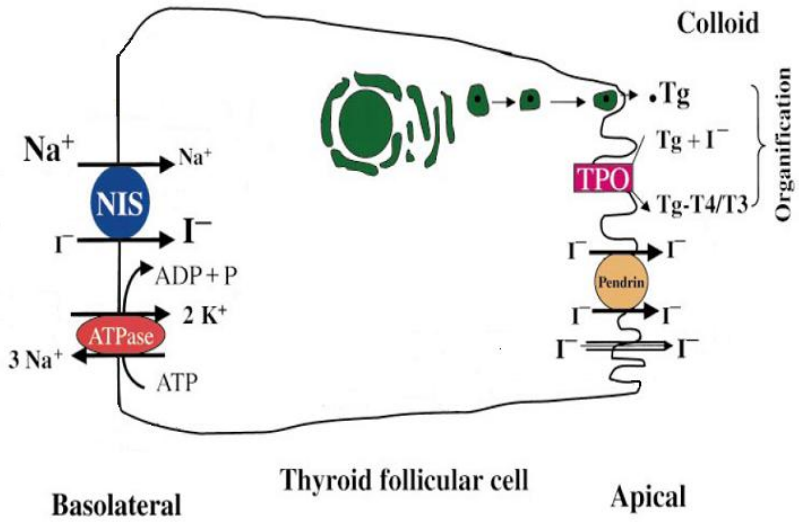

Figure 4. hNIS physiology in the thyroid. hNIS on the basolateral cell membrane of thyroid follicular cells cotransporting two sodium ions and one iodide ion into the cell, driven by a sodium gradient maintained by sodium-potassium adenosine triphosphatase (ATPase) providing energy for this transfer. Once iodide enters cell, it is transported across the apical membrane into the follicular lumen by other anion transporters including pendrin. In the follicular lumen, iodide is attached through the action of thyroid peroxidase (TPO) to tyrosyl residues along the thyroglobulin (Tg) backbone. Thyroid hormones triiodothyronine (T3) and thyroxine (T4) are synthesized by the coupling of two iodotyrosine residues and are then stored within the colloid. When thyroid hormone is needed, Tg enters the thyroid follicular cell, and thyroid hormone is released into the bloodstream. Modified from *Spitzweg et al. The sodium iodide symporter: its pathophysiological and therapeutic implications. 2002*

Once the hNIS is inserted on the basolateral cell membrane of thyroid follicular cells, it cotransports two sodium ions and one iodide ion into the cell, driven by a sodium gradient, which provides energy for this transfer and is maintained by an oubain sensitive sodium-potassium adenosine triphosphatase (ATPase) (Figure 4)[175, 176]. When iodide enters the thyroid cell, it is transported across the apical membrane into the follicular lumen by other anion transporters including pendrin, which is a chloride-iodide transporter. In the follicular lumen, iodide is attached covalently to tyrosyl residues along the thyroglobulin (Tg) backbone through the action of thyroid peroxidase (TPO). Thyroid hormones triiodothyronine (T3) and thyroxine (T4) are synthesized by the coupling of two iodotyrosine residues and are then stored within the colloid. When thyroid hormone is needed, Tg enters the thyroid follicular cell, and thyroid hormone is released into the bloodstream.

Although endogenous *NIS* is physiologically and functionally expressed in several normal tissues, so far only 2 cancers have been shown to express endogenous *NIS* functionally making them amenable to radiotherapy, those 2 being thyroid cancers (mainly papillary and follicular), and around 80% of human breast cancers including ductal carcinomas[177]. Furthermore, some thyroid tumors such as medullary and anaplastic cancers have been shown to lose *hNIS* expression making them non-amenable to radiotherapy, and some papillary cancers have even been shown to de-differentiate, also losing functional *hNIS* expression[178].

2.3.2 Imaging Potential.

hNIS gene transfer via viral vector may allow infected tumor cells to concentrate several easily attainable, commercially available, and relatively inexpensive, carrier free radioisotopes such as ^{123}I, ^{124}I, ^{125}I, ^{131}I, $^{99m}TcO_4$, rhenium, and astatine for non-invasive imaging of *NIS* expression, all of which have long been approved for human use. In contrast to the study published by McCart *et al*.[120, 152] using the VACV-expressing SSTR2, hNIS is a transporter-based reporter gene system. Whereas receptors usually have a 1:1 binding relationship with a radiolabeled ligand, transporters provide signal amplification through transport-mediated concentrative intracellular accumulation of substrate. hNIS use has also been shown to be comparable to the commonly used *HSV1-tk* reporter gene[179] and correlated with $^{99m}TcO_4$[180]. This can be very useful for viral distribution with scintigraphy or PET scanning during and after viral therapy, and may allow for correlation with efficacy and

toxicity during clinical trials, thus offering potential clinical translation of this dual therapy. Furthermore, the human origin of *hNIS* likely renders it less immunogenic than other foreign reporter genes such as *TK*.

2.3.3 Therapeutic Potential With hNIS.

In addition, although self-replicating virotherapy has shown great promise for treating cancer, the additive or synergistic effects by combining targeted therapeutic systemic radiotherapy such as ^{131}I with oncolytic virus-mediated hNIS transfer may eliminate tumors and virus-resistant tumors. Oncolytic viruses have been found to have a synergistic antitumor effect when combined with ionizing radiation[181-183]. One mechanism for such synergy appears to be radiation-induced upregulation of certain cellular DNA repair genes that result in promoting viral replication[79, 184].

Furthermore, a bystander effect may be possible as ^{131}I undergoes β-particle decay with a path length of 0.2–2.4 mm[185]. It is important to note that ^{131}I is already approved in patients for multiple ailments including thyroid cancers and palliation of bone metastasis, and was found to be safe with relatively few side effects[186]. In addition, ^{131}I is not a gene therapy and thus involves less risk and complications as compared to gene therapy of cancer.

If additive or synergistic effect is found, patients may be more safely treated with combinations of lower doses of virus and radioiodine. Application of carrier-free radioiodine would thus be extended, and the extensive experience with radioiodine in thyroid cancer management will undoubtedly be helpful in the treatment of other *NIS*-transfected tumors.

2.3.3.1 Dosimetry and Targeted Radiotherapy.

Radiation dosimetry determines the amount as well as the spatial and temporal distribution of energy deposited in matter by ionizing radiation. Internal targeted radionuclide radiation dosimetry specifically deals with the deposition of radiation energy in tissue due to a radionuclide within the body[187]. However, unlike external radiation (XRT) dose which can often be measured, internal radiation dose must be calculated. By incorporation of appropriate radionuclides in appropriately large amounts into target tissue-avid radiopharmaceuticals, a sufficiently high radiation dose may be delivered to produce a

therapeutic response in tumor or other tissue. With higher administered activities and resulting higher normal-tissue doses, however, serious radiation injury can occur.

The main differences between targeted radiotherapy and XRT are caused by dosimetry, with dose-rate effects a secondary factor[188]. In XRT, a target volume is defined, and overlapping radiation fields are arranged to treat this volume as evenly as possible. For targeted radiotherapy, the absorbed radiation dose is due to the flux of ionizing particles produced by radionuclides distributed within or around the tumor. The distribution of radionuclide depends on the biologic properties of the tumor. Factors such as the affinity of targeting molecules for the tumor cells and the extent and permeability of the tumor vasculature determine the intratumoral distribution of targeting molecules. The main theoretic advantage of targeted radionuclide therapy is that radiation can be delivered selectively to subclinical tumors and metastases that are too small to be imaged and thereby treated by surgical excision or local XRT. In addition, the absorbed doses to tumors achieved by targeting may be higher than can be delivered by systemic XRT. For any radiation-based therapy, the likelihood of tumor cure depends on three factors[188]: (1) the radiation dose absorbed in the tumor and its pattern of delivery; (2) the number of clonogenic tumor cells present. These all have to be destroyed to cure the tumor; and (3) the response of the tumor cells to radiation including their radiosensitivity, repair capacity and proliferation rate.

Radiopharmaceuticals may be structurally simple, such as ions, to complex, such as antibodies, consisting of or labeled with a radionuclide. They may be in solution or in the form of a colloid or suspension and may be administered systemically or regionally. Historically, radioiodine therapy of thyroid disease including hyperthyroidism and localized and metastatic thyroid cancer, has been the most active and successful area of radionuclide therapy. Although radioiodine therapy of thyroid disease remains the most widely used form of radionuclide therapy, there are a number of newer and/or less frequently applied radionuclide therapies including radioimmunotherapy; radiolabeled peptide octreotide or -octreotate therapy of carcinoid and other tumors over-expressing cell-surface receptors (*eg* somatostatin receptors); and palliative radionuclide therapy of bone pain secondary to skeletal metastases using radiopharmaceuticals such as rhenium-186 (^{186}Re)- or rhenium-188 (^{188}Re)[189-191].

The physical characteristics of these radionuclides impose a further level of variability with targeted radiotherapy[188, 192]. The energy spectrum of the ionizing particles determines the range of the energy emission, and the distribution of radiation dose throughout a tumor depends on tumor size, the radionuclide in use and its intratumoral distribution. This complex

situation results in a heterogeneous distribution of radiation dose, which is relatively high in some intratumoral regions, and reduced in others. Even in the case of a uniform distribution of radionuclide throughout a tumor volume, when the tumor is large in comparison to the range of the ionizing particles, most of the energy is absorbed within the tumor. When tumor dimensions are smaller than the range, a large proportion of the energy may escape. In practice, besides the dosimetric considerations, the selection of a therapeutic radionuclide depends on the availability and cost of the radionuclide and the chemical preparation and stability, particularly *in vivo*, of the radiopharmaceutical.

In a seminal paper by O'Donoghue and colleagues, the choice of how radionuclide therapy influences the relationship between tumor curability and tumor size was examined[188]. They used a mathematical model to examine tumor curability and its relationship to tumor size for twenty-two β-emitting radionuclides that may have therapeutic potential including ^{131}I. The model assumed a uniform distribution of radionuclide throughout. They found that for targeted radionuclide therapy, the relationship between tumor curability and tumor size is different from that for conventional XRT. With targeted radionuclides, there is an optimal tumor size for cure. Tumors smaller than the optimal size are less vulnerable to irradiation from radionuclides as a substantial proportion of the disintegration energy escapes and is deposited outside the tumor volume. The optimal cure size range for ^{131}I was calculated at (2.6 - 5.0mm). This may pose an issue for treating micrometastatic disease due to the relatively long path length of the β-particle. Further, they conclude that the energy emitted per disintegration may also be used to predict optimal cure size for uniform distributions of radionuclide.

In systemic therapy, a therapeutic radionuclide is administered either enterally or parenterally (typically IVly) and is thus distributed throughout the body via circulatory, secretory, metabolic, and/or excretory processes[187]. In regional therapy, the therapeutic radionuclide is introduced directly into a specific space or region of the body and is thus mechanically deposited into or on the target region which increases the specificity of dose delivery and the therapeutic index is maximized. Although this is the ideal situation for tumor therapy, this may miss regions of micrometastasis, and is technically more challenging. This thesis concentrates on the systemic therapy of pancreatic tumor xenografts in nude mice.

Serial measurements of activities in normal organs, tumor, and total body can be performed by planar gamma camera imaging, SPECT, or positron emission tomography PET[193, 194]. Three-dimensional imaging modalities such as SPECT and PET provide more accurate estimates of activities *in situ* by eliminating the confounding effect of counts from activity in

source regions surrounding the structure of interest[195, 196]. Moreover, with the introduction of SPECT-CT[197-199] and PET-CT[200-202] devices, activity distributions can be accurately correlated with anatomy, and tumor and normal-organ masses can be measured in conjunction with activity measurements. To determine these activities, regions-of interest (ROIs) may be drawn around areas of uptake of organs and/or tumors to determine their respective activities, usually expressed as the percentage injected dose per gram tissue (%ID/gm). A simplified approach to calculation of tumor and total-body %ID/gm tissue for the purposes of this thesis is explained in the methods sections of this thesis.

Although advances have been made in quantitative SPECT[203], conventional SPECT remains relatively insensitive and slow, requiring a 20- to-40-minute acquisition per bed position. Further, propagation of statistical uncertainty in the image reconstruction process degrades the precision of SPECT-based activity measurements. PET, on the other hand, offers better spatial resolution, higher sensitivity, and generally more accurate and precise activity quantitation than SPECT[204] and quantitative whole-body PET scans can be completed in 30 minutes or less. However, as discussed, a limitation of dosimetry calculation is the non-uniform dose distributions. Scintigraphic imaging modalities such as planar gamma camera imaging, SPECT, and even PET), often do not have sufficient spatial resolution to discern the heterogeneity of intra-organ and intra-tumor activity distributions[205], and normal tissue toxicity and tumor therapeutic response may not correlate with average as also demonstrated by O'Donoghue and colleagues[192]. Thus, in addition to patient-specific dosimetry, the issue of spatial non-uniformity of dose at both the macroscopic[205-230] and microscopic[231-251] levels has become an important consideration.

2.4 Preclinical Data

In order to take advantage of the therapeutic and imaging potential of *hNIS*, several groups have attempted exogenous *NIS* gene transfer in several human cancers in cell culture and in rat and mice models. These cancers include head and neck squamous cell cancers, non-small cell lung, thyroid, liver, colorectal, and prostate cancer, as well as glioma and multiple myeloma. Various gene transfer methods have been used, including direct transfer, as well as the use of replication-deficient and replication-competent viral vectors. However, these experiments have had ranging levels of success.

2.4.1 Stable and Vector-Medicated hNIS Transfections.

Several groups have attempted exogenous transfer of hNIS with the aid of electroporation, retroviruses, and replication-deficient adenoviral and baculoviral vectors with varying levels of success[166, 252, 253]. Examples of selective promoters used to drive hNIS expression include CEA[254], hTERT[255], survivin[256], and MDR1[257]. However, several studies report of the rapid efflux of iodide from NIS-transfected cells, including anaplastic thyroid and lung cancer cells, with no therapeutic effect seen[258, 259]. To circumvent this problem, Boland *et al*. constructed a recombinant adenovirus encoding the human thyroperoxidase (TPO) gene under the control of the cytomegalovirus early promoter (AdTPO). Infection of non-thyroid tumor cells with this virus led to production of an enzymatically active protein, and a significant increase in iodide organification could be observed in cells co-infected with both Ad*NIS* and AdTPO in the presence of exogenous hydrogen peroxide. However, the levels of iodide organification obtained were too low to significantly increase the iodide retention time in the target cell[260].

On the other hand, other studies have shown that *NIS* gene delivery into non-thyroidal, non-organifying tumor cells are capable of inducing accumulation of therapeutically effective radioiodine doses, and this was indeed the case in several tumor models. For example, a single therapeutic ^{131}I dose of 3 mCi was shown to elicit a dramatic therapeutic response using adenovirus-mediated *NIS* transfer into prostate cell xenografts with an average volume reduction of more than 90%[261]. Further, an Adenoviral vector expressing hNIS regulated by MUC1 promoter (Ad-MUC1-NIS) caused a more than 15-fold increase in iodide uptake in infected pancreatic cancer cells *in vivo* with ^{123}I scintigraphy and an *in vivo* therapeutic effect with 3mci of ^{131}I of >75% reduction in volume of NIS transduced tumors[262].

2.4.2 Oncolytic Viruses and hNIS for Imaging and Therapy.

The oncolytic viruses that have been investigated so far in relation to *hNIS* are adenoviruses, measles virus, and vesicular stomatitis virus. To date, however, no one has investigated the potential of an oncolytic vaccinia virus vector. A summary of the following section is presented in Table 3.

2.4.2.1 Adenovirus.

Adenoviruses have shown some success in preclinical trials, however their efficacy in phase I trials is often limited by their replication capacity and ability to spread within tumors, and there are few examples of complete tumor eradication.

Therefore, several groups have attempted NIS transfer to cells via oncolytic adenoviral vectors to improve adenoviral treatment efficacy. Merron *et al*. were the first to insert the hNIS reporter gene in a wild type replicating oncolytic adenovirus (AdlP1) and in an adenovirus in which a promoter from the human telomerase gene (RNA component) drives E1 expression (AdAM6). The virus induced functional hNIS expression and replication in cell culture and kinetics of spread of the different viruses in colorectal tumor xenografts were visualized *in vivo* after IT injection of 10^9 PFU of virus using $^{99m}TcO_4$-mediate SPECT. The time required to reach maximal spread was 48 h for AdIP1 and 72 h for AdAM6 suggesting that *hNIS* gene insertion in adenoviruses hindered spread in tumors. Maximum radiouptake was 4 days post virus injection, suggesting a delay in peak viral replication and hNIS expression. However, no significant signal could be reached by day 5 after IT adenovirus injection [263].

To further improve adenoviral selectivity, Trujillo *et al*. constructed of a MUC-1 promoter driven, conditionally replicating adenovirus that expresses the NIS (Ad5AMUCH_RSV-*NIS*) for gene therapy of breast cancer[264]. In cell culture infection of the MUC-1 positive breast cell line T47D resulted in virus replication, cytolysis, and release of infective viral particles. Conversely, the MUC-1 negative breast cancer cell line MDA-MB-231 did not support viral replication. *In vivo*, mice were maintained on a low-iodine diet and received T4 supplementation to maximize iodide uptake by tumors while reducing thyroid gland and stomach uptake. T47 xenografts were readily imaged using ^{123}I and γ-camera 2 days after IT injection of 1 x 10^{11} of the hNIS-encoding virus with almost 30% uptake 1 hour after radiotracer administration.

Hakkarainen *et al*. created the adenovirus Ad5/3-Δ24-*hNIS*, a Rb-p16 pathway selective infectivity enhanced oncolytic adenovirus encoding hNIS. Ad5/3-Δ24-*hNIS* replication effectively killed prostate cancer cells in cell culture and *in vivo*[265]. After 2 consecutive injections of $2x10^8$ virus particles ITly, PC-3MM2 tumors retained around 6% of the injected dose visualized via ^{123}I-mediated γ-scintigraphy, and interestingly this uptake plateaued until around 13 hours post radiotracer administration showing significant retention. Furthermore,

Ad5/3-Δ24-*hNIS* with radioiodide was significantly more effective than virus alone in mice with prostate cancer xenografts.

Peerlinck *et al*. generated the adenovirus AdIP2 encoding hNIS and capable of selective replication in colorectal carcinoma cells[266]. The selectivity of this virus was verified in cell culture and *in vivo*. Its spread in tumors was monitored *in vivo* using SPECT/CT imaging upon $^{99m}Tc_{O4}$- injection and confirmed by immunohistochemistry. Like AdIP1, replication of AdIP2 seemed to be affected by *hNIS* gene insertion as compared to wild type. Imaging and immunohistochemical data showed limited viral spread with maximal hNIS expression 48 hours after injection of 10^9 PFU. Administration of a single therapeutic dose of ^{131}I at this time point led to a dramatic reduction in tumor size not observed in *hNIS*-negative viruses.

Next, Merron *et al*. investigated the potential of hNIS to affect the therapeutic efficacy of parental adenovirus dl922-947 following intraperitoneal (IP) administration, in a mouse model of peritoneal ovarian carcinoma. In cell culture infection of ovarian carcinoma IGROV-1 cells with ADAM7 led to functional expression of NIS. However, the insertion of *NIS* into the viral genome resulted in a loss of efficacy of the virus in terms of replication and cytotoxicity. *In vivo*, imaging of IP ovarian xenografts infected with a single IP dose of 10^{10} PFU via $^{99m}TcO_4$-SPECT/CT was only detectable in the peritoneal cavity of animals bearing peritoneal ovarian tumors for up to 5 days after IP administration. The study interestingly demonstrated that despite the detrimental effect observed in cell culture, insertion of the reporter gene NIS in an oncolytic adenovirus did not affect its therapeutic efficacy *in vivo*[267].

Further, Trujillo *et al*. constructed another conditionally replicating adenovirus in which the E1a gene is driven by the prostate-specific promoter, Probasin Ad5PB_RSV-*NIS*[268]. In cell culture, infection of the prostate cancer cell line LnCaP resulted in virus replication, cytolysis and release of infective viral particles. Conversely, the prostate cancer cell line PC-3 (androgen receptor negative) and the pancreatic cancer cell line PANC-1 did not support viral replication. Radioiodine uptake was readily measurable in infected LnCaP cells infected with Ad5PB_ RSV-*NIS* 24 h post-infection, confirming NIS expression. *In vivo*, LnCaP tumor xenografts in nude-mice injected ITly with 10^{11} PFU of virus expressed NIS actively as evidenced by $^{99m}TcO_4$-SPECT, with signal sustained up to one month after viral therapy. Maximum uptake was 12% ID/gm 1 day post virus administration Moreover, administration of therapeutic ^{131}I after virus injection significantly increased survival of mice carrying xenografted LnCaP tumors compared with virotherapy alone.

Promise in these preclinical trials lead to plans for a phase I gene therapy trial in patients with prostate cancer utilizing the Ad5-yCD/*mut*TKSR39*rep-hNIS* adenovirus [269]. To aid in these plans, the dosimetric characteristics of the reporter gene system when coupled with IV administration of radioactive $^{99m}Tc_{O4}$ and was determined in a large animal tumor. The virus was injected into the prostate gland of dogs for dosimetry purposes, and into a canine soft tissue sarcoma for imaging purposes. Using the highest value observed, absorbed radiation dose to critical organs was calculated and found to be below U.S. Food and Drug Administration limits for diagnostic imaging. Also, $^{99m}TcO_4$ uptake was readily detected by SPECT and found to persist *in vivo* for at least 4 days. On the basis of dosimetry calculations, the authors concluded that up to five imaging procedures can be safely performed in humans after intraprostatic injection of the Ad5-yCD/*mut*TKSR39*rep-hNIS* adenovirus, and the *hNIS* reporter gene system can be used to study the dynamics of adenoviral gene therapy vectors in large animal tumors.

2.4.2.2 Measles virus.

Several groups have also attempted hNIS transfer via oncolytic measles vectors. Dingli *et al*. were the first to show the imaging and therapy potential of hNIS in an oncolytic measles vector[270]. They demonstrated noninvasively by ^{123}I- γ-scintigraphy the IT spread of measles virus encoding for *hNIS* (MV-*NIS*) in various multiple myeloma xenografts after IT injection of 2 $x10^6$ TCID50. Tumors retained up to 12% to 17% of the injected dose, and showed iodine retention up to 24 hours after xenografts. Further, KAS-6/1 xenografts regressed completely after a single IV dose of MV-*NIS* and ^{131}I.

However, due the unfavorable replication kinetics of measles viruses expressing both CEA and NIS, Hasegawa *et al*. tested MV-*NIS* in combination with another viral construct, MV-*CEA*, to treat ovarian cancer SKOV3ip.1 xenografts[271]. MV-*NIS* propagation was again mapped by serial radioiodine imaging via gamma scanner by systemic injection of $^{99m}TcO_4$. In cell culture studies showed superior replication kinetics of MV-*NIS* relative to MV-*CEA*. However, γ-scintigraphy was considerably less sensitive than the plasma *CEA* marker for monitoring virus infection. Further, Liu *et al*. demonstrated that antitumor activity of MV-*NIS* was evident only in measles naive mice-bearing disseminated myeloma, and not in passively immunized mice which may limit clinical application of this virus[272].

MV-NIS was also shown to be effective with prostate cancer cells for imaging. Infected cells concentrated radioiodide isotopes in cell culture by ^{125}I uptake assays. Virus localization and

spread *in vivo* could again be followed by γ-scintigraphy of ^{123}I uptake. After injection of 1.5 x 10^6 $TCID_{50}$ IT or IV, peak tumor uptake was observed on day 4 in IT- and on day 14 in IV-treated animals with a maximum uptake of around 13% and 14%, respectively. Absorbed dose of radiodiodine in the tumor was calculated at an average of 420 or 540 rads/mci when MV-*NIS* was administered IT or IV, respectively, at the time of maximum observed uptake. Combination therapy with ^{131}I further enhanced the antitumor effect of MV-*NIS* virotherapy [273].

Blechacz *et al*. investigated *MV-NIS's* oncolytic potential and efficiency in tracking viruses in animal models of hepatocellular carcinoma. Quantitative analysis of IT iodine uptake via γ-scintigraphy showed a median IT ^{123}I uptake of 8.41% on day 3 and 9.13% on day 10 in Hep3B xenografts with a single IV dose of 2x10^6 $TCID_{50}$ of MV-*NIS*[274].

MV-NIS was further evaluated in pancreatic cancer xenografts[275]. After injection of 3.5 x 10^6 TCID50 of virus directly into BxPC-3 tumors, the maximum average % ID/gm was quantitated using ^{123}I-SPECT of tissue and found to be 11.4% on day 2, decreasing thereafter at 8.4% on day 3, and 6. 4% on day 5 with wide ranges of uptakes noted. Uptakes continued to decrease thereafter. Mice were also maintained on a low-iodine diet and received T4 supplementation to maximize iodide uptake by NIS-positive tumors. A significant therapeutic effect with virus alone was also seen, and effects of combination therapy in this tumor model was then explored[276]. Dosimetric calculations estimated an absorbed intratumoral dose of 1008 rads after IT injection of 3.5 x 10^6 TCID50. Synergy between MV-*NIS*-induced oncolysis and *NIS*-mediated ^{131}I ablation was not seen; however, a significant correlation was observed between *NIS*-mediated IT iodide localization and peak tumor volume reduction with combination MV-*NIS* and ^{131}I therapy. They concluded that this lack of synergy in this model was not due to a lack of radiosensitivity, but rather to a nonuniform IT distribution of MV-*NIS* infection

Due to the large body of promising data with MV-*NIS*, preparations for clinical trials then ensued. Preclinical pharmacology and toxicology studies were conducted in support of the clinical protocol for the phase I trial of systemic administration of MV-*NIS* with or without cyclophosphamide in patients with recurrent or refractory multiple myeloma[277]. On the basis of this data, the safe starting dose of MV-*NIS* for the clinical protocol was set at 10^6 TCID50 per patient. Results of this trial are still pending.

2.4.2.3 Vesicular Stomatitis Virus (VSV).

In mice with established subcutaneous 5TGM1 myeloma tumors, virus replication and spread of a vesicular stomatitis virus, VSV (51)-*NIS*, was also monitored noninvasively by serial gamma camera imaging of ^{123}I biodistribution after IV or IT injection of 5 x 10^7 TCID50[278]. Maximum uptakes were noted at 33.2% and 38.5% ID/gm for the IT and IV groups, respectively, 4 days after virus treatment. Dosimetry calculations based on these images pointed to the feasibility of combination radiovirotherapy with VSV(51)-*NIS* plus ^{131}I, with a predicted absorbed dose of 1840 and 11.6 rad/mci given IT or IV, respectively, on day 1 after virus administration. Significant enhancement of tumor regression and survival was observed.

Table 3. Imaging studies with oncolytic viral vectors encoding *hNIS* in mouse models.

	Tumor	Viral dose (PFU) / route of injection	Radiotracer/ imaging modality	Imaging time points	Maximum uptake (%ID/gm) / spread	Loss of signal	T4/low iodine diet?	Dosimetry (rad/mci)	Combin-ation Therapy with ^{131}I?	Notes	Refer-ence
Adenovirus											
AdIP1	Colorectal HCT-116 SC	1 x 10^9 single IT	$^{99m}TCO_4$/ SPECT/CT	1,2,3,4 dpvi	4 dpvi	5 dpvi	No	N/A	No	Delay btw max viral replication and max radiouptake, hNIS hindered replication	263
Ad5AMUCH_ RSV-*NIS*	Breast T47D SC	1 x 10^{11} single IT	^{123}I / γ-camera	2 dpvi	30% 1 hpri	N/A	Yes	N/A	No		264
Ad5/3-Δ24-*hNIS*	Prostate PC-3MM2 SC	2 x10^8 IT 2 x IT	^{123}I / γ-camera	1 dpvi, 0.5, 1, 1.5, 2, 4 / 13 hpri	6% 2 hrs pri, plateaued 13 hpri	N/A	No	N/A	Yes	Uptake plateaued up to 13 hrs pri	265
AdIP2	Colorectal HCT-116 SC	1 x 10^9 single IT	$^{99m}TCO_4$ / X-SPECT/CT	1,2,3,4,5 dpvi / 10mins pri	N/A	3 dpvi	Yes with therapy	N/A	Yes	Replication hindered by hNIS insertion	266
ADAM7	Ovarian IGROV-1 IP	1 x 10^{10} single IP	$^{99m}TCO_4$ / X-SPECT/CT	1-5, 9 dpvi	~40/mm^3 2 dpvi	5 dpvi	No	N/A	No	No effect on therapeutic efficacy	267
Ad5PB_RSV-*NIS*)	Prostate LnCaP SC	1 x 10^{11} single IT	$^{99m}TCO_4$ / X-SPECT/CT	1-28 dpvi	12% 1 dpvi	N/A	No	N/A	Yes	Uptake sustained up to 1 month pvi	268

Measles Virus											
MV-*NIS*	Multiple myeloma ARH-77, KAS-6/1, MM1 SC	2 x 10^6 single IV	^{123}I / γ-camera	1,3,5,7,15, 24 hpri	12% - 17% 1 hpri	N/A	No	400	Yes with KAS-6/1	Complete eradication of KAS-6/1 xenografts with combination therapy	270
MV-*NIS*	Ovarian SKOV3ip.1 IP	1 x 10^6 2 x IP	$^{99m}TCO_4$ / γ-camera	1 hpri	N/A	N/A	No	N/A	No		271
MV-*NIS*	Prostate LnCaP SC	1.5x 10^6 TCID50single IT/IV	^{123}I / γ-camera	1,4,5,8,11 dpvi IT; 1,4,5,8,11, 14,18 dpvi IV	~ 13% 4 dpvi IT, ~14% 14 dpvi IV 1 hpri	N/A	No	420 IT; 540 IV at max uptake	Yes	Uptake sustained up to 36 dpvi for IV	273
MV-*NIS*	Hepatocellular Hep-3B SC	2 x 10^6 TCID50 single IV	^{123}I / γ-camera	1,3,7,10, 14 dpvi	8.41% 3 dpvi; 9.13%10 dpvi;	N/A	No	N/A	No		279
MV-*NIS*	Pancreatic BxPC-3 SC	3.5x 10^6 TCID50single IT	^{123}I / SPECT/CT	2,3,5,8 dpvi	11.4% 2 dpvi	5 dpvi	Yes	N/A	No		275
MV-*NIS*	Pancreatic BxPC-3 SC	3.5x 10^6 TCID50 single IT	^{123}I / SPECT/CT	2,3,4,6,9 dpvi	8% 4 – 6 dpvi	9 dpvi	Yes	1008	Yes		276

Vesicular Stomatitis Virus											
VSV (51)-*NIS*	Multiple myeloma 5TGM1	5 x 10^7 TCID502 x IT/IV	^{123}I and X-SPECT	1,4 dpvi / 3 hrs pri	4.1 IT, 7 IV 1 dpvi; 33.2 IT, 38.5 IV 4 dpvi	N/A	No	1840 IT; 1160 IV at max uptake	Yes		[278]

Abbreviations: dpvi = day post virus injection; hprvi = hours post radiotracer injection; IT = intratumoral; IV = intravenous.

2.5 Clinical Trials With hNIS

Preclinical imaging and therapy success with *NIS* gene delivery has lead to several completed and ongoing clinical trials (Table 4.). Clinical application of *NIS* gene delivery followed by radioiodine will require the generation and investigation of safe and efficient gene delivery systems, as well as the ability for systemic administration and regulated gene expression.

Table 4. Clinical trials with oncolytic viruses carrying hNIS. Source: www.clinicaltrials.gov.

Condition	Intervention	Phase	Sponsor
Prostate cancer	Biological: Adenovirus (Ad5-yCD/*ut*TKSR39*rep*-hNIS)	Phase I	Henry Ford Health System, Michigan
Prostate cancer	Biological: Adenovirus (Ad5CMV-NIS)	Phase I	Mayo Clinic, Rochester
Multiple Myeloma	Biological: Measles virus (MV-NIS)	Phase I	Mayo Clinic, Rochester

NIS transfer has already been attempted in clinical trials utilizing the replication-competent adenovirus Ad5-yCD/*ut*TKSR39*rep*-hNIS for the imaging of prostate cancer. Men with clinically localized prostate cancer were administered an intraprostatic injection of the adenovirus. NIS gene expression was imaged noninvasively by uptake of $^{99m}TcO_4$ in infected cells using SPECT. Therapy was shown to be safe with 98% of the adverse events being grade 1 or 2. Enhanced radiouptake was detected in the prostate in seven of nine patients at 10^{12} PFU but not at 10^{11}, again highlighting the replication inefficiency of this virus. Further, expression was monitored and found to increase to around 18% of the total prostate volume following injection of 10^{12} PFU, peaking at 1–2 days post adenovirus injection and detectable in the prostate for up to 7 days. No evidence of extraprostatic dissemination of the adenovirus was seen by SPECT imaging. The results demonstrate for the first time in humans the noninvasive imaging capability of hNIS utilizing an onolytic viral vector[269].

Another trial is also underway investigating the potential of Ad5CMV-*NIS* for gene therapy and combination with radioactive iodine in treating patients with locally recurrent prostate cancer that did not initially respond to XRT[280]. Patients receive intraprostate Ad5CMV-NIS followed by dosimetry oral ^{123}I on day 4 and undergo image studies periodically for around 24 hours for measurement of radioiodine uptake. Patients then receive therapeutic oral ^{131}I on day 5. The main aims of this study were to determine the safety and tolerance of

Ad5CMV-NIS administered intraprostatically followed by radioiodine treatment in patients with locally recurrent adenocarcinoma of the prostate following external beam radiotherapy as well as the maximum tolerated dose of Ad5CMV-NIS in these patients.

Further, a phase I trial has been initiated studying the side effects and best dose of MV-*NIS* when given with or without cyclophosphamide in treating patients with recurrent or refractory multiple myeloma[280]. The time course of viral gene expression and viral elimination, as well as the biodistribution of virally infected cells at various time points after treatment with these regimens using iodine ^{123}I gamma camera imaging will also be determined.

3.0 SPECIFIC AIMS AND HYPOTHESIS

This project centers on the construction and testing of a novel oncolytic vaccinia virus carrying the human sodium iodide symporter (*hNIS*) gene on tumor rejection, imaging, and targeted radiotherapy in cell culture and mouse models.

Hypothesis: The oncolytic vaccinia-*hNIS* construct, GLV-1h153, will allow killing of tumor by direct oncolytic means as well as by additive or synergistically targeted radiotherapy. Further, such viral constructs will allow imaging of viral therapy by PET scanning.

Specific Aim 1: **To determine if GLV-1h153 induces the expression of hNIS on the cancer cell membranes and assess the effects of gene insertion on viral replication.**
Justification: Since oncolytic viral therapy relies on the replication-competent virus to directly kill cancer cells, it is not obvious that a cell surface protein such as hNIS will be expressed by a cell infected with virus prior to cell lysis. Based on previous data, parental virus GLV-1h68 effectively infects, replicates in, and kills many cancer cell types in cell culture. GLV-1h153 will be compared to parental virus, GLV-1h68, in cell culture in order to determine whether insertion of *hNIS* alters the replication or oncolytic capability of the virus. Further, the successful expression and transported of the hNIS to the cell membrane of infected cells will be assessed in order to facilitate intracellular radiouptake, as well as the time course and dose dependency of hNIS expression and conditions that affect such gene expression.

Specific Aim 2: **To establish that GLV-1h153 specifically kills pancreatic cancer cell line PANC-1, and is safe when administered in animal models.**
Justification: GLV-1h153 will again be compared to its parental virus, GLV-1h68, in animal models in order to determine whether insertion of *hNIS* alters the cancer - or animal-related toxicity. GLV-1h68 is currently in human clinical trials. If GLV-1h153 is found to be effective and safe, clinical translation will be possible.

Specific Aim 3: **To determine if GLV-1h153-induced hNIS expression facilitates intracellular uptake of radioiodide, thus enabling imaging of tumor and viral therapy.**

Justification: Successful imaging of hNIS for tracking oncolytic therapy is related to rate of infection and internalization of virus, as well as rate of synthesis of hNIS protein and localization of protein to the cell surface. Since it is not obvious that a cell surface protein such as hNIS will be expressed by a cell infected with virus prior to cell lysis, imaging may be negatively affected by rapid cell lysis. This is why the synthetic early (SE) promoter was chosen to drive hNIS expression, as protein production under this promoter occurs within hours. In this aim, the optimal conditions for imaging will be determined in mouse models. The imaging parameters as related route of tracer administration and timing of imaging will be investigated. Finding a noninvasive means of tracking viral distribution during and after viral therapy allows potential clinical translation for correlation with efficacy and toxicity during clinical trials and therapy.

Specific Aim 4: **To determine if combination therapy with GLV-1h153 and ^{131}I produces additive or synergistic tumor killing.**

Justification: Radioiodine ^{131}I is a standard treatment for cancers that naturally have high hNIS expression, such as thyroid cancers. Oncolytic viruses have been found to have a synergistic antitumor effect when combined with ionizing radiation. In this specific aim, the ability of GLV-1h153-mediated hNIS expression to induce cancers not naturally expressing hNIS to concentrate and retain ^{131}I will be investigated. Further, assessment of whether such oncolytic viral therapy would be additive or synergistic to treatment by ^{131}I will be examined. If additive or synergistic effect is found, patients may be more safely treated with combinations of lower doses of virus and radioactive iodine.

4.0 MATERIALS AND METHODS

4.1 Cell Culture Experiments

4.1.1 Cell Culture.

African green monkey kidney fibroblast CV-1 cells and human pancreatic ductal carcinoma PANC-1 cells were purchased from American Type Culture Collection (ATCC) (Manassas, VA) and were grown in Dulbecco's modified Eagle's medium (DMEM) supplemented with 1% antibiotic-antimycotic solution (Mediatech, Inc., Herndon, VA) and 10% fetal bovine serum (FBS) (Mediatech, Inc.) at 37^{o}C under 5% CO_2. Rat thyroid PCCL3 cells were a kind gift from the lab of Dr. James Fagin at MSKCC and were maintained in Coon's modified medium (Sigma, St. Louis, MO), 5% calf serum, 2mM glutamine, 1% penicillin/streptomycin, 10mM NaHCO3, and 6H hormone (1 mU/ml bovine TSH, 10 ug/ml bovine insulin, 10 nM hydrocortisone, 5ug/ml transferrin, 10 ng/ml somatostatin, and 2ng/ml L-glycyl-histidyl-lysine) at 37^{o}C under 5% CO_2.

4.1.2 Construction of hNIS Transfer Vector.

The hNIS cDNA was amplified by polymerase chain reaction (PCR) using human cDNA clone TC124097 (SLC5A5) from OriGene as the template with primers hNIS-5 (5′-GTCGAC(Sal I) CACCATGGAGGCCGTGGAGACCGG-3′) and hNIS-3 (5′-TTAATTAA(Pac I) TCAGAGGTTTGTCTCCTGCTGGTCTCGA-3′). The PCR product was gel purified, and cloned into the pCR-Blunt II-TOPO vector using Zero Blunt TOPO PCR Cloning Kit (Incell culturegen, DeSchelp, Netherlands). The resulting construct pCRII-hNIS-2 was confirmed by sequencing to be identical to the source template TC124097. The hNIS binding test suggested that the sequence amplified from the cDNA clone TC124097 was not functional. A further sequence analysis indicated that the hNIS in the TC124097 contained a 33-bp extra sequence in the middle of the coding region when compared to the SLC5A5 sequence in GenBank (accession number NM_000453). The following procedure was employed to remove this 33-bp segment. The hNIS template in the pCRII-hNIS-2 was amplified

separately with the primer pair hNIS-5 and hNIS-a3 (5′-GAGGCATGTACTGGTCTGGGGCAGAGATGC-3′), and the primer pair hNIS-a5 (5′-CCCAGACCAGTACATGCCTCTGCTGGTGCTG-3′) and hNIS-3. The PCR products were purified from the gel, and mixed as the template for the second PCR with the primers hNIS-5 and hNIS-3. The second PCR product was then gel purified, and cloned into the pCR-Blunt II-TOPO vector. The insert was confirmed by sequencing to be identical to the SLC5A5 sequence presented in the NM_000453, and designated as hNISa (the 33-bp segment was removed). The hNIS cDNA was then released from pCRII-hNIS-2 with Sal I and Pac I, and subcloned into HA-SE-RLN-7, HA-SL-RLN-3, and HA-SEL-RLN-2 with the same cuts by replacing RLN cDNA. The resulting construct HA-SE-hNIS-1 were confirmed by sequencing and used for insertion of PE-hNIS, PL-hNIS, and PEL-hNIS into the HA locus of GLV-1h68.

4.1.3 Generation of hNIS-Expressing VACV.

CV-1 cells were infected with GLV-1h68 at a multiplicity of infection (MOI) of 0.1 for 1 hour, then transfected using Fugene (Roche, Indianapolis, IN) with the hNIS transfer vectors. GLV-1h68 was derived from VACV LIVP, as described previously[43]. Two days postinfection, infected/transfected cells were harvested and the recombinant viruses selected and plaque purified. The genotype of hNIS-expressing VACV GLV-1h153 was verified by PCR and sequencing. Also, expression of GFP and β-galactosidase was confirmed by fluorescence microscopy and 5-bromo-4-chloro-3-indolyl-β-D-galactopyranoside (X-gal, Stratagene, La Jolla, CA), respectively, and lack of expression of *gusA* was confirmed by 5-bromo-4-chloro-3-indolyl-β-D-glucuronic acid (X-GlcA, Research Product International Corp., Mt. Prospect, IL).

4.1.4 Viral Growth Curves.

PANC-1 cells were seeded onto 24-well plates at 5×10^5 cells per well. After 24 hours in culture, cells were infected with either GLV-1h153 or GLV-1h68 at an MOI of 0.01 or 1.0. Cells were incubated at 37º C for 1 hour with brief agitation every 30 minutes to allow infection to occur. The infection medium was then removed, and cells were incubated in fresh growth medium until cell harvest at 1, 24, 48, and 72 hours postinfection. Viral particles from infected cells were released by 3 freeze-thaw cycles, and titers determined as medium (PFU/mL) in duplicate by plaque assay in CV-1 cell monolayers.

4.1.5 Flow Cytometry.

Cells were seeded on 6-well plates at 5×10^5 cells per well. Wells were then infected at MOIs of 0, 0.01, and 1.0, and cells then harvested at 6, 12, 24, 48, 72, and 96 hours post infection by trypsinizing and washing with phosphate-buffered saline (PBS). GFP expression was analyzed via a Becton-Dickinson FACScan Plus cytometer (Becton-Dickinson, San Jose, CA). Analysis was performed using CellQuest software (Becton-Dickinson). Cells were seeded on 6-well plates at 5×10^5 cells per well. Wells were then infected at MOIs of 0, 0.01, 0.1, 0.5, 1.0, 2.0, and 5, and were harvested at 24 hours after infection. Cells were subsequently trypsinized, washed with phosphate-buffered saline (PBS), and assayed for GFP expression on a Becton-Dickinson FACScan Plus cytometer (Becton-Dickinson, San Jose, CA). Analysis was performed using CellQuest software (Becton-Dickinson).

4.1.6 Cytotoxicity Assay.

PANC-1 pancreatic cancer cells were plated at 2×10^4 per well in 6-well plates. After incubation for 6 hours, cells were infected with GLV-1h153 or GLV-1h68 at MOIs of 1.0, 0.10, 0.01, and 0 (control wells). Viral cytotoxicity was measured on day 1 and every second day thereafter by lactate dehydrogenase (LDH) release assay. Results are expressed as the percentage of surviving cells as compared to uninfected control.

4.1.7 hNIS mRNA Analysis Via Microarray.

To evaluate the level of hNIS mRNA production in infected cells, cells were plated at 5×10^5 cells per well and infected with GLV-1h153 at an MOI of 5.0. Six and 24 hours postinfection, 3 samples of each MOI were harvested and lysis performed directly using RNeasy mini kit protocol (Qiagen Inc., Valencia, CA). The mRNA samples were measured by spectrophotometer for proof of purity and hybridized to HG-U133A cDNA microarray chips (Affymetrix Inc, Santa Clara, CA) by the genomic core laboratory at Memorial Sloan-Kettering Cancer Center (MSKCC). The chip images were scanned and processed to CEL files using the standard GCOS analysis suite (Affymetrix Inc). The CEL files were then normalized and processed to signal intensities using the gcRMA algorithm from the Bioconductor library for the R statistical programming system. All subsequent analysis was

done on the log (base 2) transformed data. To find differentially expressed genes a moderated t-test was used as implemented in the Bioconductor LIMMA package. To control for multiple testing the False Discovery Rate (FDR) method was used with a cutoff of 0.05.

4.1.. hNIS Protein Analysis Via Western Blot.

To confirm whether the hNIS protein was being expressed in infected cells, cells were plated at 5×10^5 per well and infected with GLV-1h153 at various MOIs of virus, harvested at 24 hours, and suspended with SDS-page and 0.5-m DDT reagent. After sonication, protein samples were loaded on 10% Bis-Tris-HCl buffered polyacrylamide gels using the Bio-rad system (Bio-rad laboratories, San Francisco, CA). Following gel electrophoresis for 1 hour, proteins were transferred to nitrocellulose membranes using electroblotting. Membranes were then preincubated for 1 hour in 5% low fat dried milk in TBS-T (20 mm Tris, 137 mm NaCl, and 0.1% Tween-20) to block nonspecific binding sites. Membranes were incubated with a purified mouse antibody against hNIS at 1:100 dilution (Abcam Inc., Cambridge, MA) and incubated for 12 hour at +4°C. After washing with TBS-T, secondary antibody (horseradish peroxidase-conjugated goat antimouse IgG (Santa Cruz, San Diego) was applied for 1hour at room temperature at a 1:5,000 dilution. Peroxidase-bound protein bands were visualized using enhanced chemiluminescence Western blotting detection reagents (Amersham, Arlington Heights, IL) at room temperature for approximately 1 minute and using Kodak BIOMAX MR film for exposure. Normal human thyroid lysate was used as a positive control, and cells treated with an MOI 1.0 of GLV-1h68 and PBS were used as negative controls.

4.1.9 Immunofluorescence.

PANC-1 cells grown in a 12-well plate at 1×10^6 were mock-infected with GLV-1h68 or infected with GLV-1h153 at an MOI of 1.0. Twenty-four hours after infection the cells were fixed with 3.7% paraformaldehyde, permeabilized with methanol, blocked with PBS containing BSA, and incubated with a mouse anti-hNIS monoclonal antibody (Abcam Inc., Cambridge, MA) at a dilution of 1:100, followed by incubation with a secondary red fluorochrome-conjugated goat antimouse antibody (Incell culturegen) at a dilution of 1:100. Pictures were taken using a Nikon inverted fluorescence microscope.

4.1.10 Cell Culture Radiouptake Assay.

Radiouptake in cells infected with GLV-1h153 was compared to rat thyroid cell line endogenously expressing NIS (PCCL3) and to cells infected with an MOI of 1.0 of parental virus GLV-1h68. Cells were plated at 5×10^5 cells per well in 6-well plates. Twenty-four hours after infection, cells were treated with 500 uCi of either carrier free ^{131}I or ^{131}I with 1 mM of sodium perchlorate ($NaClO_4$), a competitive inhibitor of hNIS for a 60-minute incubation period. Media was supplemented with 10 uM of sodium iodide. Iodide uptake was terminated by removing the medium and washing cells twice with PBS. Finally, cells were solubilized in lysis buffer for residual radioactivity, and the cell pellet-to-medium activity ratio (cpm/g of pellet vs. cpm/mL of medium) calculated from the radioactivity measurements assayed in a Packard γ-counter (Perkin Elmer, Waltham, MA). Results are expressed as change in uptake relative to negative uninfected control. All samples were done in triplicate.

4.1.11 Radiopharmaceuticals.

^{124}I, ^{131}I and $^{99m}TcO_4$ were obtained from MSKCC's radiopharmacy. The maximum specific activities for the ^{124}I and ^{131}I were ~215-250 uCi/mouse and ~0.5 uCi/well, respectively. Activity of $^{99m}TcO_4$ ranged from 500-900 uCi/mouse.

4.2 Mouse Model Experiments

4.2.1 Tumor Therapy Studies and Systemic Toxicity.

All mice were cared for and maintained in accordance with animal welfare regulations under an approved protocol by the Institutional Animal Care and Use Committee at Memorial Sloan-Kettering Cancer Center, New York and San Diego Science Center, San Diego. PANC-1 xenografts were developed in 6- to 8-week-old male nude mice (NCI:Hsd:Athymic Nude-*Foxn1*nu, Harlan) by implanting 2×10^6 PANC-1 cells in PBS subcutaneously in the left hindleg. Tumor growth was recorded once a week in 3 dimensions using a digital caliper and reported in mm^3 using the formula (length × width × [height-5]). When tumors reached

100–300mm^3, mice were injected Intratumorally (ITly) or Intravnenously (IVly) via the tail vein with a single dose of 2 × 10^6 PFU GLV-1h153 or GLV-1h68 in 100 uL PBS. Animals were observed daily for any sign of toxicity, and body weight checked weekly. Animals were then euthanized and tumor harvested for viral distribution studies.

4.2.2 In vivo Viral Biodistribution Assays.

Tissue from normal organs (lung, liver, spleen, kidney, brain, testes), as well as from tumor, were harvested at 1 and 5 weeks postinjection of virus, weighed, suspended in 500 mL PBS containing protease inhibitor, and homogenized for 30 seconds at a speed of 6500 rpm. Three to four mice were used per group. After homogenization, samples were subjected to 3 freeze–thaw cycles. Samples were then centrifuged for 5 minutes at 3000 *g* at 4°C, supernatants collected, and serial dilutions made. Standard plaque assays were performed on 24-well plates of confluent CV-1 cells, with all samples assessed in duplicate. The remaining mice for each group were followed for 34 days to determine viral effect on tumor growth.

4.2.3 Optical Imaging of Pancreatic Tumor Xenografts.

GFP expression of tumors infected with GLV-1h153 was visualized directly using UV light fluorescence or utilizing the Maestro 2 system (Cambridge Research and Instrumentation, Woburn, MA). For the bioluminescence imaging, animals were analyzed for the presence of virus-dependent luciferase activity. For this purpose, mice were injected IV with a 100 uL mixture of 5 mL coelenterazine (Sigma; 0.5 mg/mL diluted ethanol solution) and 95 uL of luciferase assay buffer (0.5 M NaCl, 1 mM EDTA, and 0.1 M potassium phosphate, pH 7.4). The animals were then anesthetized with xyline IP injection and imaged using the ARGUS-100 (Hamamatsu, Hamamatsu City, Japan). Photons were collected for 1 minute from dorsal views of the animals.

4.2.4 Histologic Confirmation of GLV-1h153 Infection of Xenografts.

At 1 week post viral injection, animals were sacrificed and the tumors harvested. Tissue sections were deparaffinized by serial passages in xylene, then subjected to a graded series of ethanol washes before endogenous peroxidase activity was blocked by incubation in a 50% by volume solution of 3% H_2O_2/methanol for 10 minutes. Subsequently, slides were be pretreated by heating in citrate buffer (10 mm citric acid) for 20 minutes. Following blocking of nonspecific binding with blocking serum for 30 minutes, slides were incubated with polyclonal antibody produced in rabbits against synthetic peptide AKKIDVQTGRRPYE (the C-terminal of A27L vaccinia protein) (custom made by GenScript Corporation, Piscataway, NJ) at a dilution of 1:1000 for 30 minutes. Tissue sections were then washed and incubated with biotin-conjugated anti-mouse-immunoglobulin for 30 minutes at room temperature, followed by incubation with preformed avidin and biotinylated horseradish peroxidase macromolecular complex. Diaminobenzidine (DAB) was used as the chromogen, where a brownish precipitate would be indicative of VACV immunoreactivity. Slides were counterstained with hematoxilyn for 1–5 minutes before mounting.

4.2.5 PET, CT, and γ-Imaging.

All animal studies were performed in compliance with all applicable policies, procedures, and regulatory requirements of the MSKCC Institutional Animal Care and Use Committee, the MSKCC Research Animal Resource Center.

For the initial IT imaging experiment, 3 groups of 3 animals each, bearing subcutaneous PANC-1 xenografts on the left hindleg, were injected ITly with 2×10^7 PFU GLV-1h153, 2×10^7 PFU GLV-1h68, or PBS. Two days postinjection, ~215 uCi of ^{124}I was administered via the tail vein. At hours 1, 2, and 8 after radiotracer administration, 3-dimensional list-mode data were acquired using an energy window of 350 to 700 keV, and a coincidence timing window of 6 nanoseconds. Imaging was performed using a Focus 120 microPET dedicated small-animal PET scanner (Concorde Microsystems Inc, Knoxville, TN). This data was then sorted into 2-dimensional histograms by Fourier rebinning. The image data were corrected for (a) nonuniformity of scanner response using a uniform cylinder source-based normalization, (b) dead time count losses using a single-count rate-based global correction, (c) physical decay to the time of injection, and (d) the ^{124}I branching ratio. The count rates in

the reconstructed images were converted to activity concentration (%ID/gm) using a system calibration factor (MBq/mL per cps/voxel) derived from imaging of a mouse-size phantom filled with a uniform aqueous solution of 18F. Image analysis was performed using ASIPro (Siemens Pre-clinical Solutions, Knoxville, TN). Four ROIs were manually drawn on each tumor and %ID/gm ± SD recorded. The bar (image intensity scale) demonstrates the range of uptake intensities, with 100% representing the strongest signal in the image. One mouse in the GLV-1h153 group was also imaged with a MicroCAT II MicroCT Scanner (ImTek Inc., Knoxville, TN) 8 hours after radiotracer and obtained images fused with those obtained with PET that same hour.

For the serial imaging experiment, 2 groups of 2 animals each, bearing subcutaneous PANC-1 xenografts on the right hindleg, were injected were injected IVly or ITly with 2×10^6 PFU of GLV-1h153. Mice were serially imaged at 1 and 4 hours post ^{124}I administration via the tail vein at 1, 2, 3, and 5 weeks post viral injection. At week 1 and 2 virus postinjection, animals were also imaged 8, 24, 48, and 72hr after radiotracer administration to obtain time-activity curves. Imaging and data acquisition was done as above. Further, 1 ITly- and 1 IVly-injected mouse were also imaged with a MicroCAT II MicroCT Scanner (ImTek Inc., Knoxville, TN) 4 hours after radiotracer at week 1 and 2, and obtained images again fused with those obtained with PET that same hour.

To investigate if hNIS can also mediate imaging of viral replication with $^{99m}TcO_4$, 3 groups of 2 animals each, bearing subcutaneous PANC-1 xenografts on the right hindleg, were injected IVly (2 mice) or ITly (2 mice) with 2×10^7 PFU of GLV-1h153, or PBS (2 mice). One mouse from each group was imaged with ^{124}I-mediated PET scanning as above, and the other imaged with $^{99m}TcO_4$-mediated γ-scintigraphy 0.5, 1-2, and 3-4 hours after $^{99m}TcO_4$ radiotracer administration. Ventral and dorsal planar images of the *in vivo* distribution of $^{99m}TcO_4$ were simultaneously acquired using the dual-detector gamma camera sub-system of the XSPECT small-animal SPECT-CT system (Gamma Medica, Northridge, CA). The detectors were fitted with low-energy, high-resolution parallel-hole collimators and images acquired over 10 minutes using a 140 keV$\pm$10% $^{99m}TcO_4$ photopeak energy window and a 56x56 image matrix (pixel size: 2.2x2.2 mm). Images were corrected for non-uniformity of response using a measured “sensitivity map”; no attenuation or scatter correction was applied. The resulting images were parameterized in terms of the percent of the %ID/gm, corrected for decay to the time of injection, by applying a system calibration factor (counts per second (cps)/pixel/μCi $^{99m}TcO_4$/ml) determined by imaging a mouse-size (25 ml) cylindrical phantom filled with an aqueous solution of $^{99m}TcO_4$ with a precisely measured activity concentration and imaged in the same manner as the mice.

4.2.6 Tissue Radiouptake Assay.

Following the initial IT imaging experiment, all mice were sacrificed 8 hours post ^{124}I radiotracer injection. Organs (heart, lung, liver, spleen, kidney, thyroid, stomach, muscle, blood) and tumors were collected, weighed, and their radioactivity determined with a γ-counter (Perkin Elmer, Waltham, MA). Data was normalized as described above and also expressed as %ID/gm.

4.2.7 Autoradiography.

Three mice bearing subcutaneous PANC-1 xenografts on the right hindleg, were injected ITly with 2×10^7 PFU of GLV-1h153 (2 mice) or PBS (1 mouse). Two days after injection, ~900 uCi of $^{99m}TcO_4$ was administered via the tail vein. Images were obtained with dual-detector gamma camera sub-system of the XSPECT small-animal SPECT-CT system (Gamma Medica, Northridge, CA).0.5hr after radiotracer administration.

Following imaging of mice, the fluorescent dye Hoechst 33342 trihydrochloride (Sigma) (40 mg/kg; 1 mg in 100 uL physiological saline) was injected IVly through the tail vein. Five minutes after dye injection, animals were sacrificed and tumors excised, embedded in mounting medium (O.C.T. Compound, Sakura Finetek, Torrance, CA) and frozen on dry ice. Sets of contiguous frozen tissue sections were cut at 6 um thicknesses on a Microm HM500 cryostat microtome (Microm International GmbH, Walldorf, Germany) and collected on glass microscope slides.

To facilitate comparison of the spatial distributions of radiotracer and immunohistochemical markers at the microscopic level, digital autoradiography (DAR) was performed on tissue sections prepared as described above. Sections were placed in a film cassette against a phosphor imaging plate (Fujifilm BAS-MS2325, Fuji Photo Film, Japan). Phosphor plates were read out at a resolution of 50 × 50 um on a BAS-1800II Bio-Imaging Analyzer (Fujifilm Medical Systems, USA)

Digital images of the distributions of GFP and Hoechst 33342 in tumor sections were acquired at 100X magnification using a fluorescence microscope (Nikon Diaphot 300) equipped with a computer-controlled motorized stage and digital Coolsnap EZ camera

(Photometrics, Tuscon AZ) for image capture After acquisition of fluorescence images, tumor sections were stained with hematoxylin and eosin (H&E) and imaged by light microscopy. Composite images of whole tumor sections were obtained by stitching individual microscopic images using Image-Pro software (Image-Pro plus v. 7.0, MediaCybernetics, Bethesda, MD). All images were saved in 8-bit format and manually co-registered using Adobe Photoshop (Version 7.0, Adobe Systems, San Jose, CA).

4.2.8 Dosimetry Calculations for Combination Therapy With ^{131}I.

For dosimetry calculations of the serial imaging experiment, four ROIs were manually drawn on imaged tumors and averaged, with the mean injected value ± SD recorded. The ^{124}I image-derived time-activity concentration data were corrected for radioactive decay to the time of injection and fit to exponential functions using least-squares regression[281, 282]. The ^{131}I cumulated activity concentrations (in uCi-hr/gm/uCi ^{131}I administered) were then calculated using *EXCEL* (Microsoft Corp, Redmond, WA) by integrating the fitted time-activity functions, incorporating the physical decay constant of ^{131}I (0.0036 /hour). Mean tumor absorbed doses (rad/uCi ^{131}I administered) were calculated assuming complete local absorption of the ^{131}I β-rays (equilibrium dose constant for ^{131}I β-rays: 0.405 gm-rad/uCi-hr) and ignoring the small contribution of the ^{131}I γ-rays. In order to treat tumors, an average was obtained for the systemically virus-treated mice, with the goal of providing a radiation dose of 2000 rads. For a more detailed explanation of dosimetry calculations, please refer to the following paper and review [153, 187].

Note that cumulated activities from time-activity data were then obtained by integration from the time of administration of the radiopharmaceutical (t = 0) to the time of its complete elimination or decay (effective clearance constant, which takes into account both the physical (radioactive) decay constant of the radionuclide and its biological clearance constant). Time-activity data is the % of administered activity versus time post-administration. Function parameters of the integration from the time of administration of the radiopharmaceutical and the effective clearance constant was iteratively adjusted to minimize the sum of the squared differences between the measured data and the corresponding calculated (i.e. fitted) value. Analytic integration of the time-activity function then yielded the cumulated activity in source region.

4.2.9 Combination Therapy With ^{131}I.

For the radiotherapeutic experiment, PANC-1 xenografts were established in the right hind leg in five groups of mice: GLV-1h153 (4 mice), GLV-1h153 + ^{131}I (3 mice), GLV-1h68 (4 mice), GLV-1h68 + ^{131}I (3 mice), and PBS control (5 mice). Based on previous imaging and dosimetric calculations, 1 week following IV injection of 2 x 10^6 PFU of GLV-1h153 or control virus GLV-1h68, treated groups were administered 5 mCi of ^{131}I by single IV injection in order to achieve an IT dose of around 2000 rads, while the untreated group had 100ul of PBS administered. Tumors were measured before administration of ^{131}I and weekly thereafter. All mice were weighed weekly and followed up to 5 weeks post virus injection.

4.3 Statistical Analysis

P values were generated for cell culture and tissue radiouptake assay comparisons using Dunnett's test, and for imaging radiouptake using the Tukey multiple comparisons test[283]. For treatment experiments, the GraphPad Prism 5.0 program (GraphPad Software, San Diego, CA) was used for data handling and analysis. The significance between therapy groups was determined via two-way ANOVA with Bonferroni correction. $P < 0.05$ was considered significant.

5.0 RESULTS BASED ON SPECIFIC AIMS

5.1 Specific Aim 1: To determine if GLV-1h153 induces the expression of hNIS on cancer cell membranes and assess the effects of gene insertion on viral replication.

5.1.1 Construction of the hNIS-encoding GLV-1h153.

The GLV-1h153 construct used in this study was derived from GLV-1h68 by replacing the β-glucuronidase (*gusA*) expression cassette at the *A56R* locus with the hNIS expression cassette (SE-hNIS) containing the hNIS cDNA under the control of the VACV synthetic early promoter, by homologous recombination in infected cells. The genotype of GLV-1h153 (Figure 5a) was verified by PCR and sequencing, and the lack of β-glucuronidase expression was confirmed by X-GLcA staining (Figure 5b).

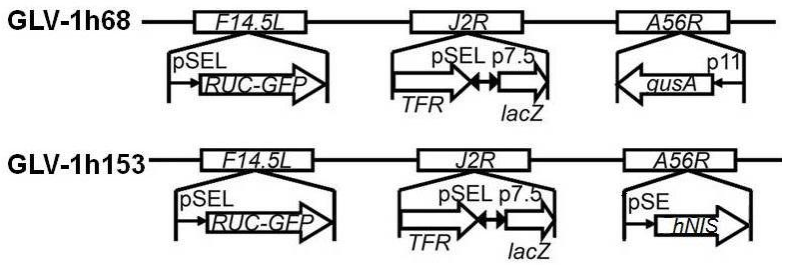

Figure 5a. GLV-1h153 construct. GLV-1h153 was derived from GLV-1h68 by replacing the *gusA* expression cassette at the *A56R* locus with the *hNIS* expression cassette through *in vivo* homologous recombination. Both viruses contain RUC-GFP and *lacZ* expression cassettes at the *F14.5L* and *J2R* loci, respectively. PE, PE/L, P11, and P7.5 are VACV synthetic early, synthetic early/late, 11K, and 7.5K promoters, respectively. TFR is human transferrin receptor inserted in the reverse orientation with respect to the promoter PE/L.

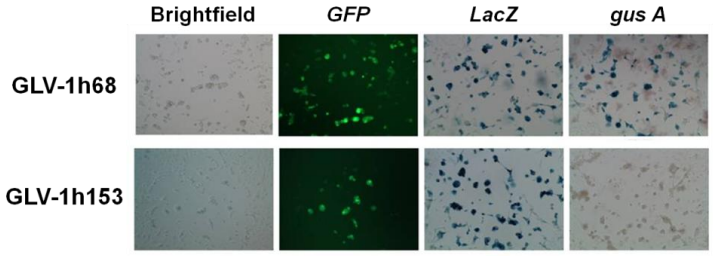

Figure 5b. Confirmation of *GFP*, *LacZ*, and lack of *gusA* marker gene expression in GLV-1h153 infected CV-1 cells. While the *gusA* gene cassette is expressed in cells infected with parent virus GLV-1h68, this has been replaced by the *hNIS* gene cassette in GLV-1h153, leading to loss of *gusA* expression.

5.1.2 GLV-1h153 Replicated Efficiently in PANC-1 Cells.

To evaluate the replication efficiency and effect of hNIS protein expression on VACV replication, PANC-1 cells were infected with either GLV-1h153 or its parental virus, GLV-1h68, at MOIs of 0.01 and 1.0, and the infected cells harvested at 1, 24, 48, and 72 hours post infection. The viral titers at each time point were determined in CV-1 cells using standard plaque assays. Both GLV-1h153 and GLV-1h68 replicated in PANC-1 cells at similar levels, indicating that the hNIS protein did not hinder viral replication within cells. GLV-1h153 yielded a 4-log, or 10,000-fold, increase of viral load with an MOI of 0.01 only 72 hours after infection. Within this time, viral load with an MOI of 0.01 reached the same levels as infection with an MOI of 1.0, again indicating efficient replication (Figure 6).

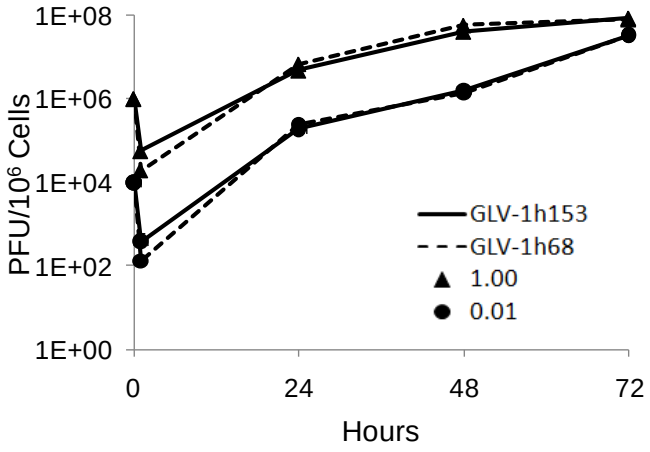

Figure 6. Viral proliferation assay of GLV-1h153-in PANC-1 cells. PANC-1 cells were grown in 6-well plates and infected with GLV-1h153 or GLV-1h68 at an MOI of 0.01 and 1.0. Three wells of each virus were harvested at 1, 24, 48, and 72 hours postinfection. GLV-1h153 replicated in a similar manner to GLV-1h68, with a 4-log increase in viral load at an MOI of 0.01 by 72 hours, reaching similar levels as that in cells infected with an MOI of 1.0 demonstrating efficient replication of GLV-1h153.

5.1.3 GLV-1h153 Replication was Assessed Via Flow Cytometric Detection of GFP.

GFP expression in cells infected with GLV-1h153 was quantified using flow analysis, and was shown to be both time- and MOI-dependent. Adjusting for background, GFP expression mimicked the viral replication growth curve, with GFP expression in cells infected at an MOI of 0.01 reaching similar levels to an MOI of 1.0 by 72 hours (Figure 7a). Further, >70% of live cells expressed GFP at an MOI of 5.0 at 24hrs postinfection (Figure 7b).

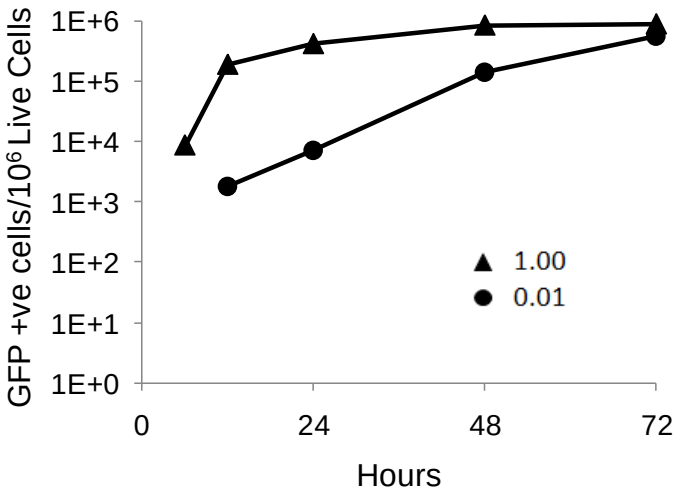

Figure 7a. Flow cytometry of time-dependent GFP expression. GFP was quantified via flow cytometry in PANC-1 cells infected with GLV-1h153 at MOIs of 1.0 and 0.01 and was shown to be MOI dependent. GFP expression mimicked the viral replication growth curve, with expression in the MOI 0.01 infected cells reaching similar levels as the MOI of 1.0 by 72 hours after infection.

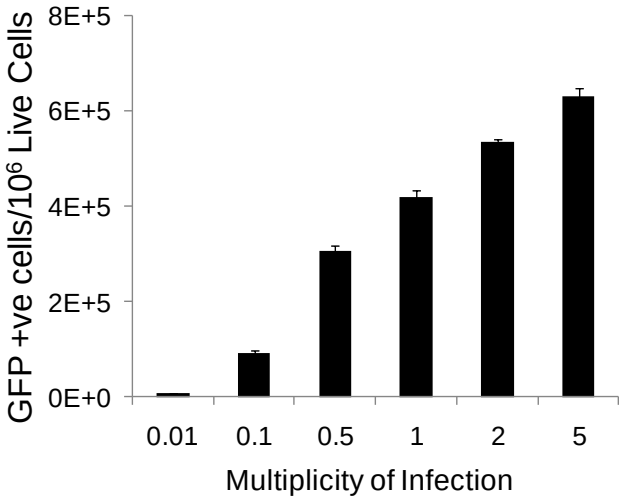

Figure 7b. Flow cytometry of MOI-dependent GFP expression. GFP expression was quantified via flow cytometry in PANC-1 cells infected with an MOI of 0.01, 0.1, 0.5, 1.0 2.0, and 5.0 at 24 hours after infection, and was shown to be MOI-dependent. >70% of live cells expressed GFP at an MOI of 5.0 at 24hrs postinfection.

5.1.4 GLV-1h153 successfully expressed hNIS mRNA and Protein in Infected Cells.

To confirm production of hNIS mRNA by GLV-1h153-infected PANC-1 cells, cells were infected at an MOI of 5.0 and mRNA isolated for analysis with Affymetrix chips. mRNA in cells had an almost 2000-fold increase by only 6 hours after infection, and a >5000-fold change by 24 hours ($P<0.05$) (Figure 8a). To show hNIS protein expression by GLV-1h153, PANC-1 cells were mock infected or infected with GLV-1h153 or parental virus GLV-1h68 at MOIs of 0.1, 1.0, and 5.0 and harvested 24 hours after infection. Production of the hNIS protein was successfully detected by Western blot between 75 and 100 kDa, with an increasing concentration of protein at higher MOIs (Figure 8b).

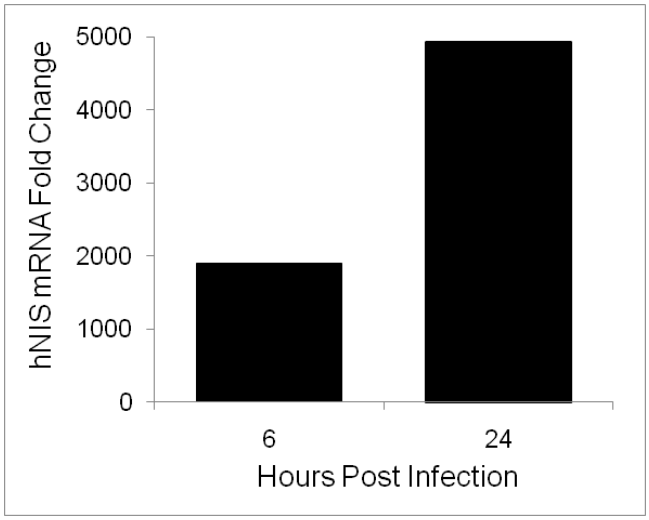

Figure 8a. Assessment of hNIS mRNA expression in GLV-1h153-infected PANC-1 cells. Microarray analysis of cells infected with an MOI of 5.0 of GLV-1h153 yielded an almost 2000-fold increase by 6 hours and an almost 5000-fold increase by 24 hours in hNIS mRNA production as compared to noninfected control.

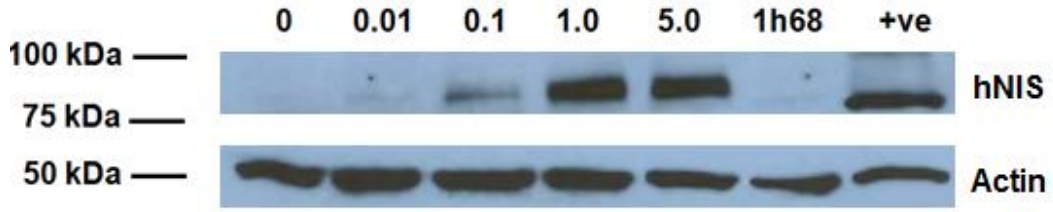

Figure 8b. Assessment of hNIS protein expression in GLV-1h153-infected PANC-1 cells PANC-1 cells were either mock infected or infected with GLV-1h68 at an MOI of 1.0 or infected with GLV-1h153 at an MOI of 1.0 or 5.0 for 24 hours. The hNIS protein was detected by Western blot analysis using monoclonal anti-hNIS antibody. Only GLV-1h153-infected cells expressed the hNIS protein, but cells either mock infected or infected with GLV-1h68 did not. The molecular weight marker bands (in kDa) are shown on the left.

5.1.5 The hNIS Protein was Localized at the Cell Membrane of PANC-1 Cells.

To determine whether the hNIS protein expressed by GLV-1h153 was successfully transported and inserted on the cell membrane, PANC-1 cells were infected with GLV-1h153 and fixed with 3.7% paraformaldehyde. The hNIS protein was visualized using a monoclonal anti-hNIS antibody that recognizes the intracellular domain of the protein. As shown in Figure 9, mock- or GLV-1h68-infected cells (as demonstrated by GFP expression) did not show hNIS protein expression, whereas the hNIS protein in cells infected with GLV-1h153 was readily detectable by immunofluorescence microscopy, and appears to be localized at the cell membrane.

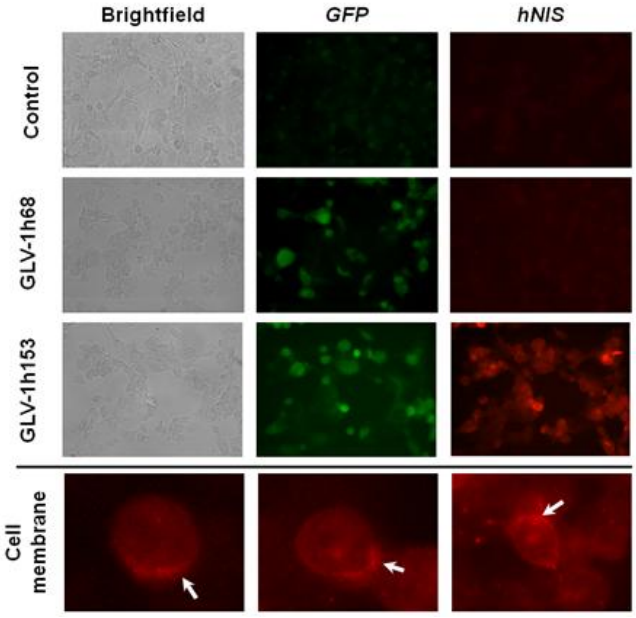

Figure 9. Immunofluorescence of hNIS protein location in GLV-1h153-infected PANC-1 cells PANC-1 cells were mock-infected or infected with GLV-1h68 or GLV-1h153 at a MOI of 1.0 for 24 hours. The hNIS protein was detected by immunofluorescence microscopy using monoclonal anti-hNIS antibody. Mock- or GLV-1h68-infected cells (as demonstrated by GFP expression) did not express the hNIS protein, whereas the hNIS immunoreactivity was readily detectable on the cell membrane of PANC-1 cells infected with GLV-1h153.

5.1.6 GLV-1h153-Infected PANC-1 Cells Showed Enhanced Dose- and Time-Dependent Uptake of Carrier-Free Radioiodide.

To establish that the hNIS symporter was functional, cells were mock infected or infected at an MOI of 1.0 with GLV-1h153 and GLV-1h68, then treated with ^{131}I at various times after infection. GLV-1h68-infected cells were treated at 24 hours postinfection. Normal rat thyroid cell line PCCL3 was used as a positive control. PANC-1 cells infected with GLV-1h153

showed a >70-fold increased radiouptake compared with negative control at 24 hours post infection (P<0.001), compared to 2.67 and 1.01 with MOIs of 0.1 and 0.01, respectively. This increased uptake correlated with peak GFP expression (Figure 10, left panel). Moreover, when cells were treated with $NaClO_4$, a competitive inhibitor of hNIS, radiouptake decreased in GLV-1h153-treated cells, from a 70- to a 1.14-fold difference at an MOI of 1.0, indicating hNIS-specific radiouptake. Radiouptake was also shown to be time-dependent, and again correlated with GFP expression, with a decrease of both radiouptake and GFP expression by 48hrs. (Figure 10, left panel).

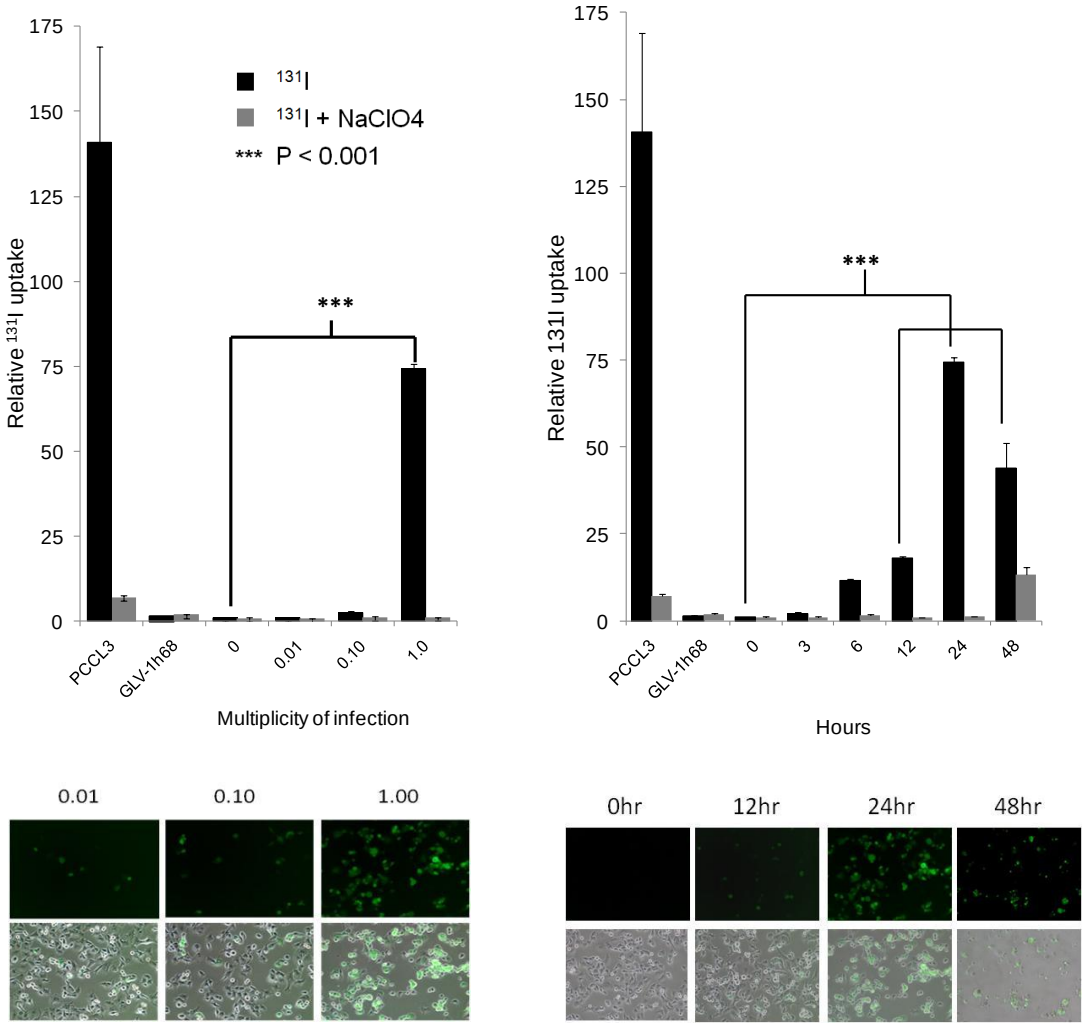

Figure 10. Assessment of cell culture ^{131}I radiouptake of GLV-1h153-infected PANC-1 cells. PANC-1 cells were infected with an MOI of 0, 0.01, 0.1, and 1.0 of GLV-1h153 and MOI of 1.0 of GLV-1h68. PCCL3 was used as a positive control. Twenty-four hours after infection, a >70-fold enhanced radiouptake was seen at an MOI of 1.0 as compared to an MOI of 0 in GLV-1h153. Uptake was MOI-dependent and hNIS-specific (as shown with blocking with competitive inhibitor of hNIS, $NaClO_4$). Maximum radiouptake with an MOI of 1.0 24 hrs after infection corresponded to maximum GFP expression (left panel). PANC-1 cells were mock infected or infected with an MOI of 1.0 of GLV-1h153 and MOI of 1.0 of GLV-1h68 (harvested at 24 hours post infection). Radiouptake was time-dependent and correlated with GFP expression, with a decrease of radiouptake and GFP expression by 48hrs (right panel).

5.2 Specific Aim 2: To establish that GLV-1h153 specifically kills pancreatic cancer cell line PANC-1, and is safe when administered in animal models.

5.2.1 Cytotoxicity Assay.

To investigate whether expression of hNIS would affect cytolytic activity of VACV in cell cultures, PANC-1 cells were mock-infected or infected with GLV-1h68 or GLV-1h153 at an MOI of 0.01 and 1.0. Viral cytotoxicity was measured every other day for 7 days. The survival curves for GLV-1h68 and GLV-1h153 were almost identical at both MOIs, indicating a similar cytopathic effect of both viruses in a time- and dose-dependent fashion (Figure 11a). By day 11, More than 60% cell kill was achieved with an MOI of 1.0 as compared to control. Cytotoxicity again correlated with GFP expression (Figure 11b).

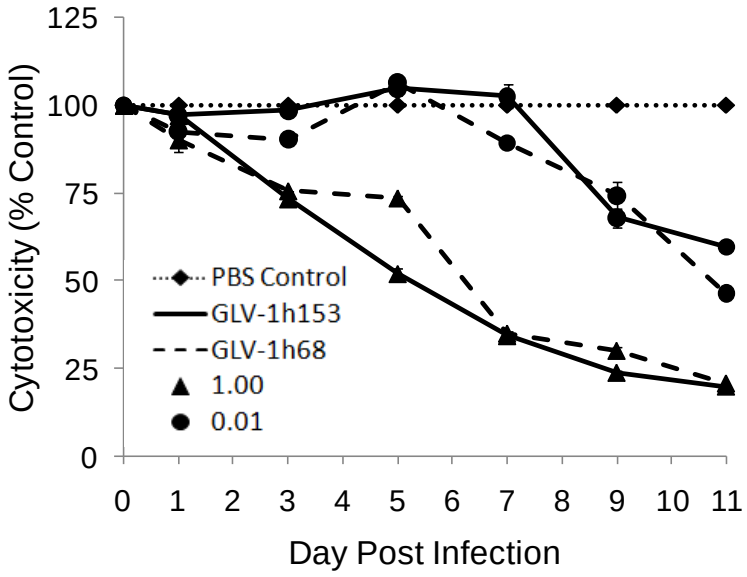

Figure 11a. GLV-1h153 infection and killing in cell culture. a. PANC-1 cells were infected by various GLV-1h153at MOIs of 0.01, 0.1, and 1.0. Cell viability was determined via lactate dehydrogenase assays, and was set at 100% before infection. GLV-1h153 infected and was cytotoxic at various MOIs, with less than 20% survival of cells as compared to control at an MOI of 1.0 by day 9. The values are the mean of triplicate samples, and bars indicate SD.

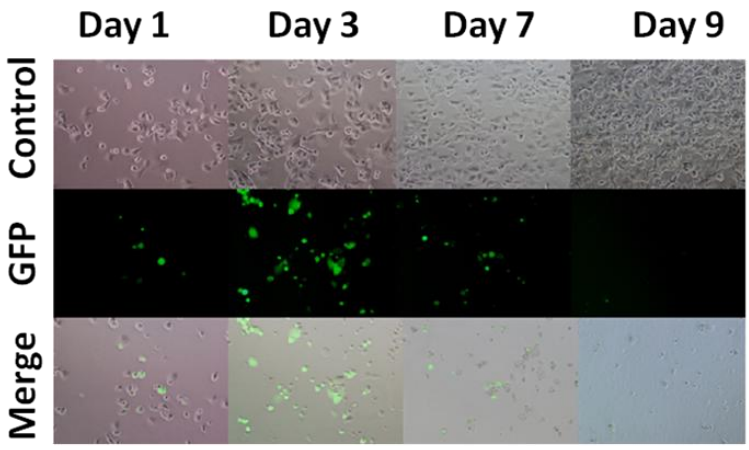

Figure 11b. Microscopy of GLV-1h153 infection and killing in cell culture. GFP expression, shown here at an MOI of 1.0, is time-dependent with abundant GFP expression by day 3. Phase overlay pictures shows gradual cell death and thus decline of GFP expression by day 7. Closer examination of infected cells reveals loss of normal morphology and cell progressive cell detachment.

5.2.2 Tumor Therapy Studies and Systemic Toxicity.

To establish cytolytic effects of GLV-1h153 in animal models, mice bearing PANC-1 hindleg xenografts were infected IT or IV with GLV-1h153 or GLV-1h168, or mock-treated with PBS. While the tumors treated with PBS continued to grow, GLV-1h153-treated tumors occurred in three distinct phases: growth, inhibition, and regression (Figure 12a). The mean relative size of tumors treated with GLV-1h153 was significantly smaller than untreated control tumors, with differences beginning as early as day 13 ($P < 0.01$), and continuing till day 34 after virus or PBS control administration ($P < 0.001$). By day 34, there was an over 4-fold difference between control and IV tumor volumes, a >6 fold difference in the IT group. Furthermore, there were no significant adverse effects seen with regard to body weight, with the IT group gaining weight as compared to control with statistically significant results by day 34 ($P < 0.001$) (Figure 12b).

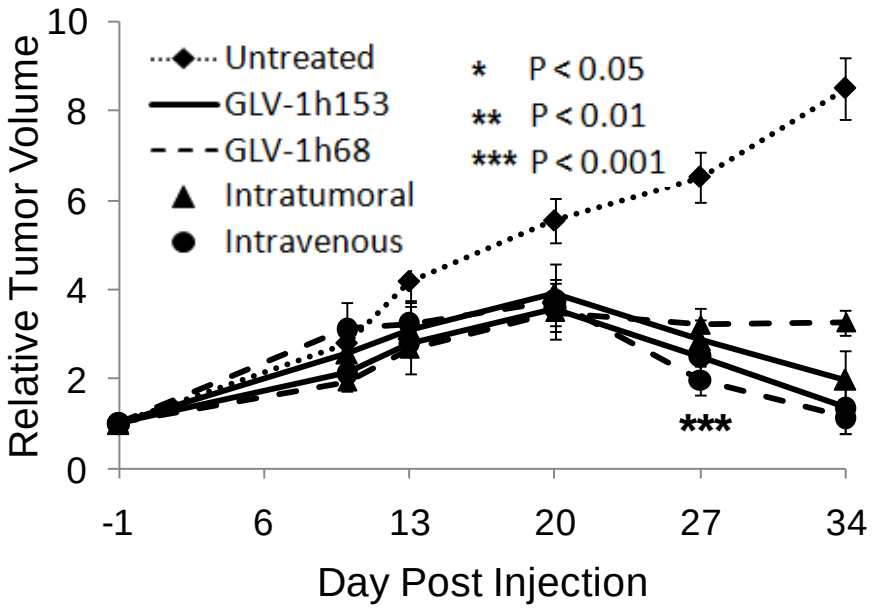

Figure 12a. GLV-1h153-mediated killing of PANC-1 tumor xenografts. Two × 10^6 PFU of GLV-1h153 or GLV-1h68, or PBS were injected IVly or ITly into nude mice bearing S.C. PANC-1 tumors (~100 mm^3). GLV-1h153 slowed growth and regressed pancreatic tumor xenografts from initial tumor volume when injected both ITly and IVly starting at day 13. The values are a mean of 4-5 mice, with bars indicating SEM.

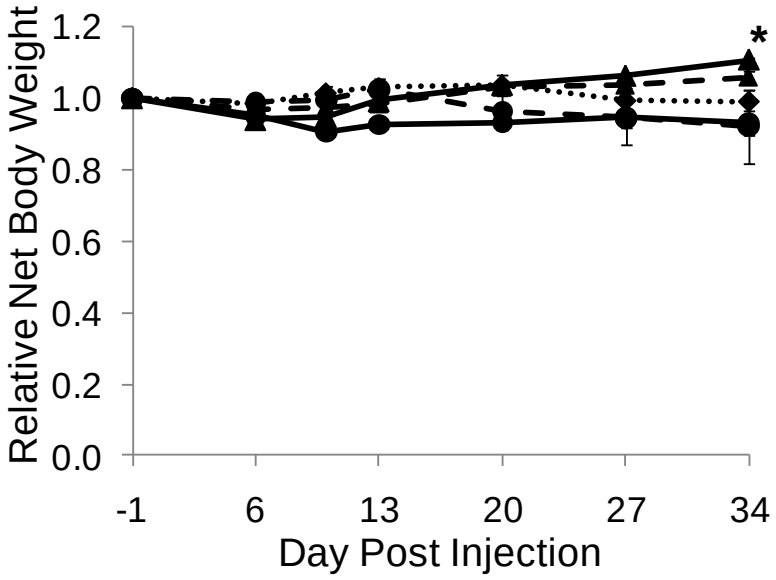

Figure 12b. Body weights of animals post GLV-1h153 treatment. GLV-1h153 treatment of pancreatic tumor xenografts did not have adverse effects on body weight at 5 weeks postinjection, with the IT group even gaining weight compared to control.

5.2.3 Viral Biodistribution Assays.

To assess viral biodistribution in animal models, GLV-1h153 particles were recovered from tumor tissues of virus-treated animals at 1 and 5 weeks in the order of 10^9 virus particles per gram tissue in both the IT and IV groups (3-4 mice per group per time point). Only trace amounts of virus were detected in the spleen and lungs for the IT and IV groups and in the spleen for the IT group at 1 week. By 5 weeks, virus replication persisted at almost 10^9 virus particles per gram of tissue in the tumors, while residual viral particles were mostly cleared in other organs with only trace amounts remaining in the lung and kidney in the IV and IT groups, respectively (Figure 13).

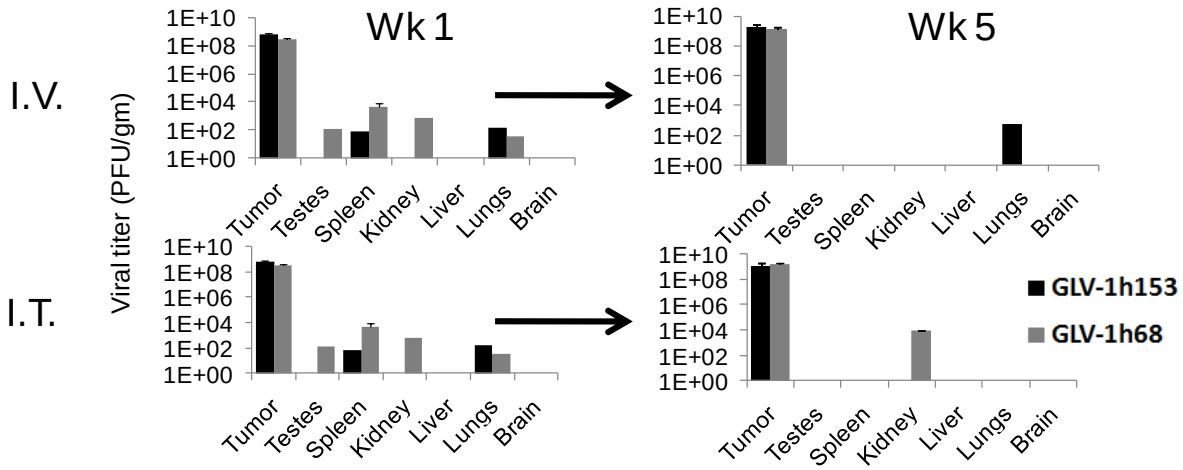

Figure 13. GLV-1h153 biodistribution in animal models. GLV-1h153 and GLV-1h68 particles were recovered from tumor tissues of virus-treated animals at 1 and 5 weeks post IT or IV injection of virus in the order of 10^9 viral particles in both groups (log scale, 3-4 mice per group per time point). Trace amounts of virus were detected in the testes, spleen, kidney and lungs for both viruses and for both the IV and IT group at 1 week. By 5 weeks, virus replication persisted at almost 10^9 virus particles per gram of tissue in the tumors, while residual viral particles were cleared in most organs.

5.2.4 Histologic and Optical Confirmation GLV-1h153 Infection of Tumor Xenografts.

To confirm virus presence in tumors, 2 animals from GLV-1h153 and GLV-1h68 IT and IV groups, as well as PBS controls, were sacrificed 1 week after treatment. All tumors treated with either GLV-1h153 or GLV-1h68 stained positive for vaccinia A27L antigen, yielding a brownish precipitate compared to the blue-purple hematoxylin background seen with uninfected areas and control tumors. Tumors injected ITly showed more homogenous areas of brown precipitation as compared to a more dispersed pattern in the IV-infected group, which is explained by the systemic rather than local spread of virus within the tumor. Tumors infected with GLV-1h153 expressed GFP, which persisted 5 weeks after injection. Furthermore, virus was detectable in virus-infected tumors by bioluminescence imaging of luciferase activity 1 week after viral administration (Figure 14).

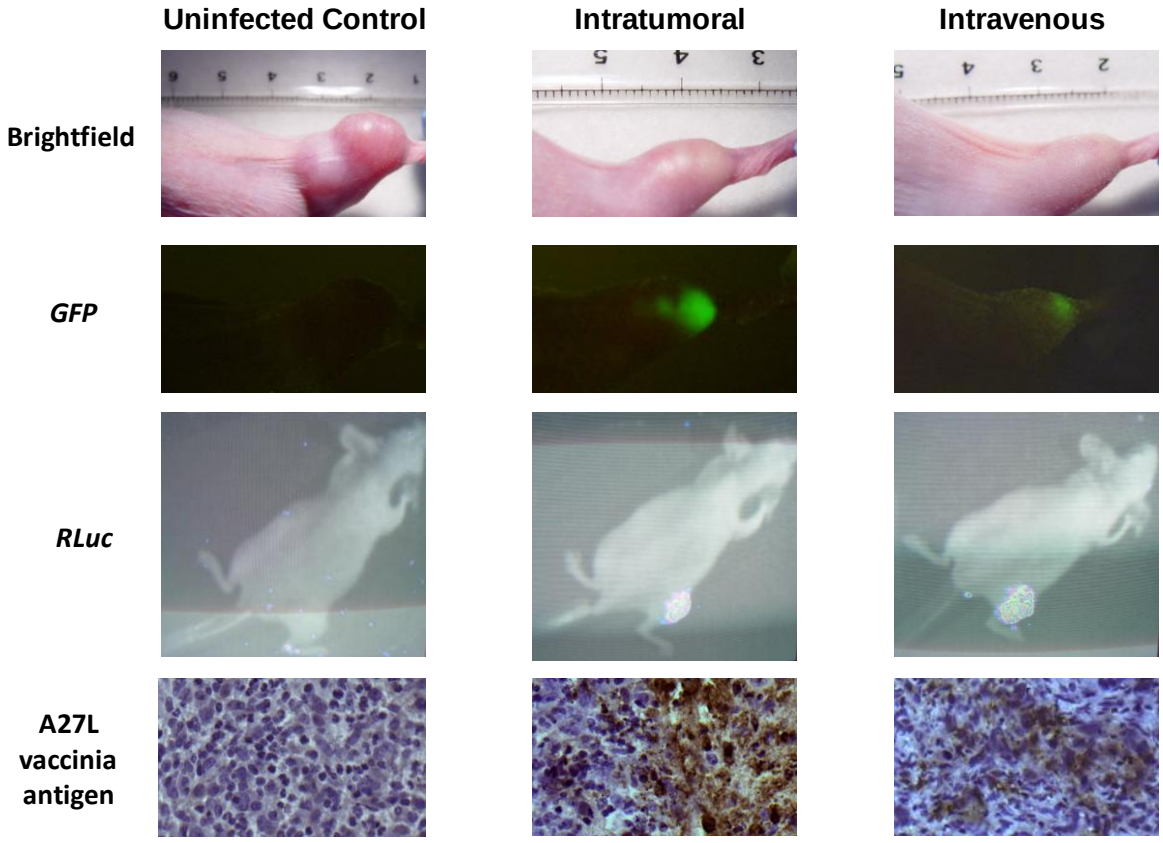

Figure 14. Histologic and optical detection of viral replication using vaccinia marker genes. GFP expression was monitored at 1, 3, and 5 weeks after GLV-1h153 injection and persisted 5 weeks posttreatment. GLV-1h153 was also detected via *RLuc* bioluminescence imaging 1 week posttreatment. Presence of GLV-1h153 in tumors was confirmed histologically, shown here with the brownish precipitate against vaccinia A27L antigen in the IT and IV groups at 400x magnification.

5.3 Specific Aim 3: To determine if GLV-1h153-induced hNIS expression facilitates intracellular uptake of radioiodide, thus enabling imaging of tumor and viral therapy.

5.3.1 GLV-1h153 Enhanced Radiouptake in Tumor Xenografts and was Imaged Via PET.

After successful cell culture radiouptake studies, the feasibility of using GLV-1h153 in combination with carrier-free ^{124}I radiotracer to image infected PANC-1 tumors was investigated. hNIS protein expression in the PANC-1 tumor-bearing animals after GLV-1h153 administration was visualized by ^{124}I-PET. Carrier free ^{124}I was IVly administered 48 hours after IT virus injection and PET imaging was performed 1, 2, and 8 hours after radiotracer administration. Tumor radioactivity values (%ID/gm) were measured and compared to background. The maximum average levels of radioactivity in GLV-1h153-injected tumors were 3.82 ± 0.46 1 hour after radiotracer administration, whereas GLV-1h68- and PBS-injected tumors could not be visualized, and therefore were not significantly above background ($P < 0.001$). The stomach and thyroid were also imaged due to native NIS expression, and the bladder due to tracer excretion (Figure 15).

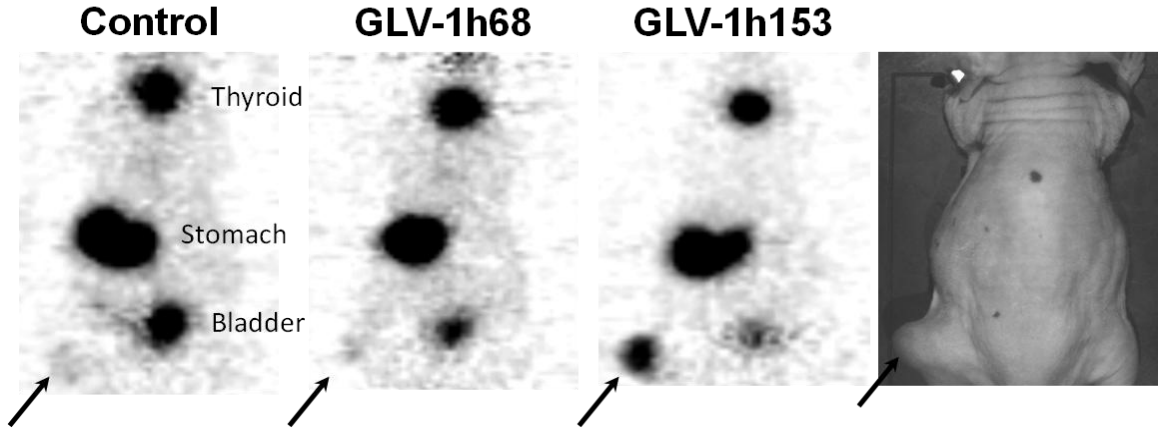

Figure 15. PET imaging of enhanced radiouptake in GLV-1h153-infected PANC-1 xenografts. Two × 10^7 PFU of GLV-1h153, GLV-1h68, or PBS was injected ITly into PANC-1 hindleg tumor-bearing mice. ^{124}I PET scanning was obtained 48 hours after infection and 1 hour after radiotracer administration. GLV-1h153-infected PANC-1 tumors were easily visualized, while no enhanced signal was seen in the PBS- or GLV-1h68 injected tumors. Stomach and thyroid were also imaged due to native NIS expression, and the bladder due to tracer excretion

5.3.2 GLV-1h153-Enhanced Radiouptake Was Retained In PANC-1 Tumor Xenografts.

When the ITly-injected mice were imaged serially over 1, 2, and 8 hours, absolute activity in tumors declined. However, the ratio of activity to background increased from 9.11 ± 1.48 ($P<0.001$) to 25.0 ± 7.05 ($P<0.01$) (Figure 16b and 16c).

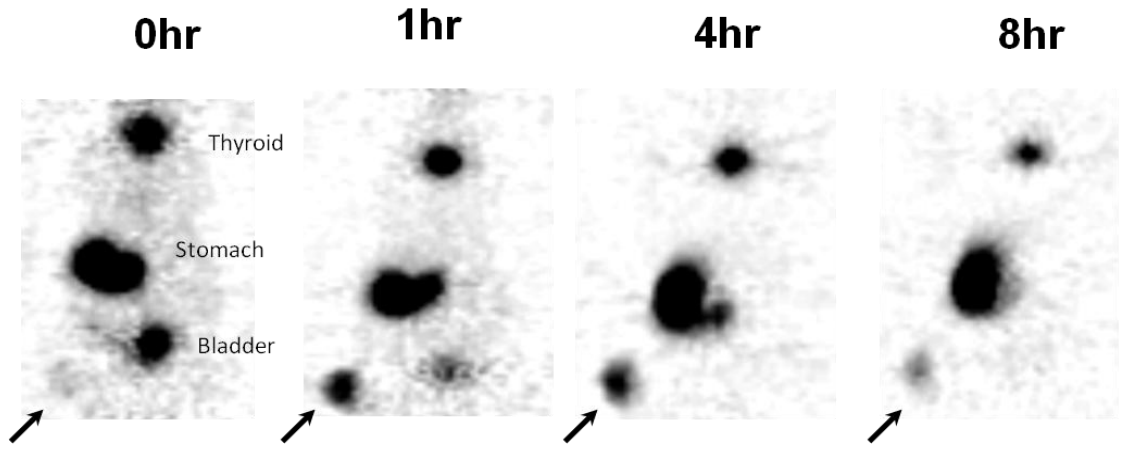

Figure 16a. Timing characteristics of radiouptake in GLV-1h153-infected PANC-1 xenografts. Two × 10^7 PFU of GLV-1h153 or PBS was injected ITly into PANC-1 hindleg tumor-bearing mice. ^{124}I-PET scanning was performed 48 hours after infection and 1, 4, and 8 hrs after radiotracer administration.

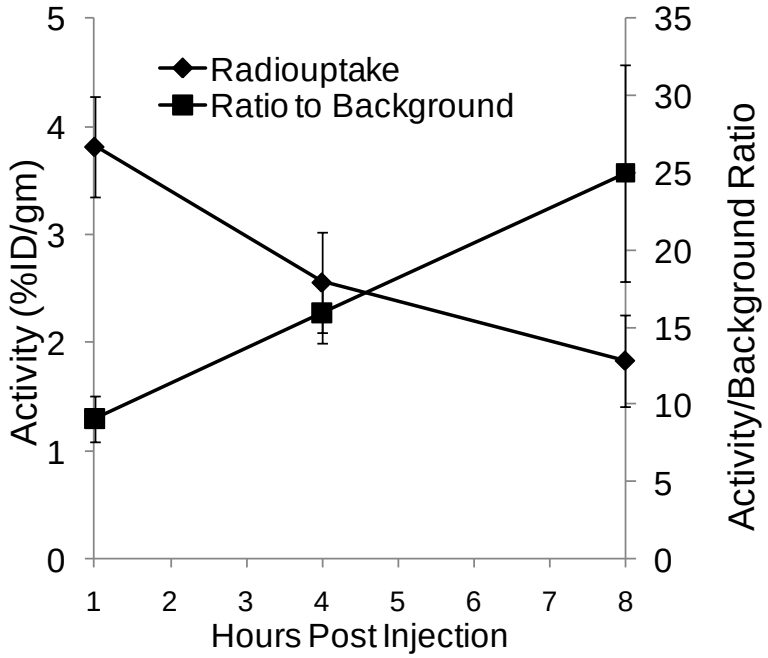

Figure 16b. Ratio of radiouptake to background in PANC-1 xenografts. Although absolute radiouptake decreased between 1 and 8 hours post radiotracer administration, ratio of uptake versus background steadily increased, showing successful retention of radiotracer in tumors.

5.3.3 GLV-1h153-Mediated Tissue Radiouptake Correlated Well With Quantative PET.

Enhanced radiouptake in ITly GLV-1h153-injected tumors to other organs as well as GLV-1h68- and PBS-injected tumors was confirmed in ITly-injected mice (2-3 mice per group) via tissue radiouptake assay at 8 hours post radiotracer administration. The activity in GLV-1h153-infected tumors correlated well with PET images, at 1.71 ± 0.30 ($P<0.001$ compared to both PBS and GLV-1h68 groups) and 1.84 ± 0.42 ($P<0.01$ also compared to both PBS and GLV-1h68), respectively, whereas tumors in the control groups were again not above background (Figure 17).

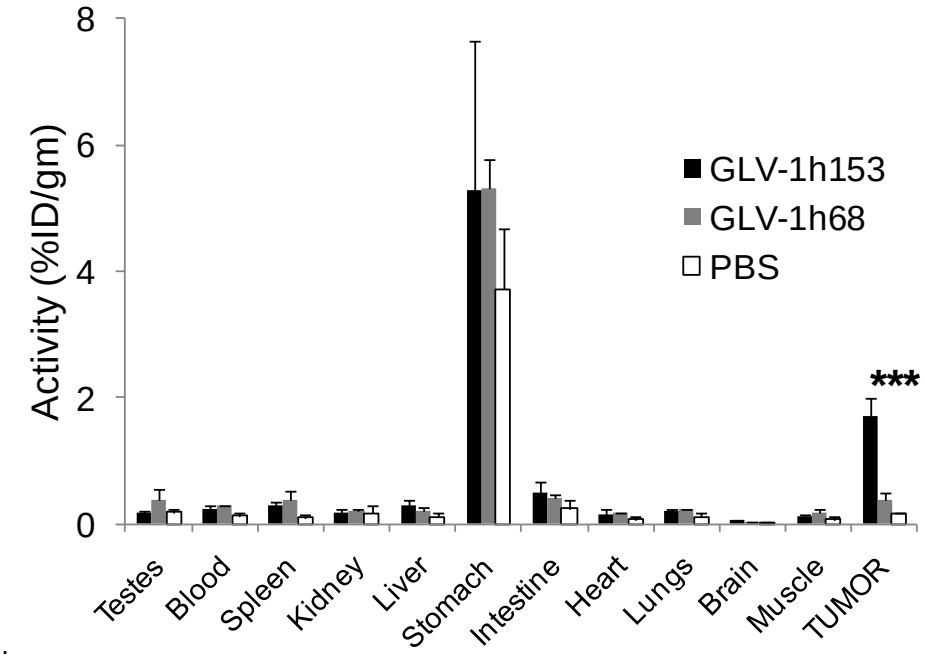

Figure 17. Tissue radiouptake assay. Enhanced radiouptake in tumors infected with GLV-1h153 compared to GLV-1h68 and PBS 8 hrs after radiotracer injection was confirmed via tissue radiouptake assays and correlated well with quantitative PET. Native NIS expression in the stomach also leads to enhanced radiouptake in all groups, but only in the GLV-1h153-mediated NIS expression in infected tumors.

5.3.4 GLV-1h153 Facilitated Serial Monitoring Of Systemic and IT Viral Therapy.

After establishing that GLV-1h153 enhances radiouptake in animal models, is detected by PET, and induces radiouptake retention, GLV-1h153 facilitation of serial imaging and monitoring of both IT and systemic viral therapy was then determined. Two mice were injected either ITly or IVly with 2×10^6 PFU of virus, which was the same dose used in the therapeutic and biodistribution assay experiments. Mice were imaged at 1, 2, 3, and 5 weeks

post virus injection and 1 and 4 hours post radiotracer administration to determine radiouptake in tumors. At week 1 and 2 post virus injection, mice were also imaged at 1, 4, 8, 24, 48, and 72 hours post injection in order to calculate absorbed doses in the tumor with dosimetry. As can be seen in the Figure 18, PET imaging readily detected virus replication in tumors as late as 5 weeks postinjection. While the GFP signal continued to be strong, hNIS-mediated radiouptake peaked at around 2 weeks post virus injection, and gradually declined by week 3 and 5. This is despite a persistent strong GFP signal by 5 weeks.

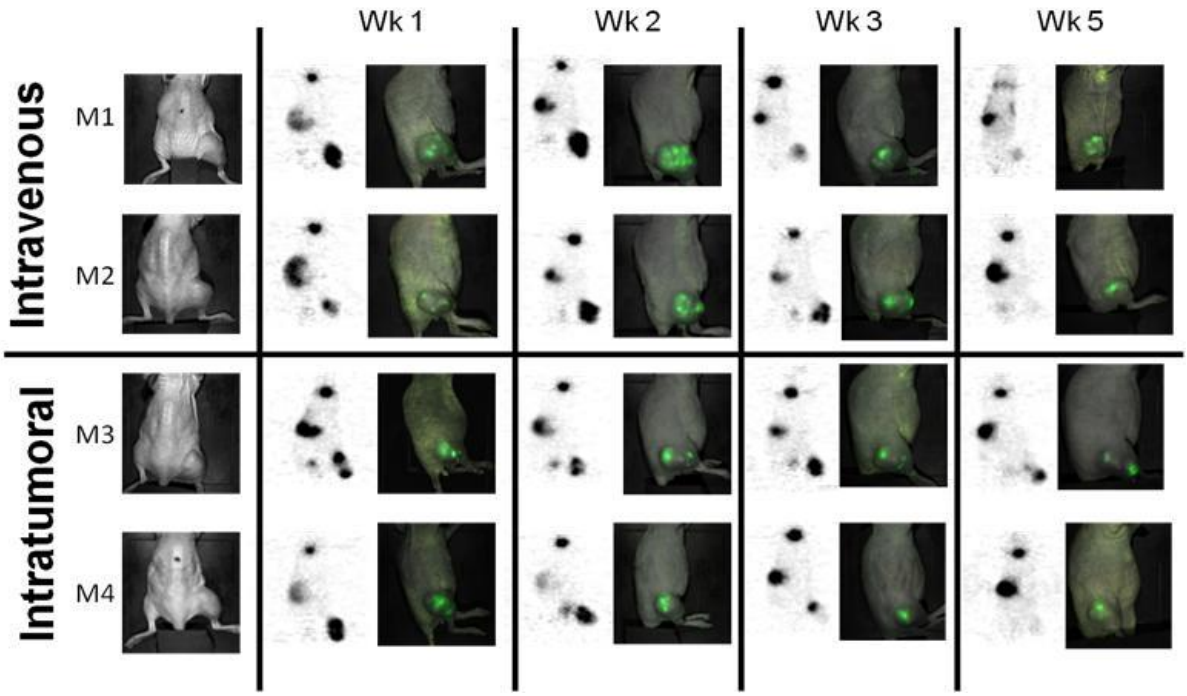

Figure 18. Serial monitoring of GLV-1h153 treatment of PANC-1 tumor xenografts. Two × 10^6 PFU of GLV-1h153 was injected IVly or ITly into PANC-1 right hindleg tumor-bearing mice. ^{124}I PET scanning was obtained 1, 2, 3, and 5 weeks post virus injection, and 4 hours post radiotracer administration at each week. hNIS-mediated enhanced radiouptake in GLV-1h153-infected tumors could be serially monitored, being strong at week 1 and 2 post virus injection, with gradual declined by week 3 and 5 despite strong GFP expression remaining.

5.3.5 GLV-1h153 Tumor Infection was Confirmed Via GFP, Bioluminescence, and CT-PET.

GLV-1h153 presence in tumors, mediating radiouptake, was confirmed via GFP, bioluminescense, and CT-PET imaging 1 and 2 weeks post viral injection in both the IV and IT groups. As can be seen in Figure 19, all reporter genes were detectable, and fusion of PET and CT images correlated enhanced signals anatomically to the location of the tumor, stomach, bladder, and thyroid.

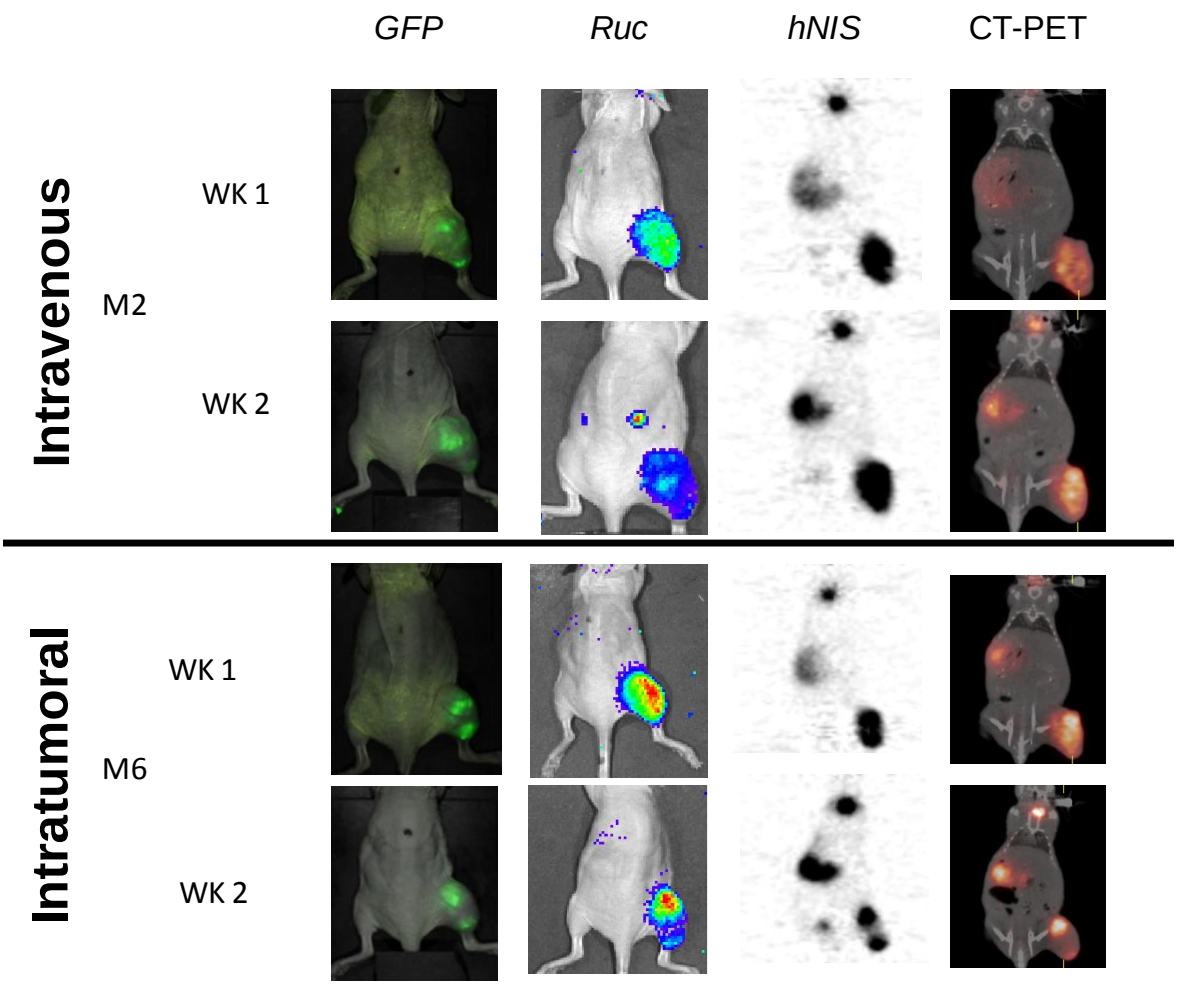

Figure 19. GLV-1h153 reporter genes were detectable in PANC-1 xenografts. GFP, bioluminescence, and hNIS signal could all be detected in GLV-1h153-infected tumors. Fusion of PET and CT images correlated uptake signal anatomically to the location of the thyroid, stomach, bladder, and tumor, while GFP and bioluminescense signals located only to the tumor.

5.3.6 Correlation of PET Signal Pattern With Tumor Regression.

When comparing PET signal intensity with tumor growth patterns in mice over 5 weeks, enhanced radiosignal appears to correlate with initial tumor growth, growth retardation, and eventual regression. The PET signal remained strong during the first 2 weeks postinjection of virus, which reflected initial tumor growth. However, when tumor growth began entering a plateau phase, PET signal began to decrease and almost disappear by week 5, when tumors have entered the regression phase. Interestingly, M3's tumor took longer to regress, and maintained a signal up to 5 weeks post virus injection (Figure 20).

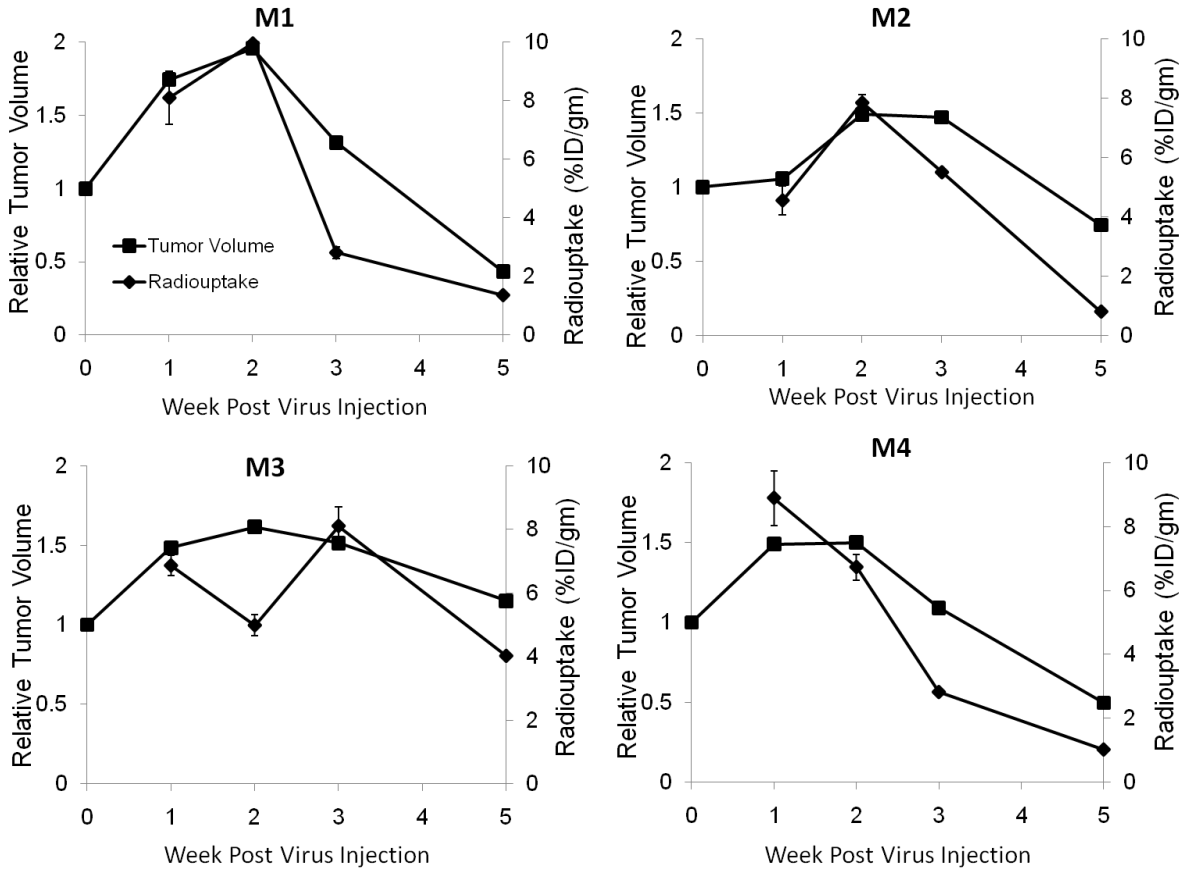

Figure 20. PET signal intensity and tumor growth characersitics. The PET signal remained strong during initial tumor growth for serially imaged mice. When tumor growth entered a plateau phase, PET signal began to decrease. By week 5, tumors have entered the regression phase, and PET signal almost disappears.

5.3.7 Histology of GLV-1h153-Treated Tumors 5 Weeks Postinjection.

Histology of serially imaged tumors confirmed wide areas of necrosis and inflammatory infiltrate (Figure 21). Necrotic areas were more homogenous in the IVly-treated group, whereas „islands“of necrosis surrounded by inflammatory infiltrate was seen in the IT group, reflecting virus route of administration. Interestingly, no viable cells were detected histologically in all mice tumors except M3, which retained some viable tumor proliferation activity.

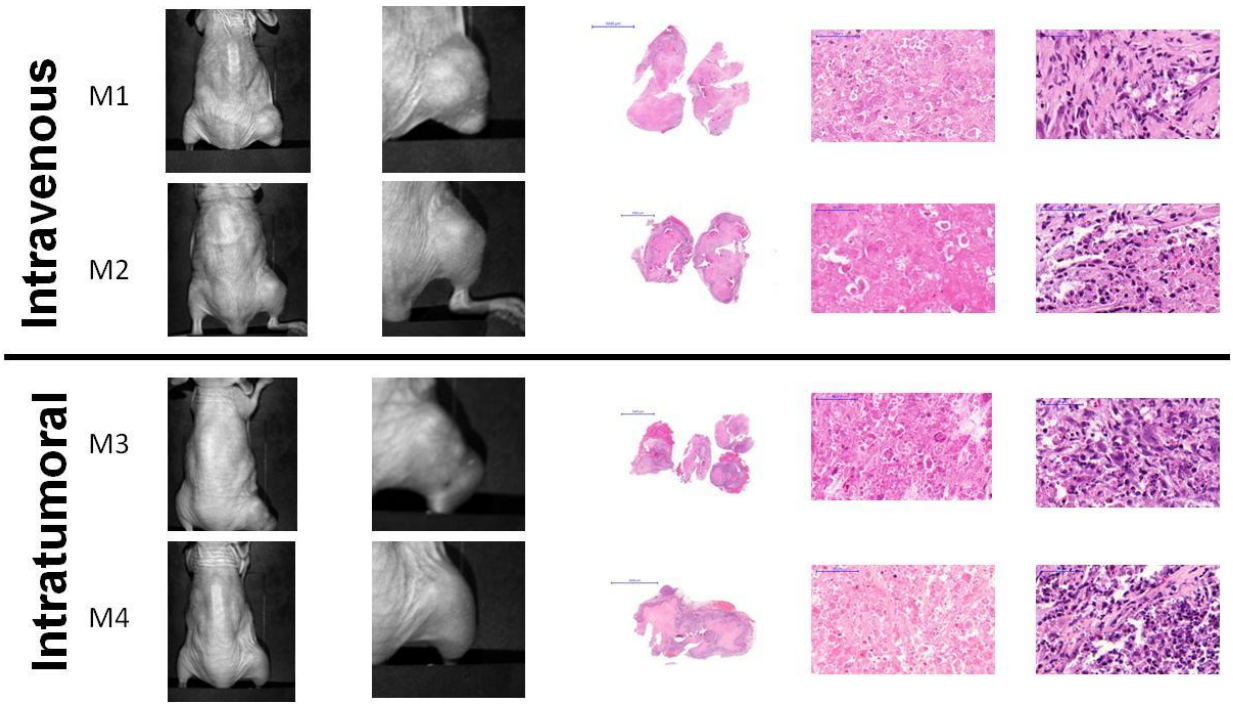

Figure 21. Histology of GLV-1h153-treated tumors 5 weeks postinjection. All mice were sacrificed 5 weeks post virus injection and serial imaging, and tumors harvested for histology. H&E staining of imaged tumors confirmed wide areas of necrosis and inflammatory infiltrate. No viable cells were detected histologically in all mice tumors except M3, which retained some viable tumor proliferation activity.

5.3.8 Viral Dose Comparisons.

To investigate the effects of viral dose administered on the hNIS-mediated PET signal, 2 groups of 1 animal each, bearing subcutaneous PANC-1 xenografts on the right hindleg, were injected IVly (2 mice) or ITly (2 mice) with 2 x 10^7 or 2 x 10^6 PFU of GLV-1h153. Mice were imaged with ^{124}I-mediated PET scanning as above at 4 hours post radiotracer injection. IT injection of 2 x 10^7 PFU caused a weaker initial (Figure 22a) and more rapid loss of signal (Figure 22b) than the IT injection with 2 x 10^6. However, injection IVly with 2 x 10^7 PFU lead to a higher initial uptake (Figure 22a), although this also rapidly decreased over 5 weeks post viral injection (Figure 22b). This suggests that virally-mediated tumor cell death and/or necrosis, and thus hNIS functionality, is dose-dependent.

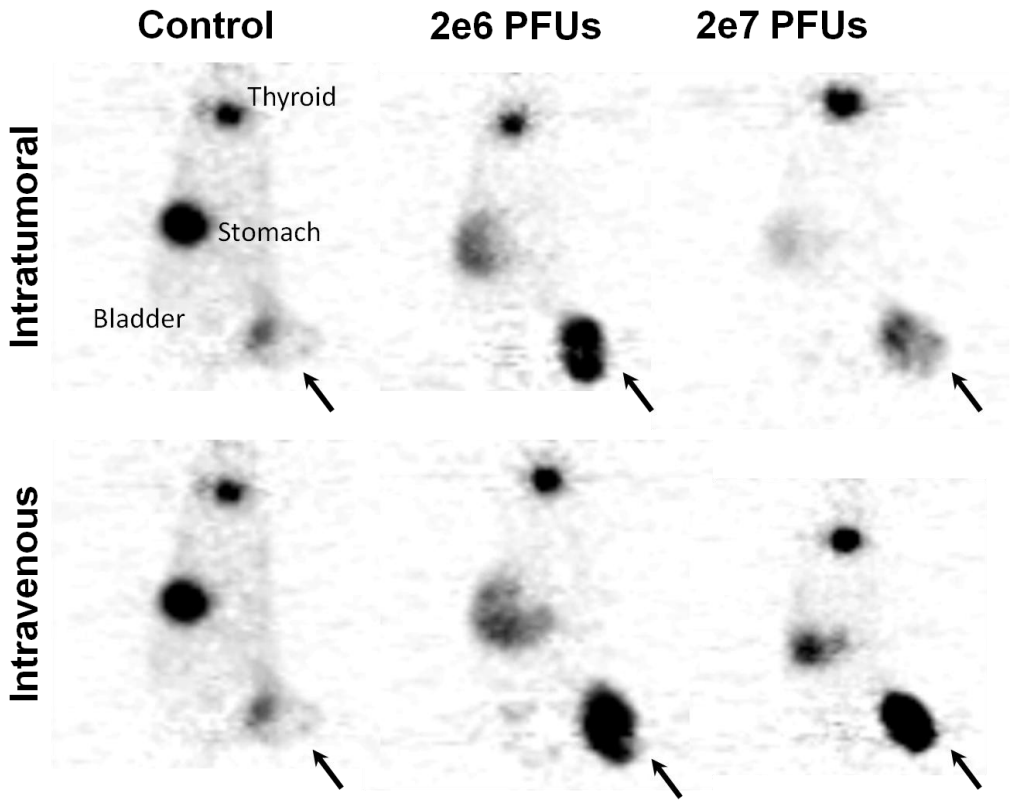

Figure 22a. Imaging of viral dose comparisons. Mice were injected IVly or ITly with 2 x 10^7 or 2 x 10^6 PFU of GLV-1h153 and imaged with ^{124}I-mediated PET 4 hours post radiotracer injection. The IT injection of 2 x 10^7 PFU caused a weaker initial signal than the IT injection with 2 x 10^6. However, injection IVly with 2 x 10^7 PFU lead to a strong initial signal similar to the 2 x 10^6 group.

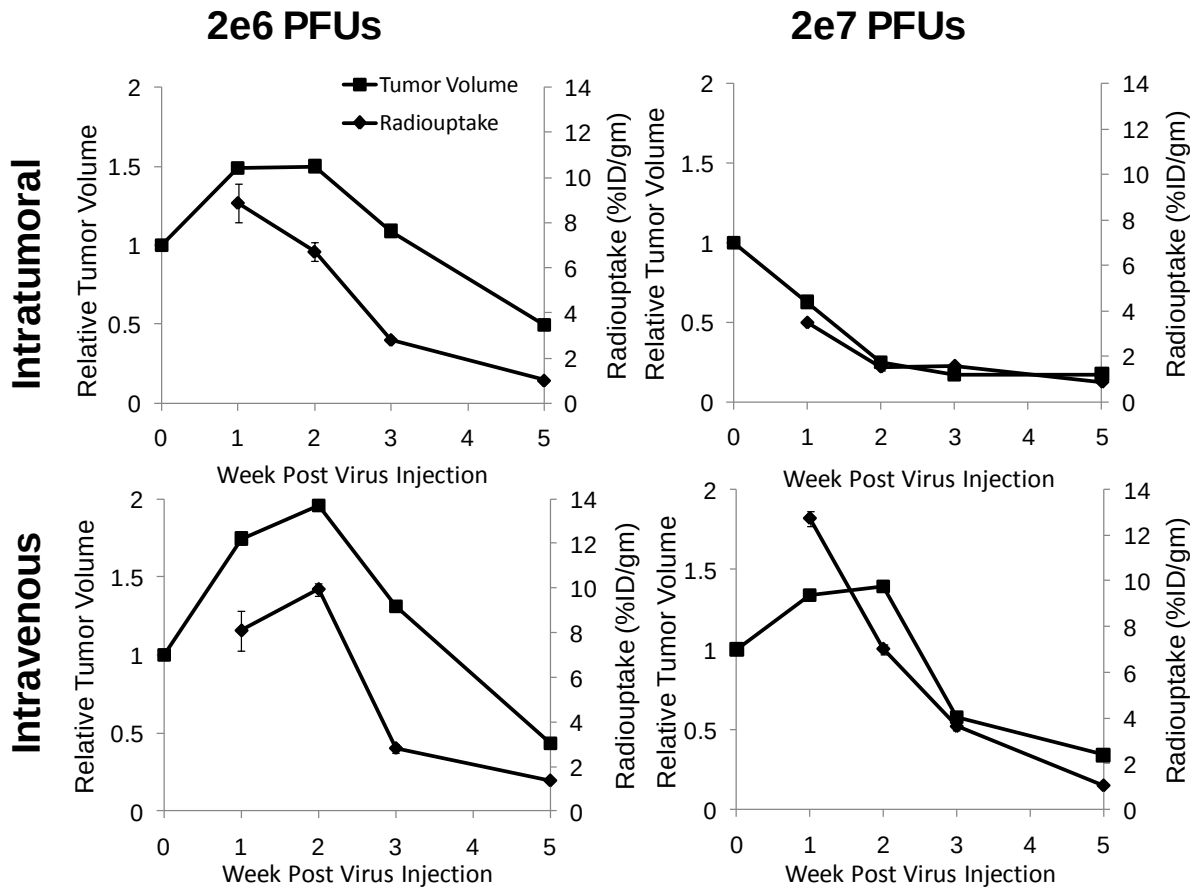

Figure 22b. Serial PET signal intensity and tumor growth characteristics of different viral doses. IT injection of 2 x 10^7 PFU causes a weaker initial and more rapid loss of signal than the IT injection with 2 x 10^6. Injection IVly with 2 x 10^7 PFU lead to a higher initial uptake which also rapidly decreased over 5 weeks post viral injection.

5.3.9 GLV-1h153 can be Detected Via $^{99m}TcO_4$-Mediated γ-Scanning.

To determine if GLV-1h153-mediated hNIS transfer can also be detected with $^{99m}TcO_4$, 3 groups of 2 animals each, bearing subcutaneous PANC-1 xenografts on the right hindleg, were injected IVly (2 mice) or ITly (2 mice) with 2×10^7 PFU of GLV-1h153, or PBS (2 mice). One mouse from each group was imaged with ^{124}I-mediated PET scanning and the other imaged with $^{99m}TcO_4$-mediated γ-scanning. Viral-mediated uptake was successfully detected and easily visualized with $^{99m}TcO_4$, although image resolutions were less than ^{124}I-mediated PET scanning (Figure 23). Like the PET images, uptake was also noted in the bladder due to radiotracer excretion, as well as the thyroid and stomach due to intrinsic hNIS expression.

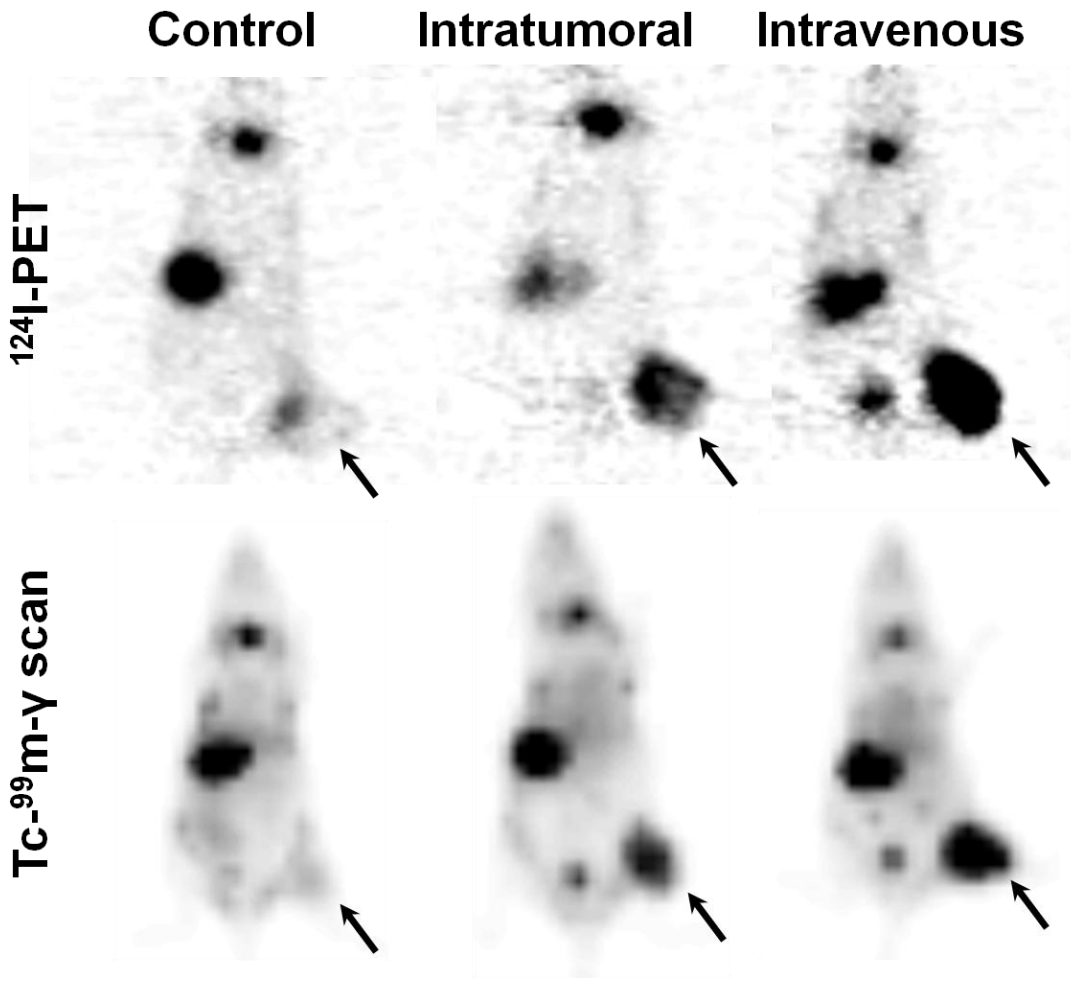

Figure 23. Detection of GLV-1h153 with TcO_4-mediated γ-scintigraphy. Three groups of 2 animals each bearing subcutaneous PANC-1 xenografts on the right hindleg, were injected IVly (2 mice) or ITly (2 mice) with 2 × 107 PFU of GLV-1h153, or PBS (2 mice). Mice were imaged ^{124}I-mediated PET or $^{99m}TcO_4$-mediated γ-scanning. Viral-mediated uptake was successfully detected and easily with $^{99m}TcO_4$-mediated γ-scintigraphy, ^{124}I-mediated PET scanning. Uptake was also noted in the bladder due to radiotracer excretion, as well as the thyroid and stomach due to intrinsic NIS expression.

5.3.10 hNIS-Mediated Uptake Requires Presence of Virus and Adequate Blood Flow.

To determine what conditions are therefore needed for adequate GLV-1h153-mediated radiouptake and retention in tumors, autoradiography was performed. Using $^{99m}TcO_4$ and γ-scintigraphy, 2 mice with tumors injected ITly with GLV-1h153 and 1 control mouse injected with PBS were imaged 2 days posttreatment. Mice were then IVly injected with hoechst dye to stain for blood flow, and tumors then harvested and sectioned in order to determine regions of uptake. The short viral treatment duration and localized IT administration enabled „hotspots“ of radiouptake in the tumor, which when compared to adjacent slices for GFP and hoechst staining revealed the need for both blood flow and GLV-1h153 infection to be present. Areas that lacked GFP (and thus virus), and areas noted to be necrotic on H&E staining with lack of blood flow did not support uptake. No uptake was noted in control tumors despite adequate blood flow (Figure 24a and 24b).

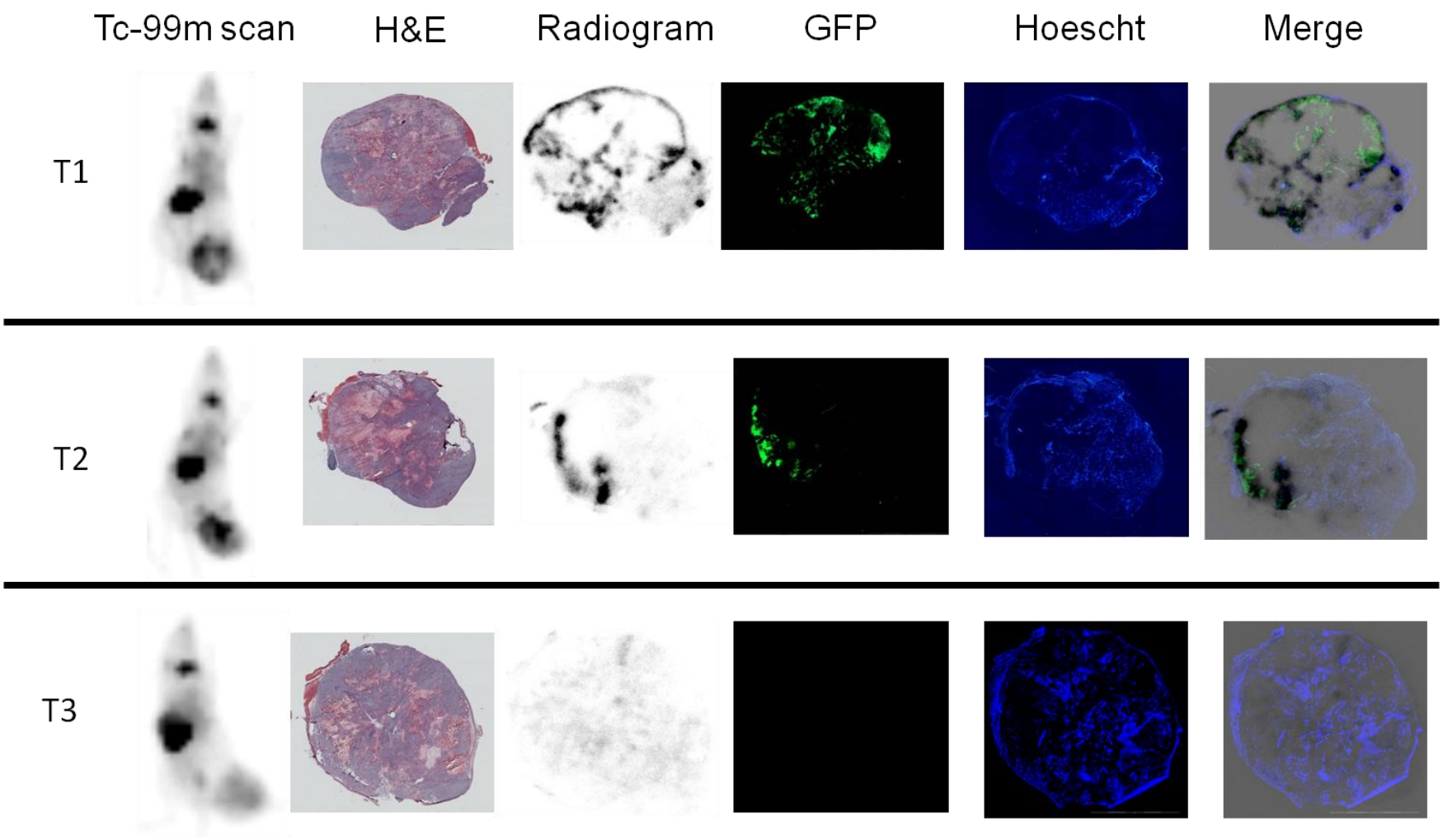

Figure 24a. Autoradioraphy of tumor samples injected with GLV-1h153. Using $^{99m}TcO_4$ and γ-scintigraphy, 2 mice with tumors injected ITly with GLV-1h153 and 1 control mouse were imaged 2 days posttreatment. Mice were then injected with hoechst dye to stain for blood flow and tumors harvested and sectioned in order to determine regions of uptake. „Hotspots“ of radiouptake in tumors (T1 and T2) correlated with GFP and hoechst staining revealing the need for both blood flow and virus to be present. Areas that lacked GFP (and thus virus), and areas noted to be necrotic on H&E stain with lack of blood flow did not support uptake. No uptake was noted in control tumors despite adequate blood flow (T3).

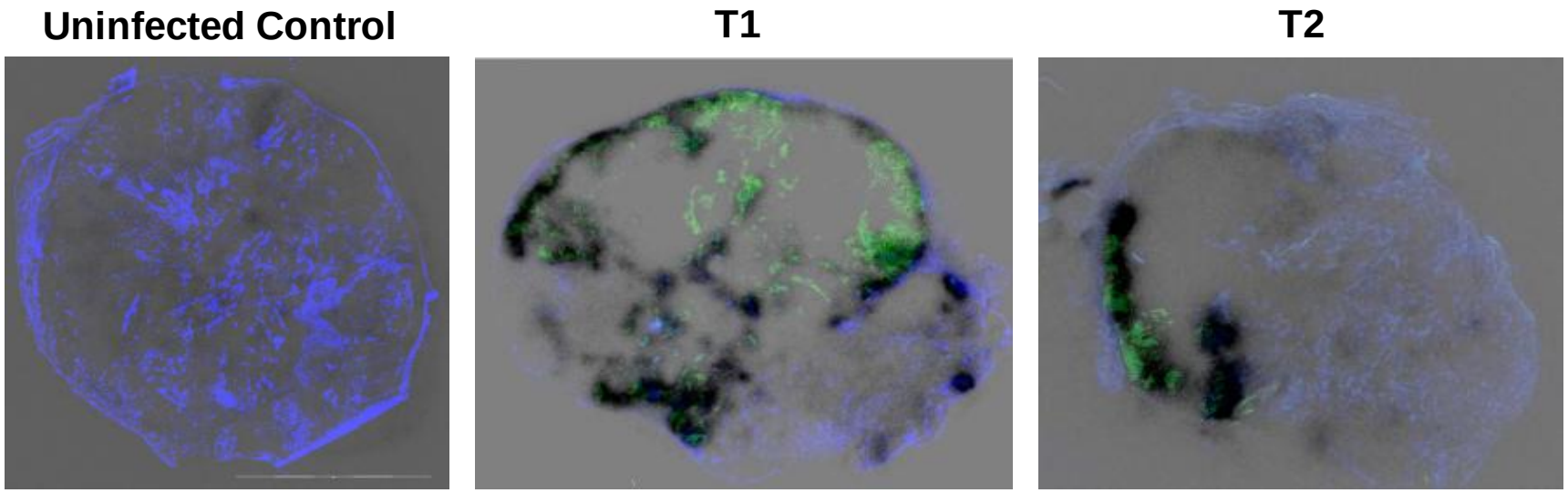

Figure 24b. Enlarged merged sections correlating areas of uptake hotspots with GFP and hoechst dye. Areas that lacked GFP (and thus virus) and areas noted to be necrotic on H&E stain with lack of blood flow (and thus hoechst staining) did not support uptake. No uptake was noted in control tumors despite adequate blood flow.

5.4 Specific Aim 4: To determine if combination therapy with GLV-1h153 and ^{131}I produces additive or synergistic tumor killing.

5.4.1 Time-Activity Curves.

To calculate absorbed doses in tumors, time-activity concentration data was generated from previous mice injected IVly or ITly with 2 x 10^6 PFU of GLV-1h153. Mice were serially imaged at 1, 4, 8, 24, 48, and 72 hours after radiotracer administration at 1 and 2 weeks post viral injection. At 1 week post virus injection, ^{124}I Uptake was maximal at 1 hour post radiotracer injection at an average of 8.39 ± 1.23 %ID/gm for the IV group and 10.81 ± 1.10 for the IT group. Uptake exponentially declined over 72 hours (Figure 25a and 5b). Interestingly, image and time activity data were similar in week 2, with a slight increased maximal 1 hour uptake of 10.14 ± 1.43 %ID/gm for the IV group and decreased maximal uptake of 8.05 ± 0.01 for the IT group (Figure 26a and 26b).

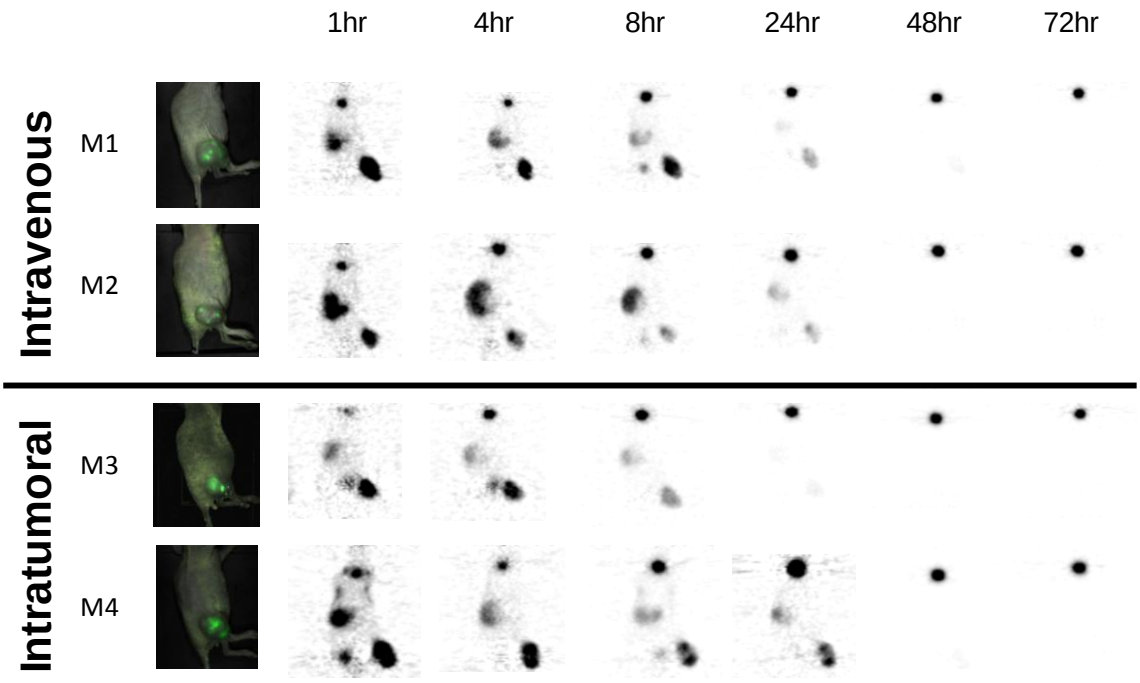

Figure 25a. Timing characteristics of radiouptake in GLV-1h153-infected PANC-1 xenografts 1 week post virus injection. Image signal was strongest 1 hour postinjection and gradually declined over 72 hours.

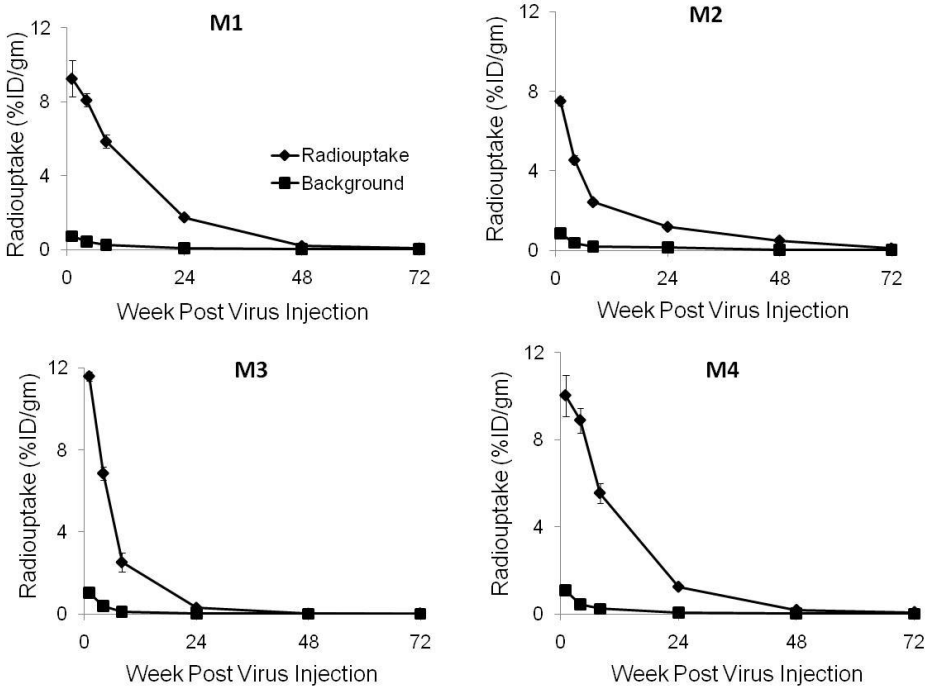

Figure 25b. Time activity concentration data generated from image-derived radiouptakes 1 week post virus injection. Time activity concentration data derived from serial images at 1 week post virus injection revealed a maximal radiouptake at 1 hour post radiotracer injection, with an exponential decrease in uptake over 72 hours.

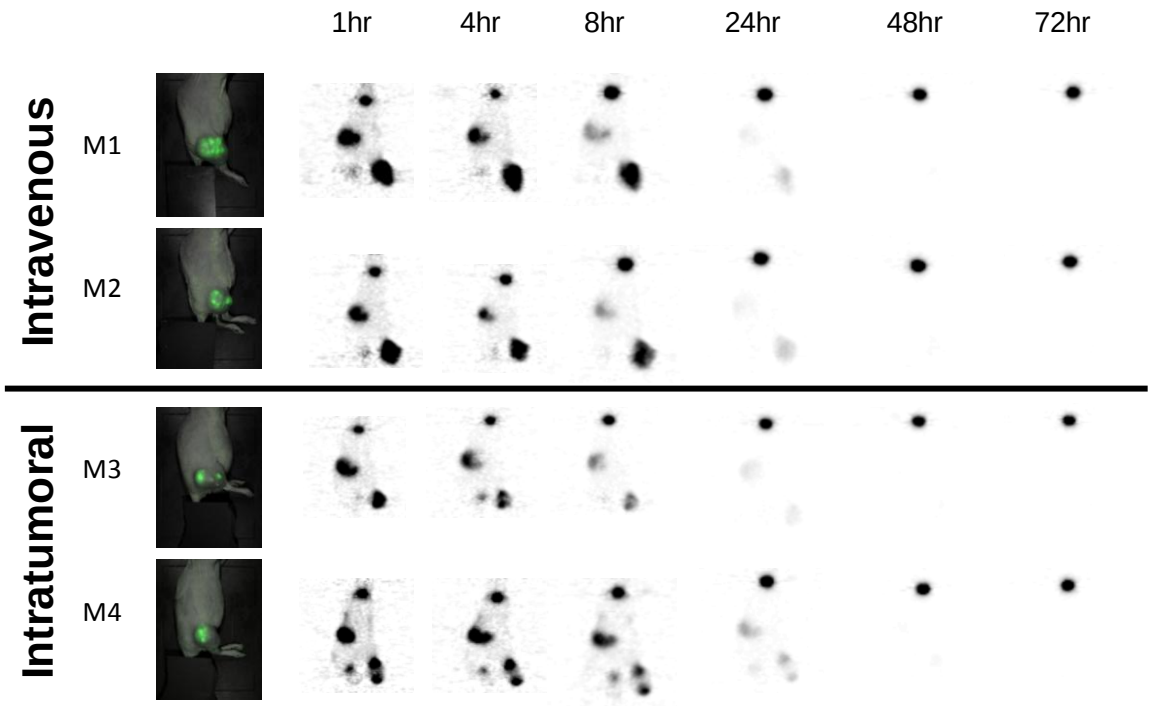

Figure 26a. Timing characteristics of radiouptake in GLV-1h153-infected PANC-1 xenografts 2 weeks post virus injection. Image signal was strongest 1 hour postinjection and gradually declined over 72 hours.

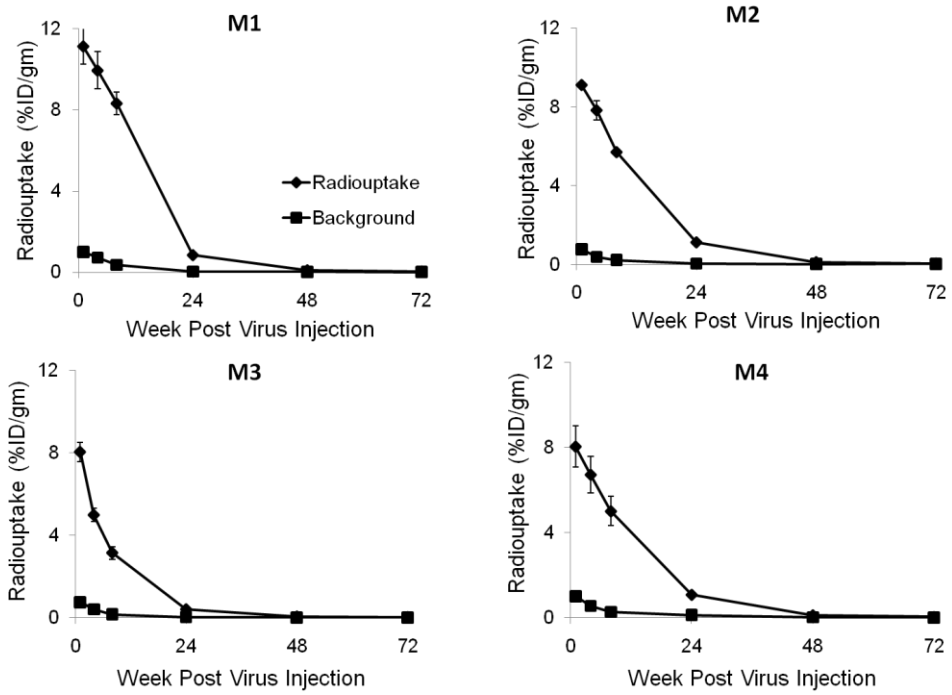

Figure 26b. Time activity concentration data generated from image-derived radiouptakes 2 weeks post virus injection. Time activity concentration data derived from serial images at 2 weeks post virus injection revealed a maximal radiouptake at 1 hour post radiotracer injection with an exponential decrease in uptake over 72 hours.

5.4.2 GLV-1h153 has Potential to Deliver Targeted and Therapeutic Radioiodine to Tumors.

To calculate absorbed doses in tumors, image-derived time-activity concentration data obtained above were corrected for radioactive decay to the time of injection and fit to exponential functions using least-squares regression. The ^{131}I cumulated activity concentrations (in uCi-hr/gm/uCi ^{131}I administered) were then calculated by integrating the fitted time-activity functions, incorporating the physical decay constant of ^{131}I. For the IV group, the average absorbed dose was 416.83 ± 130.68 rad/mci at week 1 and 514.57 ± 22.70 at week 2 post virus injection. The For the IT group, average absorbed doses were 387.02 ± 104.60 rad/mci at week 1 and 352.88 ± 95.45 at week 2. The absorbed dose at week 1 post virus injection appears higher in the IV group despite a lower maximal radiouptake, signifying longer retention time in the tumor. An estimated 2000 rad dose is required for a therapeutic effect to be seen in tumors. Therefore, in order to achieve a rad dose of 2000 in the IV-treated group 1 week post injection, around 4-5 mci of ^{131}I is required. Table 5 shows a summary of uptakes, effective ½ lives, and absorbed calculated doses in tumors.

.

Table 5. Dosimetric calculations of radiouptake in tumor xenografts.

			Week 1 Post Virus Injection							Week 2 Post Virus Injection						
			Uptake	Dosimetry						Uptake	Dosimetry					
				124I			131I				124I			131I		
				Effective 1/2 time (hr)		Absorbed dose (rad/mci)	Effective 1/2 time (hr)		Absorbed dose (rad/mci)		Effective 1/2 time (hr)		Absorbed dose (rad/mci)	Effective 1/2 time (hr)		Absorbed dose (rad/mci)
		Hour		1	2		1	2			1	2		1	2	
2e6 PFUs Ivtravenous	M1	1	9.26	7.39	65.08	**489**	7.68	98.21	**509**	11.14	5.65	53.48	**520**	5.82	73.99	**531**
		4	8.10							9.95						
		8	5.86							8.33						
		24	1.75							0.84						
		48	0.20							0.09						
		72	0.07							0.04						
	M2	1	7.52	2.54	15.17	**312**	2.58	16.46	**324**	9.13	7.39	65.08	**487**	7.68	98.21	**499**
		4	4.55							7.84						
		8	2.43							5.71						
		24	1.18							1.12						
		48	0.50							0.12						
		72	0.10							0.05						
2e6 PFUs Intratumoral	M3	1	11.58	3.35	65.08	**304**	3.41	98.21	**313**	8.04	4.63	65.08	**273**	4.74	98.20	**285**
		4	6.86							4.99						
		8	2.53							3.15						
		24	0.31							0.41						
		48	0.04							0.06						
		72	0.03							0.03						
	M4	1	10.03	4.75	16.57	**452**	4.87	18.12	**461**	8.05	7.39	65.08	**407**	7.68	98.21	**420**
		4	8.89							6.73						
		8	5.55							5.01						
		24	1.24							1.09						
		48	0.18							0.13						
		72	0.08							0.05						

5.4.3 Combining GLV-1h153 and Radioiodine Mediates Greater Therapeutic Efficacy.

For the combination therapy experiment, PANC-1 xenografts were established in the right hind leg in five groups of mice: GLV-1h153, GLV-1h153 + ^{131}I, GLV-1h68, GLV-1h68 + ^{131}I, and PBS control. Based on previous imaging and dosimetric calculations, one week following IV injection of 2x10^{6} PFU of GLV-1h153 or control virus GLV-1h68, treated groups were administered ~5 mCi of ^{131}I by a single IV injection in order to achieve an absorbed dose of around 2000 rads in tumors. Control tumors continued to grow, and while GLV-1h153, GLV-1h68, and GLV-1h68 +^{131}I mediated similar therapy effects, the GLV-1h153 +^{131}I group seemed to have more rapid and greater tumor regression (Figure 27). This effect, however, was not statistically significant.

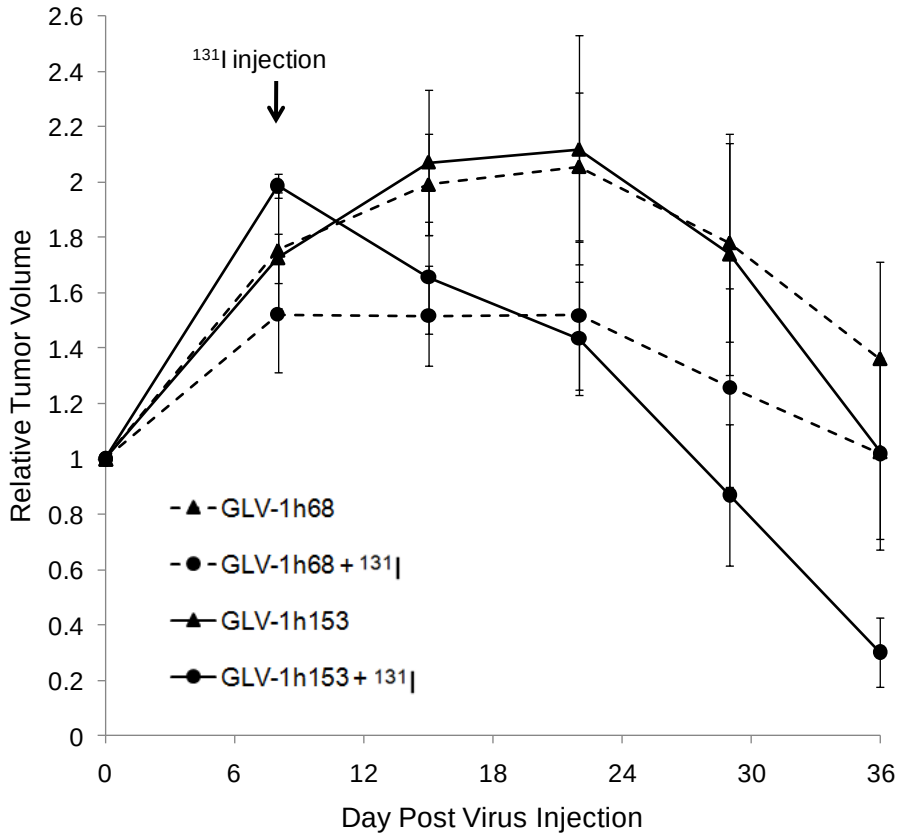

Figure 27. Combination therapy with GLV-1h153 and ^{131}I. For the radiotherapeutic experiment, PANC-1 xenografts were established in the right hind leg in five groups of mice: GLV-1h153 (4 mice), GLV-1h153 + ^{131}I (3 mice), GLV-1h68 (4 mice), GLV-1h68 + ^{131}I (3 mice), and PBS control (5 mice, not shown in graph). One week following IV injection of 2x10^{6} PFU of GLV-1h153 or control virus GLV-1h68, treated groups of mice were administered 5 mCi of ^{131}I by a single IV injection. GLV-1h153, GLV-1h68, and GLV-1h68 +^{131}I mediated similar therapy effects, while the GLV-1h153 +^{131}I group seemed to have more rapid and greater tumor regression.

6.0 DISCUSSION

Twelve million people worldwide will be diagnosed with cancer this year, and 7 million will die from cancer-related causes despite advances in conventional therapies[1]. Therefore, developing novel therapies, which may also work synergistically in combination with conventional treatment options, is vital. Oncolytic viral therapies have made their mark on the cancer research world as another potential therapeutic option, with the possible advantages of lessening side effects as well as strengthening treatment efficacy due to higher tumor selectivity[9]. Results have been so promising that oncolytic viral treatments have now been approved for clinical trials in several countries[280], and the first oncolytic viral therapy has now been marketed as a treatment for head and neck cancers in China[284]. Pancreatic cancer in particular is a deadly disease with poor response single agent or combination chemotherapies, and explains the active investigation underway seeking novel therapeutic strategies for this disease[6, 7].

Several clinical trials are underway to assess the effects of viral therapies[280]. However, future clinical studies may benefit from the ability to noninvasively and serially identify sites of viral targeting and to measure the level of viral infection in order to provide important safety, efficacy, and toxicity information[135, 285, 286]. Such real-time tracking would also provide useful viral dose and administration schedule information for optimization of therapy and would obviate the need for multiple and repeated tissue biopsies.

VACV is arguably the most successful biologic therapy agent, since versions of this virus were given to millions of humans during the smallpox eradication campaign[46]. More recently, engineered VACVs have also been successfully used as direct oncolytic agents, capable of preferentially infecting, replicating within, and killing a wide variety of cancer cell types[9, 43, 72, 96, 97, 110, 287-290]. Vaccinia displays many of the qualities thought necessary for an effective oncolytic antitumor agent[77, 289, 291]. In particular, the large insertional cloning capacity allows for the inclusion of several functional and therapeutic transgenes. With the insertion of reporter genes not expressed in uninfected cells, viruses can be localized and the course of viral therapy monitored in patients.

One such promising virus strain is GLV-1h68. This strain has shown efficacy in the treatment of breast tumors[43], mesothelioma[96], pancreatic cancers[72], anaplastic thyroid cancer[97, 287], and melanoma[110], and is currently being tested in phase I human trials with substantial data showing promising safety and therapeutic responses[280].

This work centers on the generation of a novel recombinant VACV, GLV-1h153, derived from GLV-1h68, which has been engineered for specific targeted treatment of cancer and the additional capability of facilitating noninvasive imaging of tumors and metastases. To date, GLV-1h153 is the first vaccinia oncolytic virus expressing the hNIS protein that can efficiently eliminate tumors and simultaneously facilitate deep tissue imaging of infected tumors.

The reporter gene chosen for insertion into GLV-1h153 was based on the already successful PET and SPECT imaging characteristics of the hNIS and carrier free radioiodine reporter imaging system. hNIS is an intrinsic plasma membrane protein which mediates the active transport and concentration of iodide in the thyroid gland cells and some extra-thyroidal tissues[166, 167, 292, 293]. It is also one of several human reporter genes currently being used in preclinical studies and has even been used in clinical studies imaging adenoviral-mediated hNIS transfer in prostate cancer[269, 280]. hNIS gene transfer via viral vector may allow infected tumor cells to concentrate several radionuclide probes which have long been approved for human use. The hNIS's transporter based system also allows signal amplification rather than, for example, a 1:1 binding relationship with radiolabelled ligands as seen with the human somatostatin receptor hSSTR2[120]. Furthermore, imaging with hNIS has been comparable to the commonly used *HSV1-tk* reporter gene[179] and correlated with $^{99m}TcO4$[180].

Oncolytic viruses encoding hNIS that have been investigated to date include several adenoviruses[263, 264, 266-268] and measles viruses[270-276], as well as a vesicular stomatitis virus (VSV)[278]. Results have been promising; however, there are several disadvantages to each strain. Although it can transduce a broad spectrum of cells with high infection efficiency, lack of replication and tumor transduction capacity due to gene insertion have limited clinical application of adenoviruses. Uptake in tumors has required high MOIs of initial virus administration, and imaging signals in tumors often did not last beyond 5 days[263, 264, 266]. Furthermore, the capsid proteins of adenoviral vectors have been found to be toxic to host cells and may raise host immune response against infected cells in humans. Therefore, the safety of adenoviral vectors has been questioned[294]. Similarly, measles viruses have also been reported to have inefficient transduction within tumors, when investigations of possible synergistic application of MV-*NIS* and radioiodine failed to produce synergistic therapeutic effects[276]. The VSV encoding hNIS also showed promise. However, VACV's safety profile is unsurpassed, and its high replication capacity and efficient cell to cell spread may enable it to overcome many of the limitations with other oncolytic viral vectors.

It has been previously discussed[86] that VACV gene transcription occurs in a temporal manner, with early genes transcribed within the core of the virus particle soon after infection, whereas intermediate and late genes transcribe in the cytoplasm of infected cells after viral DNA replication[295]. Early, intermediate, and late mRNA synthesis was detectable within 20, 100, and 140 minutes of infection, respectively. The strength of VACV promoters, early (PE), synthetic early/late (PE/L), and synthetic late (PL) also varies. PE is the weakest among these three but is stronger than native early promoters, whereas PE/L has been found to be comparable to or slightly stronger than PL. We initially attempted to generate recombinant VACVs expressing the hNIS protein under the control of all three promoters (PE, PE/L and PL) in order to evaluate the effect of the levels and temporal manner of the hNIS protein expression on virus replication, therapy, and imaging. The use of PE/L or PL at the HA locus failed to generate any recombinants, as overexpression and/or constitutive expression of hNIS seemed to be toxic to the virus. We were able to generate, however, a recombinant virus strain that expressed the hNIS protein under the control of PE, GLV-1h153.

GLV-1h153 was effective at infecting, replicating within, and killing PANC-1 cells in cell culture and eradicating tumor xenografts as efficiently as parental virus GLV-1h68. This indicated that insertion of the hNIS protein did not negatively affect virus replication in animal models which was already the case in cell culture, or the cytolytic activity in cell culture and virotherapeutic efficacy in tumor xenografts. Since the genes exchanged under the HA locus were both under the control of the early promoter PE, these results are not surprising. Furthermore, similar effects were seen between the IT and IV groups treated with GLV-1h153 or GLV-1h68, indicating the inherent affinity of both genetically modified vaccinia viruses to tumors. Administration of GLV-1h153 did not have any significant effects on mean net body weights of the animals 34 days after treatment, with the IT group even gaining weight as compared to untreated control. Furthermore, viral distribution revealed persistence of viral infection of tumors even 5 weeks after viral administration at ~10^9 viral particles per gram tissue, with most of the virus cleared from all other organs and trace residual amounts found in the lung and kidney.

Microarray analysis revealed an almost 2000-fold change increase in hNIS mRNA and an almost 5000-fold change increase by 24 hours after PANC-1 infection with GLV-1h153 at a multiplicity of infection of 5.0. Western blot studies showed hNIS protein expression as a band between 75 and 100 kDa in PANC-1 cells infected with GLV-1h153, with higher concentrations of the protein at higher MOIs. This band also appears in normal human thyroid lysates which should contain intrinsic hNIS protein, at a slightly lower molecular weight, which is likely explained by differences in glycosylation within cells[168]. Differences in

the expected weight of 97 kDa was seen by other groups, with most also obtaining a band between 75 – 100kDa [172, 261, 296, 297]. The hNIS protein was successfully transported and inserted into the cell membrane, as demonstrated by fluorescence microscopy.

In cell culture, GLV-1h153-mediated expression of the hNIS protein in infected PANC-1 cells resulted in specific uptake of the radiotracer ^{131}I in a time and dose-dependent manner, indicating that the hNIS protein was functional, The uptake levels were lower in the GLV-1h153–infected cells compared with the NIS-expressing rat thyroid cell line PCCL3, however, in viral-treated cultures, it is likely that not all cells are simultaneously infected with virus and express the reporter gene during the early phase of viral infection. During the late, prelytic phase of viral infection (48 hours and beyond), the hNIS transporter could be impaired due to loss of cell membrane integrity, and following cell lysis, the accumulated ^{131}I radiotracer would be lost. Thus, there seems to be a relatively narrow window, ~24 to 48 hours after viral infection of PANC-1 cells, during which the hNIS reporter is maximally functional in cell culture at an MOI of 1.0. These results reflect the dynamic state between viral infection, replication, and lysis of tumor cells, and were also seen with the hNET-expressing virus GLV-1h99[86, 159].

In mice, PANC-1 tumors infected with GLV-1h153 were readily detectable by PET, with no enhancement above background of either GLV-1h68- or PBS-treated tumors. Mice were treated intratumorally with GLV-1h153, non-hNIS expressing parent virus GLV-1h68, and PBS, and imaged 48 hours after with carrier free 124I. The quantitative ^{124}I-PET showed that the three GLV-1h153-infected PANC-1 tumors were readily detectable with an average uptake of 3.82 ± 0.46 %ID/gm 1 hour after radiotracer administration, and no enhancement above background of either GLV-1h68- or PBS-treated tumors. Presence of virus in tumors was also readily visualized via GFP and bioluminescence imaging. It should be noted that the whole tumor is only partially infected with virus and tumor cells are at different stages of virus infection at any given time (shown by immunohistochemistry).

The timing of PET imaging after ^{124}I administration was also shown to be important, as radioactivity levels (% ID/gm) in GLV-1h153-infected tumors was highest during the first 1-hour period after tracer administration. This difference is likely the effect of a degree of radioefflux from cells, however, the tumor uptake to background ratio actually increased in tumors with time, suggesting adequate retention of radioiodine even 8 hours after radiotracer injection. This was also seen with other hNIS-encoding viruses[264, 270, 271]. An exception was the adenovirus Ad5/3-24-hNIS, which retained its maximal uptake value 13 hours post injection[265]. Enhanced radiouptake in GLV-1h153-injected tumors compared to other organs,

as well as GLV-1h68- and PBS-injected tumors was confirmed in these mice via tissue radiouptake assay at 8 hours post radiotracer administration, and correlated well with quantative PET.

After establishing that GLV-1h153 enhances radiouptake in tumors in animal models, is detected by PET, and induces radiouptake retention, the potential of GLV-1h153 for serial imaging and monitoring of both IT and systemic viral therapy was assessed. PET imaging readily detected virus replication in tumors as late as 5 weeks post injection. This is in contrast to some studies with other oncolytic viruses such as measles and adenoviruses, which had signals lasting only around 5 days post virus injection[263, 267, 275]. Other studies, on the other hand, reported the ability of hNIS signal to be detected as far as 30 days post virus treatment[268, 273]. Further, hNIS-mediated radiouptake with GLV-1h153 seemed to peak at 2 weeks, and gradually decline by week 3 and 5 in both the IT and IV injected groups. This is interesting, as although the signal timing pattern in the IV group was similar to other what others have found, such as with VSV (51)-NIS and MV-NIS[273, 278], the IT group had a much more prolonged uptake enhancement. This may be due to the fast replication and spread of vaccinia, and could also be due to more rapid cell lysis caused by intratumoral injection of the other viruses, which would compromise cell membrane integrity and thus hNIS functionality. It should be noted that it is difficult to compare exact values found with other oncolytic viruses, as dose effects may differ and are unlikely to be directly comparable. Decrease in signal enhancement with GLV-1h153 was despite persistent strong GFP expression by 5 weeks posttreatment. GLV-1h153-mediated radiouptake was confirmed via GFP, bioluminescence, and CT-PET imaging 1 and 2 weeks post viral injection in both the IV and IT groups. All reporter genes were detectable, and fusion of PET and CT images correlated enhanced signals anatomically to the location of the tumor, stomach, bladder, and thyroid.

When comparing PET signal intensity with tumor growth patterns in mice over 5 weeks, enhanced radiosignal appears to correlate with the initial tumor growth, retardation, and eventual regression phases. The PET signal remained strong during the first 2 weeks postinjection of virus, which reflected initial tumor growth. However, when tumor growth began entering a retardation phase, PET signal began to decrease and almost disappear by week 5, when tumors have entered the regression phase. Correlation of hNIS-mediated uptake and signal patterns was not explored in any other paper investigating oncolytic viruses encoding hNIS. It is known that some delay occurs before an actual difference in tumor size is noted even after cell death and or necrosis has occurred post viral treatment. The only exception was one ITly-treated mouse (M3), where signal persisted up to 5 weeks

post GLV-1h153 injection, with an initial decrease in signal suggesting initial cellular death, and re-increase in signal, suggesting further tumor cellular proliferation within the tumor. Interestingly, the tumor took longer to regress, and maintained a signal up to 5 weeks post virus injection. These data suggest that the *hNIS* reporter gene is able to give insight into the biological activity of tumor cells, and whether cell death or necrosis is occurring. Non-viability of cells and loss of cell membrane integrity is likely to affect functionality of the hNIS protein as shown in cell culture radiouptake experiments, while the GFP reporter protein simply suggests viral activity, and once produced seems to persist despite non-viability of tumor cells. A similar pattern was observed in the cell culture ^{131}I uptake studies, showing decreasing radiotracer uptake at later time points after GLV-1h153 infection also likely due to cell lysis and loss of cell membrane integrity.

Histology of serially imaged tumors confirmed wide areas of necrosis and inflammatory infiltrate. Necrotic areas were more homogenous in the IVly-treated group, whereas „islands“ of necrosis surrounded by inflammatory infiltrate was seen in the IT group, reflecting virus route of administration. Interestingly, no viable cells were detected histologically in all mice tumors except M3 which retained viable tumor proliferation activity. This may again explain lack of PET signal in the other imaged mice at 5 weeks post virus injection, and persistence of signal in M3. However, it is known from previous viral biodistribution assays that virus can persist at even 5 weeks post injection. This may be explained by the fact that virus particles can persist in the tumor microenvironment despite non-viability of actual tumor cells, but like the GFP signal, persistence of virus does not give insight into the biological activity occurring in the tumor cells in response to viral therapy. Further, when higher doses of virus are used, ^{124}I-mediated PET signals declined more rapidly than with lower doses, suggesting that cell death occurs more rapidly with higher doses of virus, especially in the IT groups. This again correlated with more rapid tumor retardation and regression. This suggested that virally-mediated tumor cell death and/or necrosis, and thus hNIS functionality, is dose dependent, which was also seen in our in cell culture radiouptake assay.

To determine what conditions are therefore needed for adequate GLV-1h153-mediated radiouptake and retention in tumors, autoradiography was performed utilizing $^{99m}TcO_4$-mediated Gamma scintigraphy and autoradiography. Areas that lacked GFP, and thus virus, and areas noted to be necrotic on H&E staining with lack of blood flow did not support uptake. Necrosis could have been virally-mediated or intrinsic due to tumor enlargement. However, this further may explain the loss of signal noted with serial monitoring of infected tumors, as necrotic areas occurring secondary to viral treatment lacked blood flow and likely

functional cell membranes, and thus are unlikely to facilitate hNIS-mediated uptake in tumors. No GFP and no uptake were noted in uninfected control tumors despite adequate blood flow.

Time-activity concentration data over 72 hours post radiotracer injection generated from imaged mice revealed that ^{124}I uptake was maximal at 1 hour post radiotracer injection at an average of 8.39 ± 1.23 %ID/gm for the IV group and 10.81 ± 1.10 for the IT group1 week post virus injection. Uptake declined over 72 hours in a classic exponential manner, but could still be visualized at 24 and even 48 hours after radiotracer injection. Interestingly, image and time activity data were similar in week 2, with a slight increased maximal 1 hour uptake of 10.14 ± 1.43 %ID/gm for the IV group and decreased maximal uptake of 8.05 ± 0.01 for the IT group. The decreased uptake in the IT group by week 2 may be due to more rapid cell death occurring in the tumors. Uptakes seem to be similar to those mediated by all MV-NIS papers and some adenoviruses, but were also much lower than some reported[278], especially when diet was supplemented with thyroxine and low iodine intake[265]. This highlights the potential of maximizing radioiodine uptake by blocking intrinsic hNIS uptake in the stomach and thyroid.

Absorbed doses from image-derived time-activity concentration data of GLV-1h153-infected PANC-1 tumors were then calculated assuming ^{131}I treatment. The average absorbed doses were 387.02 ± 104.60 rad/mci at week 1 and 352.88 ± 95.45 at week 2 for the IT group. The absorbed dose at week 1 post virus injection appears higher in the IV group despite a lower maximal radiouptake, signifying longer retention time in the tumor. An estimated 2000 rad dose is required for a therapeutic effect to be seen in tumors. Therefore, in order to achieve a rad dose of 2000 in the IV-treated group 1 week post injection, around 4-5 mci of ^{131}I was estimated to be required. These results are similar to those with MV-NIS in the treatment of prostate cancer, with a calculated absorbed dose of 420 and 540rads/mci if injected IT or IV[273]. However, absorbed doses of over 1000 has been calculated with MV-NIS[276] and VSV[278]. This could be due to thyroxine supplementation in MV-*NIS*, but this was not the case with VSV. Other factors could include greater viral replication at injected doses, or stronger promoter expression of hNIS by these viruses.

Combination therapy of GLV-1h153 and ^{131}I revealed a modest additive effect over GLV-1h153 alone. While GLV-1h68, and GLV-1h68 with ^{131}I mediated similar therapy effects, the GLV-1h153 with ^{131}I group seemed to have more rapid and greater tumor regression. This effect, however, was not statistically significant. This is in contrast to several other papers showing the potential of enhanced treatment efficacy by combining ^{131}I treatment with hNIS

encoding OVs in several different tumor models[265, 266, 270, 273, 276, 278]. This could be due to several factors, including the study not being sufficiently powered, possible lack of radiosensitivity of PANC-1 to radioiodine, lack of complete tumor transduction by virus, and large tumor volume. A likely explanation, however, is that lower doses of virus are needed to show an additive or synergistic effect, as the virus appears to work very well on its own at the selected dose of 2×10^6 PFU. Further work is required to assess the optimum doses of virus to be combined with radiotherapy in order to obtain an additive or synergistic effect.

As with any translational therapy, concerns over immune responses remain. Since *hNIS* is a human derived gene, it is unlikely to be immunogenic[138]. However, application of GLV-1h153-mediated hNIS transfer raises concerns over the possibility of autoimmunity in patients. Several papers have already shown that hNIS is not a major candidate for autoimmune disease in patients with patients with Graves' disease and Hashimoto's thyroiditis[298, 299]. Moreover, the clinical trial assessing adenoviral-mediated hNIS transfer in humans did not report any serious adverse effects due to autoimmunity in patients treated for prostate cancer[269]. Further studies and caution are needed to assess the potential of autoimmunity with hNIS transfer in humans.

7.0 CONCLUSIONS

The two most important factors that eventually determine the clinical safety and efficacy of any cancer therapeutic are tumor selectivity and anti-tumor potency. Vaccinia virus strains are a promising oncolytic virotherapy candidate capable of producing potent antitumor effects via cell lysis as well as tumor rejection by stimulating antitumoral immunity. So far, clinical trials with oncolytic vaccinia virus constructs indicate that oncolytic vaccinia viruses are generally safe and well tolerated in patients with advanced tumors, with certain degrees of antitumoral activity demonstrated. However, efforts are still needed to further improve safety and efficacy. With many oncolytic viral constructs currently being tested in varied phases of clinical trials, intense efforts are now being dedicated to improve efficacy, ability to non-invasively monitor therapy, and combine virotherapy with existing treatments for human malignancies.

The GLV-1h153 vaccinia construct is a promising candidate for future clinical studies combining deep tissue imaging and oncolytic virotherapy. This novel new oncolytic VACV engineered to carry the human sodium iodide symporter gene (*hNIS*) can successfully replicate within pancreatic cancer cells as efficiently as its parental virus GLV-1h68, and expresses the hNIS reporter gene, which readily facilitated ^{131}I radiouptake in cells. The cytotoxicity and safety, as well as tumor-specific imaging, has also been shown following treatment of pancreatic tumor xenografts with GLV-1h153. GLV-1h153-treated pancreatic tumors were readily imaged with the clinically approved radiopharmaceutical ^{124}I and PET, as well as $^{99m}TcO_4$–mediated gamma scintigraphy. Furthermore, radioiodine dose accumulation and retention time in infected tumors reached potentially therapeutic levels, and combination of GLV-1h153 and ^{131}I seems promising for more rapid and potent tumor regression.

Thus, the ability of GLV-1h153 to infect and image pancreatic cancer, a uniformly fatal disease resistant to conventional therapy, justifies further studies as well as the initiation of clinical trials. Further, this imaging system could be directly translated to human studies, and clinical trials of oncolytic viral therapy would benefit from this noninvasive monitoring modality. These findings also warrant further investigation into possible synergistic or additive effects of radioiodine combined with this novel new treatment and imaging modality. Further investigation is required into the effects of viral dose, tumor size, and metastatic disease on imaging capability and potential for targeted radiotherapy with this novel virus.

CURRICULUM VITAE

Personal Information:

Name:	Dana Haddad
Date of Birth :	26.02.1984
Place of Birth:	Kuwait City
Nationality:	New Zealander
Address:	504 E 81st Street Apartment 3E New York, NY 10028 USA

Education:

01/1996 – 11/2000	High School Bursary Dipolma, Macleans College, Auckland, New Zealand

Higher Education:

03/2001 – 11/2003	Bachelor of Human Biology, The University of Auckland, Auckland, New Zealand
03/2004 – 11/2006	Bachelor of Medicine, Bachelor of Surgery (Dr. Med), The University of Auckland, Auckland, New Zealand

Doctoral Studies:

03/2008 – the present	Doctoral studies supervised by Professor Aladar A. Szalay, Julius-Maximilians-Universität, Würzburg, Germany; Memorial Sloan-Kettering Cancer Center, New York, USA; and Genelux Corporation, San Diego, USA

LIST OF ORIGINAL PUBLICATIONS

Reviews

Worschech A, **Haddad D**, Stroncek DF, Wang E, Marincola FM, Szalay AA. The immunologic aspects of poxvirus oncolytic therapy. Cancer Immunology Immunotherapy. 2009 Sep; 58(9): 1355-1362. Cited in PubMed; PMID: 19266198.

Carson J, **Haddad D**, Bressman M, Fong Y. Oncolytic herpes simplex virus 1 vectors: Increasing treatment efficacy and range through strategic virus design. Drugs of the Future. Publication Status: Accepted

Book Chapter

Haddad, D., Gentschev, I., Stritzker, J., Szalay, A.A. (2010). Cancer therapy and diagnostics (theranostics) following treatment with recombinant oncolytic vaccinia virus strains. In R.M. Mohan (Ed.), *Research Advances in Biotechnology and Bioengineering* (pp. In Press). Kerala, India. Global Research Network.

Manuscripts

Haddad D*, Chen N*, Zhang Q, Chen C, Yu YA, Gonzalez L, Carpenter SG, Carson J, Au J, Mittra A, Gonen M, Zanzonico P, Fong Y, Szalay AA. (2011, March). Insertion of the human sodium iodide symporter to facilitate deep tissue imaging does not alter oncolytic or replication capability of a novel vaccinia virus. Accepted by the Journal of Translational Medicine.

Gholami S***, Haddad D***, Chen C, Chen N, Zhang Q, Zanzonico P, Szalay AA, Fong Y. (March 2011) Novel therapy for anaplastic thyroid carcinoma cells utilizing an oncolytic vaccinia virus carrying the human sodium iodide symporter. Submitted to the Journal of Surgery.

Posters

Haddad, D., Chen, N., Zhang, Q., Chen, C., Chen, C., Yu, Y., Stritzker, J., Carpenter, S., Gonzalez, L., Aguilar, J., Au, J., Mittra, A., Zanzonico, P., Szalay, AA., Fong, Y. (2010, October). Imaging and treating pancreatic cancer with an oncolytic vaccinia virus carrying the human sodium iodide symporter. Poster presentation finalist at: Memorial Sloan-Kettering Cancer Symposium; New York, NY.

Abstracts

Haddad, D., Chen, N., Zhang, Q., Chen, C, Yu, Y., Stritzker, J., Carpenter, S., Gonzalez, L., Aguilar, J., Au, J., Mittra, A., Zanzonico, P., Szalay, AA., Fong, Y. (2011, May). Imaging and treating pancreatic cancer with an oncolytic vaccinia virus carrying the human sodium iodide symporter. Oral Presentation accepted for: The American Society of Gene and Cell Therapy. Seattle, WA, USA

Carson J,, **Haddad D.**, Gholami S., Chen N,, Seung TJ., Jun K., Au J., Rusch VW., Szalay AA., Fong Y. (June 2011) The hNIS expressing oncolytic virus GLV-1h153 is a promising agent for the imaging and treatment of non-small cell lung cancer. Oral Presentation accepted for: The Western Thoracic Surgical Association. Colorado Springs, Colorado, USA.

Gholami S**, Haddad, D**., Chen, C., Chen, N., Zhang, Q, Zanzonico, P., Szalay, AA., Fong, Y. (2011, April). Novel therapy for anaplastic thyroid carcinoma cells utilizing oncolytic vaccinia virus carrying the human sodium iodine symporter. Oral Presentation accepted for: The American Society of Endocrine Surgeons. Houston, TX, USA

Haddad, D., Chen, N., Zhang, Q., Chen, C., Gonzalez, L., Aguilar, J., Li, P., Wong, J., Szalay, AA., Fong, Y. (2011, March). A novel genetically modified oncolytic vaccinia virus is effective against a wide range of human cancers and is safe when administered *in vivo*. Oral Presentation presented at: Society of Surgical Oncology. San Antonio, TX, USA.

Haddad, D., Carpenter, S., Socci, N., Fong, Y. (2011, October). Molecular network pathway and functional analysis of tumor signatures associated with colon cancer stem cells. Oral Presentation presented at: American College of Surgeons Surgical Forum; Washington, D.C., DC, USA.

Haddad, D., Song, T.J., Adusumilli, P., Kim, T., Hezel, M., Mullerad, M., Chan, M., Socci, N., Gonen, M., Fong, Y. (2009, October). Molecular network pathway and functional analysis of tumor signatures associated with development of resistance to viral gene therapy. Oral Presentation presented at: American College of Surgeons Surgical Forum; Chicago, IL, USA.

ACKNOWLEDGMENTS

This work was carried out at the Department of Biochemistry, The University of Wuerzburg, Bavaria, Germany, the Department of Surgery at Memorial Sloan-Kettering Cancer Center, New York, New York, USA, and Genelux Corporation at San Diego Science Center, San Diego, California, USA, and between March 2008 and March 2011. This study was supported financially by grants from the University of Wuerzburg, Memorial Sloan-Kettering Cancer Center and Genelux Corporation.

This work could not have been accomplished without the help of the people on the next few pages, to which I extend my sincerest thanks and gratitude.

I would like to acknowledge the University and the Graduate School of Life Sciences for giving me the opportunity to start my PhD program at the University, and the faculty of Biology for enabling me to continue my studies. Thanks also to Professor Utz Fischer for providing a great home for our lab at the department of Biochemistry.

I am most grateful to my supervisor, Professor Aladar A. Szalay, for giving me the opportunity to carry out my PhD studies in his group, and for his guidance and mentorship. Thanks to Professor Friedrich Grummt, for critical review of this manuscript and his support of all AG Szalay's students. Appreciation is given to Professor Buchner who reviewed my initial minithesis and undertook my oral examination to qualify for the PhD program.

Sincerest appreciation to Dr. Yuman Fong at Memorial Sloan-Kettering Cancer Center, New York, NY, for providing me an amazing opportunity to carry out my studies at his institution, facilitating a state of the art small imaging center to conduct my experiments, and also for his guidance and mentorship. These experiments could not have been done without the help and expertise of Dr. Pat B. Zanzonico, head of the small animal imaging facility at MSKCC, and Valerie Longo for her technical expertise. Pat, your help and guidance will never be forgotten, and you have had such a large and positive impact during my time at MSKCC. Further, thanks to Associate Professor Sean Carlin for his help and advice with hNIS physiology and autoradiography experiments, as well as his technical assistant Megan Reese for her help with experiments.

Special mention to my mentor in New Zealand, Mr. Jonathan Koea, who empowered me to take on this adventure, which took me from Wuerzburg to New York, and San Diego.

Appreciation to Mithat Gonen for help with statistical analysis, Nicholas Socci for assistance with microarray analysis, and Victor Andrade for help with histologic interpretation. Thanks also to the guidance of the genomics, microscopy, and histology core facilities, especially Sho Fujisawa, Yevgeniy Romin, Mesruh Turkh, Ning Fan, and Afsar Barlas.

I am grateful to all members of the Wuerzburg group, especially Jochen Stritzker for critical assessment of this work, Ivo Gentschev, Elizabeth Hoffman, Steffi Weibel, Johanna Langbein, Julia Sturm, Thu Ha Lee, Huiqiang Wang, Viktoria Raab, and Carolin Suebert. Ulrike Donat, thank you for being such a special friend to me during my time in Wuerzburg, your hospitality and friendship during this time meant so very much.

I am very thankful to all members of Genelux Corporation including Nanhai Chen, Tony Yu, Qian Zhang, Sunil Advani, Ulrike Geissinger, Alexa Frentzen, Martina Zimmermann, Jennifer Reinboth, Klaas Ehring, Lisa Buckel, Vanessa Cook, Duong Nguyen, and Camha Hoang.

Gratitude also to all past and present members of the Fong lab including Lorena Gonzalez, Joyce Wong, Gerd Silberhumer, Alley Schulman, Susanne Carpenter, Joyce Au, Joshua Carson, Tae-Jin Song, Jun Kyonghwa, Sepideh Gholami, and Kelly Mojia. Thanks to other members of MSKCC, especially Chun-Hao Chen, Pingdong Lee, Narcisso Olvera, Fahina Bogomolniy, Maria Bisogna, Rita Sakr, Hyaehwan Kim, Tommy Chen, David Liska, Russell Holmes, Desiree Dubon, and Linda Wilkins.

I am very grateful for technical assistance from Terry Trevino, Melody Fells, and Jason Aguilar. Thanks also to Eric Rosenfield, Mordechai Smith, Jonathan Katz, and Laura Weber for assistance with experiments.

To my friends, Anu, Arjun, Alex, Aspan, Eesvan, Deepti, Jawad, Luvern, Marya, Marianna, Mehershad, Mohsen, and Patty who have supported me through this journey, I am so very thankful.

To my father Bassam, mother Afaf, Rasha, and Tariq, thank you for being my foundation and strength during this time and always.

This work is dedicated to my sister Rasha. Thank you for being my companion in life.

New York, 2011.

REFERENCES

1. World Health Organization. The global burden of cancer in: World cancer report. 2008. http://www.iarc.fr/en/publications/pdfs-online/wcr/2008/index.php. Updated Last Updated Date.

2. American Cancer Society. Cancer facts and figures. 2009. http://www.cancer.org/downloads/STT/500809web.pdf. Updated Last Updated Date.

3. German cancer research centre. http://www.dkfz.de/en/krebsatlas/total/einleitung_e.html, 2008.

4. Leaf C. Why we're losing the war on cancer (and how to win it). *Fortune.* Mar 22 2004;149(6):76-82, 84-76, 88 passim.

5. Garattini S, Bertele V. Efficacy, safety, and cost of new anticancer drugs. *BMJ.* Aug 3 2002;325(7358):269-271.

6. Galasso D, Carnuccio A, Larghi A. Pancreatic cancer: diagnosis and endoscopic staging. *Eur Rev Med Pharmacol Sci.* Apr;14(4):375-385.

7. Squadroni M, Fazio N. Chemotherapy in pancreatic adenocarcinoma. *Eur Rev Med Pharmacol Sci.* Apr;14(4):386-394.

8. Vaha-Koskela MJV, Heikkila JE, Hinkkanen AE. Oncolytic viruses in cancer therapy. *Cancer Letters.* Sep 8 2007;254(2):178-216.

9. Chen N, Szalay A. Oncolytic vaccinia virus: a theranostic agent for cancer. *Future Virol.* 2010;5(6):763-784.

10. Garber K. China approves world's first oncolytic virus therapy for cancer treatment. *Journal of the National Cancer Institute.* Mar 1 2006;98(5):298-300.

11. Parato KA, Senger D, Forsyth PAJ, Bell JC. Recent progress in the battle between oncolytic viruses and tumours. *Nature Reviews.* Dec 2005;Cancer. 5(12):965-976.

12. Woo Y, Adusumilli PS, Fong Y. Advances in oncolytic viral therapy. *Current Opinion in Investigational Drugs.* Jun 2006;7(6):549-559.

13. Sinkovics J. [The effect of oxygenation on the biological behaviour of tumours].[comment]. *Orvosi Hetilap.* Oct 28 2007;148(43):2056-2057; author reply 2057.

14. Dock G. Rabies virus vaccination in a patient with cervical carcinoma. *American Journal of Medical Science.* 1904;127:563.

15. Dock G. Influence of complicating diseases upon leukemia. *Am J Med Sci.* 1904;127(563).

16. Pace NGD. Sulla scomprasa di un enorme cancro vegetante del collo dell'utero senza cura chirurgica. *Ginecologica.* 1912;9:82-88.

17. Sinkovics JG, Horvath JC. Natural and genetically engineered viral agents for oncolysis and gene therapy of human cancers. *Arch Immunol Ther Exp (Warsz).* Dec 2008;56 Suppl 1:3s-59s.

18. Levaditi C, Nicolau S. Affinite du virus herpetique pour les neoplasmes epitheliaux. *Comptes Rendus Societe Biologie.* 1922;87:498-500.

19. Higgins GK, Pack GT. Virus therapy in the treatment of tumors. *Bull Hosp Joint Dis.* Oct 1951;12(2):379-382.

20. Higgins GK, Pack GT. The effects of virus therapy on the microscopic structure of human melanomas. *Am J Pathol.* Jul-Aug 1951;27(4):728-729.

21. Pack GT. Note on the experimental use of rabies vaccine for melanomatosis. *AMA Arch Derm Syphilol.* Nov 1950;62(5):694-695.

22. Moore AE. The destructive effect of the virus of Russian Far East encephalitis on the transplantable mouse sarcoma 180. *Cancer.* 1949;2(3):525-534.

23. Moore AE. Oncolytic properties of viruses. *Tex Rep Biol Med.* 1957;15(3):588-599; discussion 599-602.

24. Moore AE. The oncolytic viruses. *Prog Exp Tumor Res.* 1960;1:411-439.

25. Hoster HA, Zanes, R.P. Jr., Von, H.E. . Studies in Hodgkin's syndrome; the association of viral hepatitis and Hodgkin's disease; a preliminary report. *Cancer Res* 1949;9(8):473-480.
26. Smith RR, Huebner, R.J., Rowe, W.P., Schatten, W.E., Thomas, L.B. Studies on the use of viruses in the treatment of carcinoma of the cervix. *Cancer.* 1956;9(6):1211-1218.
27. Bischoff JR, Kirn DH, Williams A, et al. An adenovirus mutant that replicates selectively in p53-deficient human tumor cells. *Science.* Oct 18 1996;274(5286):373-376.
28. Breitbach CJ, Reid T, Burke J, Bell JC, Kirn DH. Navigating the clinical development landscape for oncolytic viruses and other cancer therapeutics: no shortcuts on the road to approval. *Cytokine Growth Factor Rev.* Apr-Jun;21(2-3):85-89.
29. Breitbach CJ, Paterson JM, Lemay CG, et al. Targeted inflammation during oncolytic virus therapy severely compromises tumor blood flow. *Mol Ther.* Sep 2007;15(9):1686-1693.
30. Yang H, Kim SK, Kim M, et al. Antiviral chemotherapy facilitates control of poxvirus infections through inhibition of cellular signal transduction. *J Clin Invest.* Feb 2005;115(2):379-387.
31. Park BH, Hwang T, Liu TC, et al. Use of a targeted oncolytic poxvirus, JX-594, in patients with refractory primary or metastatic liver cancer: a phase I trial. *Lancet Oncol.* Jun 2008;9(6):533-542.
32. Fielding AK. Measles as a potential oncolytic virus. *Rev Med Virol.* Mar-Apr 2005;15(2):135-142.
33. Vile R, Ando D, Kirn D. The oncolytic virotherapy treatment platform for cancer: unique biological and biosafety points to consider. *Cancer Gene Ther.* Dec 2002;9(12):1062-1067.
34. Sinkovics J. Die Grundlagen der Virusforschung verlag der Ungarischen Akademie der Wissenschaften. 1956:3-420. Published Last Modified Date|. Accessed Dated Accessed|.
35. Cassel WA, Garrett RE. Relationship between viral neurotropism and oncolysis. I. Study of vaccinia virus. *Cancer.* Mar 1967;20(3):433-439.
36. DiStefano AD, Buzdar AU. Viral-induced remission in chronic lymphocytic leukemia? *Arch Intern Med.* Aug 1979;139(8):946.
37. Hansen RM, Libnoch JA. Remission of chronic lymphocytic leukemia after smallpox vaccination. *Arch Intern Med.* Jul 1978;138(7):1137-1138.
38. Kawa A, Arakawa S. The effect of attenuated vaccinia virus AS strain on multiple myeloma; a case report. *Jpn J Exp Med.* Feb 1987;57(1):79-81.
39. Arakawa S, Jr., Hamami G, Umezu K, Kamidono S, Ishigami J, Arakawa S. Clinical trial of attenuated vaccinia virus AS strain in the treatment of advanced adenocarcinoma. Report on two cases. *J Cancer Res Clin Oncol.* 1987;113(1):95-98.
40. Everall JD, O'Doherty CJ, Wand J, Dowd PM. Treatment of primary melanoma by intralesional vaccinia before excision. *Lancet.* Sep 27 1975;2(7935):583-586.
41. Hunter-Craig I, Newton KA, Westbury G, Lacey BW. Use of vaccinia virus in the treatment of metastatic malignant melanoma. *Br Med J.* May 30 1970;2(5708):512-515.
42. Merrick AE, Ilett EJ, Melcher AA. JX-594, a targeted oncolytic poxvirus for the treatment of cancer. *Curr Opin Investig Drugs.* Dec 2009;10(12):1372-1382.
43. Zhang Q, Yu YA, Wang E, et al. Eradication of solid human breast tumors in nude mice with an intravenously injected light-emitting oncolytic vaccinia virus. *Cancer Res.* Oct 15 2007;67(20):10038-10046.
44. Esposito JJ, and Frenner, F. . *Poxviruses*. 4th ed. Philadelphia: Lippincott Williams & Wilkins; 2001.
45. Moss B. *Poxviridae: the Viruses and Their Replication*. 4th ed. Philadelphia: Lippincott Williams & Wilkins; 2001.
46. Fenner F. *Smallpox and its eradication*. Geneva; 1988.

47. Jenner E. *An inquiry into the causes and effects of the variolae vaccinae, a disease discovered in some of the Western counties of England, particularly Gloucestershire, and known by the name of the cow pox*. New York: Dover; 1959.
48. Shen Y, Nemunaitis J. Fighting cancer with vaccinia virus: teaching new tricks to an old dog. *Mol Ther.* Feb 2005;11(2):180-195.
49. Boone RF, Moss B. Sequence complexity and relative abundance of vaccinia virus mRNA's synthesized in vivo and in vitro. *J Virol.* Jun 1978;26(3):554-569.
50. Paoletti E, Grady LJ. Transcriptional complexity of vaccinia virus in vivo and in vitro. *J Virol.* Sep 1977;23(3):608-615.
51. Smith GL, Vanderplasschen A, Law M. The formation and function of extracellular enveloped vaccinia virus. *J Gen Virol.* Dec 2002;83(Pt 12):2915-2931.
52. Roberts KL, Smith GL. Vaccinia virus morphogenesis and dissemination. *Trends Microbiol.* Oct 2008;16(10):472-479.
53. Mercer J, Helenius A. Apoptotic mimicry: phosphatidylserine-mediated macropinocytosis of vaccinia virus. *Ann N Y Acad Sci.* Oct;1209:49-55.
54. Mercer J, Helenius A. Vaccinia virus uses macropinocytosis and apoptotic mimicry to enter host cells. *Science.* Apr 25 2008;320(5875):531-535.
55. Tolonen N, Doglio L, Schleich S, Krijnse Locker J. Vaccinia virus DNA replication occurs in endoplasmic reticulum-enclosed cytoplasmic mini-nuclei. *Mol Biol Cell.* Jul 2001;12(7):2031-2046.
56. Harrison SC, Alberts B, Ehrenfeld E, et al. Discovery of antivirals against smallpox. *Proc Natl Acad Sci U S A.* Aug 3 2004;101(31):11178-11192.
57. Schramm B, Locker JK. Cytoplasmic organization of POXvirus DNA replication. *Traffic.* Oct 2005;6(10):839-846.
58. Pichlmair A, Reis e Sousa C. Innate recognition of viruses. *Immunity.* Sep 2007;27(3):370-383.
59. Fukuhara H, Todo T. Oncolytic herpes simplex virus type 1 and host immune responses. *Current Cancer Drug Targets.* Mar 2007;7(2):149-155.
60. Hangartner L, Zinkernagel RM, Hengartner H. Antiviral antibody responses: the two extremes of a wide spectrum. *Nat Rev Immunol.* Mar 2006;6(3):231-243.
61. Zhu J, Martinez J, Huang X, Yang Y. Innate immunity against vaccinia virus is mediated by TLR2 and requires TLR-independent production of IFN-beta. *Blood.* Jan 15 2007;109(2):619-625.
62. Quigley M, Martinez J, Huang X, Yang Y. A critical role for direct TLR2-MyD88 signaling in CD8 T-cell clonal expansion and memory formation following vaccinia viral infection. *Blood.* Mar 5 2009;113(10):2256-2264.
63. Buller RM, Palumbo GJ. Poxvirus pathogenesis. *Microbiol Rev.* Mar 1991;55(1):80-122.
64. van Den Broek M, Bachmann MF, Kohler G, et al. IL-4 and IL-10 antagonize IL-12-mediated protection against acute vaccinia virus infection with a limited role of IFN-gamma and nitric oxide synthetase 2. *J Immunol.* Jan 1 2000;164(1):371-378.
65. Ada GL, Blanden RV. CTL immunity and cytokine regulation in viral infection. *Res Immunol.* Oct-Dec 1994;145(8-9):625-628; discussion 628-629.
66. Cole GA, and Blanden, R. V. . *Immunology of Poxviruses*. New York: Plenum; 1982.
67. Smith GL, Symons JA, Khanna A, Vanderplasschen A, Alcami A. Vaccinia virus immune evasion. *Immunol Rev.* Oct 1997;159:137-154.
68. Belyakov IM, Earl P, Dzutsev A, et al. Shared modes of protection against poxvirus infection by attenuated and conventional smallpox vaccine viruses. *Proc Natl Acad Sci U S A.* Aug 5 2003;100(16):9458-9463.
69. Perdiguero B, Esteban M. The interferon system and vaccinia virus evasion mechanisms. *J Interferon Cytokine Res.* Sep 2009;29(9):581-598.
70. Mastrangelo MJ, Maguire HC, Jr., Eisenlohr LC, et al. Intratumoral recombinant GM-CSF-encoding virus as gene therapy in patients with cutaneous melanoma. *Cancer Gene Ther.* Sep-Oct 1999;6(5):409-422.

71. Thorne SH, Hermiston T, Kirn D. Oncolytic virotherapy: approaches to tumor targeting and enhancing antitumor effects. *Seminars in Oncology.* Dec 2005;32(6):537-548.
72. Yu YA, Galanis C, Woo Y, et al. Regression of human pancreatic tumor xenografts in mice after a single systemic injection of recombinant vaccinia virus GLV-1h68. *Mol Cancer Ther.* Jan 2009;8(1):141-151.
73. Gentschev I, Donat U, Hofmann E, et al. Regression of human prostate tumors and metastases in nude mice following treatment with the recombinant oncolytic vaccinia virus GLV-1h68. *J Biomed Biotechnol.* 2010:489759.
74. Worschech A, Kmieciak M, Knutson KL, et al. Signatures associated with rejection or recurrence in HER-2/neu-positive mammary tumors. *Cancer Res.* Apr 1 2008;68(7):2436-2446.
75. Worschech A, Chen N, Yu YA, et al. Systemic treatment of xenografts with vaccinia virus GLV-1h68 reveals the immunologic facet of oncolytic therapy. *BMC Genomics.* 2009;10:301.
76. Worschech A, Haddad D, Stroncek DF, Wang E, Marincola FM, Szalay AA. The immunologic aspects of poxvirus oncolytic therapy. *Cancer Immunol Immunother.* Sep 2009;58(9):1355-1362.
77. Thorne SH, Hwang TH, Kirn DH. Vaccinia virus and oncolytic virotherapy of cancer. *Curr Opin Mol Ther.* Aug 2005;7(4):359-365.
78. Fenner F. Risks and benefits of vaccinia vaccine use in the worldwide smallpox eradication campaign. *Res Virol.* Sep-Oct 1989;140(5):465-466; discussion 487-491.
79. Adusumilli PS, Chan MK, Hezel M, et al. Radiation-induced cellular DNA damage repair response enhances viral gene therapy efficacy in the treatment of malignant pleural mesothelioma. *Ann Surg Oncol.* Jan 2007;14(1):258-269.
80. Gammon DB, Gowrishankar B, Duraffour S, Andrei G, Upton C, Evans DH. Vaccinia virus-encoded ribonucleotide reductase subunits are differentially required for replication and pathogenesis. *PLoS Pathog.*6(7):e1000984.
81. Thorne SH, Hwang TH, O'Gorman WE, et al. Rational strain selection and engineering creates a broad-spectrum, systemically effective oncolytic poxvirus, JX-963. *J Clin Invest.* Nov 2007;117(11):3350-3358.
82. Kim JH, Oh JY, Park BH, et al. Systemic armed oncolytic and immunologic therapy for cancer with JX-594, a targeted poxvirus expressing GM-CSF. *Mol Ther.* Sep 2006;14(3):361-370.
83. Frentzen A, Yu YA, Chen N, et al. Anti-VEGF single-chain antibody GLAF-1 encoded by oncolytic vaccinia virus significantly enhances antitumor therapy. *Proc Natl Acad Sci U S A.* Aug 4 2009;106(31):12915-12920.
84. Guse K, Sloniecka M, Diaconu I, et al. Antiangiogenic arming of an oncolytic vaccinia virus enhances antitumor efficacy in renal cell cancer models. *J Virol.* Jan 2010;84(2):856-866.
85. Hiley CT, Yuan M, Lemoine NR, Wang Y. Lister strain vaccinia virus, a potential therapeutic vector targeting hypoxic tumours. *Gene Ther.* Feb 2010;17(2):281-287.
86. Chen N, Zhang Q, Yu YA, et al. A novel recombinant vaccinia virus expressing the human norepinephrine transporter retains oncolytic potential and facilitates deep-tissue imaging. *Mol Med.* May-Jun 2009;15(5-6):144-151.
87. Tysome JR, Briat A, Alusi G, et al. Lister strain of vaccinia virus armed with endostatin-angiostatin fusion gene as a novel therapeutic agent for human pancreatic cancer. *Gene Ther.* Oct 2009;16(10):1223-1233.
88. Chuang CM, Monie A, Wu A, Pai SI, Hung CF. Combination of viral oncolysis and tumor-specific immunity to control established tumors. *Clin Cancer Res.* Jul 15 2009;15(14):4581-4588.
89. Kirn DH, Wang Y, Liang W, Contag CH, Thorne SH. Enhancing poxvirus oncolytic effects through increased spread and immune evasion. *Cancer Res.* Apr 1 2008;68(7):2071-2075.

90. Gentschev I, Stritzker J, Hofmann E, et al. Use of an oncolytic vaccinia virus for the treatment of canine breast cancer in nude mice: preclinical development of a therapeutic agent. *Cancer Gene Ther.* Apr 2009;16(4):320-328.
91. Gentschev I. Significant growth inhibition of canine mammary carcinoma xenografts following treatment with oncolytic vaccinia virus GLV-1h68. *J. oncol.* 2010;In press.
92. Thorne SH, Negrin RS, Contag CH. Synergistic antitumor effects of immune cell-viral biotherapy. *Science.* Mar 24 2006;311(5768):1780-1784.
93. Lun XQ, Jang JH, Tang N, et al. Efficacy of systemically administered oncolytic vaccinia virotherapy for malignant gliomas is enhanced by combination therapy with rapamycin or cyclophosphamide. *Clin Cancer Res.* Apr 15 2009;15(8):2777-2788.
94. Gil M, Bieniasz M, Wierzbicki A, Bambach BJ, Rokita H, Kozbor D. Targeting a mimotope vaccine to activating Fcgamma receptors empowers dendritic cells to prime specific CD8+ T cell responses in tumor-bearing mice. *J Immunol.* Nov 15 2009;183(10):6808-6818.
95. Yu Z, Li S, Brader P, et al. Oncolytic vaccinia therapy of squamous cell carcinoma. *Mol Cancer.* 2009;8:45.
96. Kelly KJ, Woo Y, Brader P, et al. Novel oncolytic agent GLV-1h68 is effective against malignant pleural mesothelioma. *Hum Gene Ther.* Aug 2008;19(8):774-782.
97. Lin SF, Price DL, Chen CH, et al. Oncolytic vaccinia virotherapy of anaplastic thyroid cancer in vivo. *J Clin Endocrinol Metab.* Nov 2008;93(11):4403-4407.
98. Deng H, Tang N, Stief AE, et al. Oncolytic virotherapy for multiple myeloma using a tumour-specific double-deleted vaccinia virus. *Leukemia.* Dec 2008;22(12):2261-2264.
99. Lee JH, Roh MS, Lee YK, et al. Oncolytic and immunostimulatory efficacy of a targeted oncolytic poxvirus expressing human GM-CSF following intravenous administration in a rabbit tumor model. *Cancer Gene Ther.* Feb 2010;17(2):73-79.
100. McCart JA, Ward JM, Lee J, et al. Systemic cancer therapy with a tumor-selective vaccinia virus mutant lacking thymidine kinase and vaccinia growth factor genes. *Cancer Res.* Dec 15 2001;61(24):8751-8757.
101. Ziauddin MF, Guo ZS, O'Malley ME, et al. TRAIL gene-armed oncolytic poxvirus and oxaliplatin can work synergistically against colorectal cancer. *Gene Ther.* Apr;17(4):550-559.
102. Guo ZS, Naik A, O'Malley ME, et al. The enhanced tumor selectivity of an oncolytic vaccinia lacking the host range and antiapoptosis genes SPI-1 and SPI-2. *Cancer Res.* Nov 1 2005;65(21):9991-9998.
103. Yang S, Guo ZS, O'Malley ME, Yin X, Zeh HJ, Bartlett DL. A new recombinant vaccinia with targeted deletion of three viral genes: its safety and efficacy as an oncolytic virus. *Gene Ther.* Apr 2007;14(8):638-647.
104. Foloppe J, Kintz J, Futin N, et al. Targeted delivery of a suicide gene to human colorectal tumors by a conditionally replicating vaccinia virus. *Gene Ther.* Oct 2008;15(20):1361-1371.
105. Kirn DH, Wang Y, Le Boeuf F, Bell J, Thorne SH. Targeting of interferon-beta to produce a specific, multi-mechanistic oncolytic vaccinia virus. *PLoS Med.* Dec 2007;4(12):e353.
106. Chalikonda S, Kivlen MH, O'Malley ME, et al. Oncolytic virotherapy for ovarian carcinomatosis using a replication-selective vaccinia virus armed with a yeast cytosine deaminase gene. *Cancer Gene Ther.* Feb 2008;15(2):115-125.
107. Hung CF, Tsai YC, He L, et al. Vaccinia virus preferentially infects and controls human and murine ovarian tumors in mice. *Gene Ther.* Jan 2007;14(1):20-29.
108. Chang CL, Ma B, Pang X, Wu TC, Hung CF. Treatment with cyclooxygenase-2 inhibitors enables repeated administration of vaccinia virus for control of ovarian cancer. *Mol Ther.* Aug 2009;17(8):1365-1372.
109. Kim HS, Kim-Schulze S, Kim DW, Kaufman HL. Host lymphodepletion enhances the therapeutic activity of an oncolytic vaccinia virus expressing 4-1BB ligand. *Cancer Res.* Nov 1 2009;69(21):8516-8525.

110. Kelly KJ, Brader P, Woo Y, et al. Real-time intraoperative detection of melanoma lymph node metastases using recombinant vaccinia virus GLV-1h68 in an immunocompetent animal model. *Int J Cancer.* Feb 15 2009;124(4):911-918.
111. Chen N. Personal communication; 2010.
112. Kaufman HL, Deraffele G, Mitcham J, et al. Targeting the local tumor microenvironment with vaccinia virus expressing B7.1 for the treatment of melanoma. *J Clin Invest.* Jul 2005;115(7):1903-1912.
113. Kaufman HL, Cohen S, Cheung K, et al. Local delivery of vaccinia virus expressing multiple costimulatory molecules for the treatment of established tumors. *Hum Gene Ther.* Feb 2006;17(2):239-244.
114. Goldman CK, Kendall RL, Cabrera G, et al. Paracrine expression of a native soluble vascular endothelial growth factor receptor inhibits tumor growth, metastasis, and mortality rate. *Proc Natl Acad Sci U S A.* Jul 21 1998;95(15):8795-8800.
115. Kim KJ, Li B, Winer J, et al. Inhibition of vascular endothelial growth factor-induced angiogenesis suppresses tumour growth in vivo. *Nature.* Apr 29 1993;362(6423):841-844.
116. Mahasreshti PJ, Navarro JG, Kataram M, et al. Adenovirus-mediated soluble FLT-1 gene therapy for ovarian carcinoma. *Clin Cancer Res.* Jul 2001;7(7):2057-2066.
117. Sallinen H, Anttila M, Narvainen J, et al. Antiangiogenic gene therapy with soluble VEGFR-1, -2, and -3 reduces the growth of solid human ovarian carcinoma in mice. *Mol Ther.* Feb 2009;17(2):278-284.
118. Manegold C. Bevacizumab for the treatment of advanced non-small-cell lung cancer. *Expert Rev Anticancer Ther.* May 2008;8(5):689-699.
119. Savona MR, Cruz WP, Thornton JA, Danaher PJ. Comparison of a semipermeable dressing bonded to an absorbent pad and a semipermeable dressing over a separate gauze pad for containment of vaccinia virus at the vaccination site. *Infect Control Hosp Epidemiol.* Dec 2007;28(12):1339-1343.
120. McCart JA, Mehta N, Scollard D, et al. Oncolytic vaccinia virus expressing the human somatostatin receptor SSTR2: molecular imaging after systemic delivery using 111In-pentetreotide. *Mol Ther.* Sep 2004;10(3):553-561.
121. Gnant MF, Puhlmann M, Alexander HR, Jr., Bartlett DL. Systemic administration of a recombinant vaccinia virus expressing the cytosine deaminase gene and subsequent treatment with 5-fluorocytosine leads to tumor-specific gene expression and prolongation of survival in mice. *Cancer Res.* Jul 15 1999;59(14):3396-3403.
122. Erbs P, Findeli A, Kintz J, et al. Modified vaccinia virus Ankara as a vector for suicide gene therapy. *Cancer Gene Ther.* Jan 2008;15(1):18-28.
123. Kanai F, Kawakami T, Hamada H, et al. Adenovirus-mediated transduction of Escherichia coli uracil phosphoribosyltransferase gene sensitizes cancer cells to low concentrations of 5-fluorouracil. *Cancer Res.* May 1 1998;58(9):1946-1951.
124. Erbs P, Regulier E, Kintz J, et al. In vivo cancer gene therapy by adenovirus-mediated transfer of a bifunctional yeast cytosine deaminase/uracil phosphoribosyltransferase fusion gene. *Cancer Res.* Jul 15 2000;60(14):3813-3822.
125. Seubert. Submitted. 2010.
126. McCart JA, Puhlmann M, Lee J, et al. Complex interactions between the replicating oncolytic effect and the enzyme/prodrug effect of vaccinia-mediated tumor regression. *Gene Ther.* Jul 2000;7(14):1217-1223.
127. Harrington KJ, Melcher A, Vassaux G, Pandha HS, Vile RG. Exploiting synergies between radiation and oncolytic viruses. *Curr Opin Mol Ther.* Aug 2008;10(4):362-370.
128. Ottolino-Perry K, Diallo JS, Lichty BD, Bell JC, McCart JA. Intelligent design: combination therapy with oncolytic viruses. *Mol Ther.* Feb;18(2):251-263.
129. Kumar S, Gao L, Yeagy B, Reid T. Virus combinations and chemotherapy for the treatment of human cancers. *Curr Opin Mol Ther.* Aug 2008;10(4):371-379.
130. Le Boeuf F, Diallo JS, McCart JA, et al. Synergistic Interaction Between Oncolytic Viruses Augments Tumor Killing. *Mol Ther.* Mar 16 2010.

131. Symons JA, Alcami A, Smith GL. Vaccinia virus encodes a soluble type I interferon receptor of novel structure and broad species specificity. *Cell.* May 19 1995;81(4):551-560.
132. Colamonici OR, Domanski P, Sweitzer SM, Larner A, Buller RM. Vaccinia virus B18R gene encodes a type I interferon-binding protein that blocks interferon alpha transmembrane signaling. *J Biol Chem.* Jul 7 1995;270(27):15974-15978.
133. Alcami A, Symons JA, Smith GL. The vaccinia virus soluble alpha/beta interferon (IFN) receptor binds to the cell surface and protects cells from the antiviral effects of IFN. *J Virol.* Dec 2000;74(23):11230-11239.
134. Kuruppu D, Brownell A-L, Zhu A, et al. Positron emission tomography of herpes simplex virus 1 oncolysis. *Cancer Research.* Apr 1 2007;67(7):3295-3300.
135. Serganova I, Ponomarev V, Blasberg R. Human reporter genes: potential use in clinical studies. *Nucl Med Biol.* Oct 2007;34(7):791-807.
136. Zhou X, Liu B, Yu X, et al. Controlled release of PEI/DNA complexes from PLGA microspheres as a potent delivery system to enhance immune response to HIV vaccine DNA prime/MVA boost regime. *Eur J Pharm Biopharm.* Mar 2008;68(3):589-595.
137. Lin MZ, McKeown MR, Ng HL, et al. Autofluorescent proteins with excitation in the optical window for intravital imaging in mammals. *Chem Biol.* Nov 25 2009;16(11):1169-1179.
138. MacLaren DC, Toyokuni T, Cherry SR, et al. PET imaging of transgene expression. *Biol Psychiatry.* Sep 1 2000;48(5):337-348.
139. SR C, Y S, RW S, K M, S S, AF C. MicroPET: A high resolution PET scanner for imaging small animals. . *IEEE Trans Nucl Sci.* 1997;44:1161-1166.
140. Chatziioannou AF, Cherry SR, Shao Y, et al. Performance evaluation of microPET: a high-resolution lutetium oxyorthosilicate PET scanner for animal imaging. *J Nucl Med.* Jul 1999;40(7):1164-1175.
141. Chatziioannou AF. Instrumentation for molecular imaging in preclinical research: Micro-PET and Micro-SPECT. *Proc Am Thorac Soc.* 2005;2(6):533-536, 510-511.
142. Bogdanov A, Jr., Weissleder R. The development of in vivo imaging systems to study gene expression. *Trends Biotechnol.* Jan 1998;16(1):5-10.
143. Contag PR, Olomu IN, Stevenson DK, Contag CH. Bioluminescent indicators in living mammals. *Nat Med.* Feb 1998;4(2):245-247.
144. Phelps ME. PET: a biological imaging technique. *Neurochem Res.* Sep 1991;16(9):929-940.
145. Hermiston T. Gene delivery from replication-selective viruses: arming guided missiles in the war against cancer. *J Clin Invest.* May 2000;105(9):1169-1172.
146. Sharma V, Luker GD, Piwnica-Worms D. Molecular imaging of gene expression and protein function in vivo with PET and SPECT. *J Magn Reson Imaging.* Oct 2002;16(4):336-351.
147. Namavari M, Barrio JR, Toyokuni T, et al. Synthesis of 8-[(18)F]fluoroguanine derivatives: in vivo probes for imaging gene expression with positron emission tomography. *Nucl Med Biol.* Feb 2000;27(2):157-162.
148. Gambhir SS, Bauer E, Black ME, et al. A mutant herpes simplex virus type 1 thymidine kinase reporter gene shows improved sensitivity for imaging reporter gene expression with positron emission tomography. *Proc Natl Acad Sci U S A.* Mar 14 2000;97(6):2785-2790.
149. Bennett JJ, Tjuvajev J, Johnson P, et al. Positron emission tomography imaging for herpes virus infection: Implications for oncolytic viral treatments of cancer. *Nat Med.* Jul 2001;7(7):859-863.
150. Slooter GD, Mearadji A, Breeman WA, et al. Somatostatin receptor imaging, therapy and new strategies in patients with neuroendocrine tumours. *Br J Surg.* Jan 2001;88(1):31-40.
151. Zinn KR, Buchsbaum DJ, Chaudhuri TR, Mountz JM, Grizzle WE, Rogers BE. Noninvasive monitoring of gene transfer using a reporter receptor imaged with a

high-affinity peptide radiolabeled with 99mTc or 188Re. *J Nucl Med.* May 2000;41(5):887-895.

152. Akinlolu O, Ottolino-Perry K, McCart JA, Reilly RM. Antiproliferative effects of 111In- or 177Lu-DOTATOC on cells exposed to low multiplicity-of-infection double-deleted vaccinia virus encoding somatostatin subtype-2 receptor. *Cancer Biother Radiopharm.* Jun;25(3):325-333.

153. Ugur O, Kothari PJ, Finn RD, et al. Ga-66 labeled somatostatin analogue DOTA-DPhe1-Tyr3-octreotide as a potential agent for positron emission tomography imaging and receptor mediated internal radiotherapy of somatostatin receptor positive tumors. *Nucl Med Biol.* Feb 2002;29(2):147-157.

154. Henze M, Schuhmacher J, Hipp P, et al. PET imaging of somatostatin receptors using [68GA]DOTA-D-Phe1-Tyr3-octreotide: first results in patients with meningiomas. *J Nucl Med.* Jul 2001;42(7):1053-1056.

155. Moroz MA, Serganova I, Zanzonico P, et al. Imaging hNET reporter gene expression with 124I-MIBG. *J Nucl Med.* May 2007;48(5):827-836.

156. Shulkin BL, Shapiro B, Tobes MC, et al. Iodine-123-4-amino-3-iodobenzylguanidine, a new sympathoadrenal imaging agent: comparison with iodine-123 metaiodobenzylguanidine. *J Nucl Med.* Jul 1986;27(7):1138-1142.

157. Axelrod J, Kopin IJ. The uptake, storage, release and metabolism of noradrenaline in sympathetic nerves. *Prog Brain Res.* 1969;31:21-32.

158. Buursma AR, Beerens AM, de Vries EF, et al. The human norepinephrine transporter in combination with 11C-m-hydroxyephedrine as a reporter gene/reporter probe for PET of gene therapy. *J Nucl Med.* Dec 2005;46(12):2068-2075.

159. Brader P, Kelly KJ, Chen N, et al. Imaging a Genetically Engineered Oncolytic Vaccinia Virus (GLV-1h99) Using a Human Norepinephrine Transporter Reporter Gene. *Clin Cancer Res.* Jun 1 2009;15(11):3791-3801.

160. Riesco-Eizaguirre G, Santisteban P. A perspective view of sodium iodide symporter research and its clinical implications. *Eur J Endocrinol.* Oct 2006;155(4):495-512.

161. Baumann E. Uber den Jodgehalt der Schilddrusen von Menchen und tieren *Hoppe-Seyler's Zeitsehrift fu¨r Physiologische Chemie.* 1986;22:1-17.

162. Dai G, Levy O, Carrasco N. Cloning and characterization of the thyroid iodide transporter. *Nature.* Feb 1 1996;379(6564):458-460.

163. Smanik PA, Liu Q, Furminger TL, et al. Cloning of the human sodium lodide symporter. *Biochem Biophys Res Commun.* Sep 13 1996;226(2):339-345.

164. Dadachova E, Carrasco N. The Na/I symporter (NIS): imaging and therapeutic applications. *Semin Nucl Med.* Jan 2004;34(1):23-31.

165. De La Vieja A, Dohan O, Levy O, Carrasco N. Molecular analysis of the sodium/iodide symporter: impact on thyroid and extrathyroid pathophysiology. *Physiol Rev.* Jul 2000;80(3):1083-1105.

166. Hingorani M, Spitzweg C, Vassaux G, et al. The biology of the sodium iodide symporter and its potential for targeted gene delivery. *Curr Cancer Drug Targets.* Mar 1;10(2):242-267.

167. Baker CH, Morris JC. The sodium-iodide symporter. *Curr Drug Targets Immune Endocr Metabol Disord.* Sep 2004;4(3):167-174.

168. Levy O, De la Vieja A, Ginter CS, Riedel C, Dai G, Carrasco N. N-linked glycosylation of the thyroid Na+/I- symporter (NIS). Implications for its secondary structure model. *J Biol Chem.* Aug 28 1998;273(35):22657-22663.

169. Ohno M, Zannini M, Levy O, Carrasco N, di Lauro R. The paired-domain transcription factor Pax8 binds to the upstream enhancer of the rat sodium/iodide symporter gene and participates in both thyroid-specific and cyclic-AMP- transcription. *Mol Cell Biol.* Mar 1999;19(3):2051-2060.

170. Cass LA, Meinkoth JL. Ras signaling through PI3K confers hormone-independent proliferation that is compatible with differentiation. *Oncogene.* Feb 17 2000;19(7):924-932.

171. Garcia B, Santisteban P. PI3K is involved in the IGF-I inhibition of TSH-induced sodium/iodide symporter gene expression. *Mol Endocrinol.* Feb 2002;16(2):342-352.
172. Levy O, Dai G, Riedel C, et al. Characterization of the thyroid Na+/I- symporter with an anti-COOH terminus antibody. *Proc Natl Acad Sci U S A.* May 27 1997;94(11):5568-5573.
173. Riedel C, Levy O, Carrasco N. Post-transcriptional regulation of the sodium/iodide symporter by thyrotropin. *J Biol Chem.* Jun 15 2001;276(24):21458-21463.
174. Dohan O, Carrasco N. Advances in Na(+)/I(-) symporter (NIS) research in the thyroid and beyond. *Mol Cell Endocrinol.* Dec 31 2003;213(1):59-70.
175. Filetti S, Bidart JM, Arturi F, Caillou B, Russo D, Schlumberger M. Sodium/iodide symporter: a key transport system in thyroid cancer cell metabolism. *Eur J Endocrinol.* Nov 1999;141(5):443-457.
176. Spitzweg C, Morris JC. The sodium iodide symporter: its pathophysiological and therapeutic implications. *Clin Endocrinol (Oxf).* Nov 2002;57(5):559-574.
177. Kogai T, Taki K, Brent GA. Enhancement of sodium/iodide symporter expression in thyroid and breast cancer. *Endocr Relat Cancer.* Sep 2006;13(3):797-826.
178. Lazar V, Bidart JM, Caillou B, et al. Expression of the Na+/I- symporter gene in human thyroid tumors: a comparison study with other thyroid-specific genes. *J Clin Endocrinol Metab.* Sep 1999;84(9):3228-3234.
179. Miyagawa M, Anton M, Wagner B, et al. Non-invasive imaging of cardiac transgene expression with PET: comparison of the human sodium/iodide symporter gene and HSV1-tk as the reporter gene. *Eur J Nucl Med Mol Imaging.* Sep 2005;32(9):1108-1114.
180. Moon DH, Lee SJ, Park KY, et al. Correlation between 99mTc-pertechnetate uptakes and expressions of human sodium iodide symporter gene in breast tumor tissues. *Nucl Med Biol.* Oct 2001;28(7):829-834.
181. Advani SJ, Sibley GS, Song PY, et al. Enhancement of replication of genetically engineered herpes simplex viruses by ionizing radiation: a new paradigm for destruction of therapeutically intractable tumors. *Gene Ther.* Feb 1998;5(2):160-165.
182. Kim SH, Wong RJ, Kooby DA, et al. Combination of mutated herpes simplex virus type 1 (G207 virus) with radiation for the treatment of squamous cell carcinoma of the head and neck. *Eur J Cancer.* Jan 2005;41(2):313-322.
183. Blank SV, Rubin SC, Coukos G, Amin KM, Albelda SM, Molnar-Kimber KL. Replication-selective herpes simplex virus type 1 mutant therapy of cervical cancer is enhanced by low-dose radiation. *Hum Gene Ther.* Mar 20 2002;13(5):627-639.
184. Mezhir JJ, Advani SJ, Smith KD, et al. Ionizing radiation activates late herpes simplex virus 1 promoters via the p38 pathway in tumors treated with oncolytic viruses. *Cancer Res.* Oct 15 2005;65(20):9479-9484.
185. Boyd M, Sorensen A, McCluskey AG, Mairs RJ. Radiation quality-dependent bystander effects elicited by targeted radionuclides. *J Pharm Pharmacol.* Aug 2008;60(8):951-958.
186. Chatal JF, Hoefnagel CA. Radionuclide therapy. *Lancet.* Sep 11 1999;354(9182):931-935.
187. Zanzonico P, Brill A, Becker D. Radiation dosimetry. In: Wagner H, Szabo Z, Buchanan J, eds. *Principles of Nuclear Medicine, 2nd ed*. Philadelphia: WB Saunders Comp; 1995:106-134.
188. O'Donoghue JA, Bardies M, Wheldon TE. Relationships between tumor size and curability for uniformly targeted therapy with beta-emitting radionuclides. *J Nucl Med.* Oct 1995;36(10):1902-1909.
189. Bombardieri E, Buscombe J, Lucignani G, Schober O, eds. *Advances in Nuclear Oncology: Diagnosis and Therapy* London: Informa Healthcare; 2007.
190. Harbert J, ed. *Nuclear Medicine Therapy*. New York: Thieme Medical Publishers; 1987.
191. Knox (Ed) SJ. Systemic Radiation Therapy. *Semin Rad Oncology.* 2000;10:71-167.

192. O'Donoghue JA. Implications of nonuniform tumor doses for radioimmunotherapy. *J Nucl Med.* 1999;40(8):1337-1341.
193. Agarwal V, Sgouros J, Smithson J, et al. Sinusoidal obstruction syndrome (veno-occlusive disease) in a patient receiving bevacizumab for metastatic colorectal cancer: a case report. *J Med Case Reports.* 2008;2:227.
194. Stabin MG, Brill AB. State of the art in nuclear medicine dose assessment. *Semin Nucl Med.* Sep 2008;38(5):308-320.
195. Zanzonico P. Technical requirements for SPECT: Instrumentation, data acquisition and processing, and quality control. In: Kramer EL, Sanger JJ, eds. *Clinical SPECT Imaging*. New York: Raven Press; 1995:7-41.
196. Zanzonico P. Positron emission tomography: a review of basic principles, scanner design and performance, and current systems. *Semin Nucl Med.* Apr 2004;34(2):87-111.
197. Israel O, Godlsmith SJ, eds. *Hybrid SPECT/CT: Imaging in Clinical Practice*. New York: Taylor & Francis Group; 2006.
198. O'Connor MK, Kemp BJ. Single-photon emission computed tomography/computed tomography: basic instrumentation and innovations. *Semin Nucl Med.* Oct 2006;36(4):258-266.
199. Roach PJ, Schembri GP, Ho Shon IA, Bailey EA, Bailey DL. SPECT/CT imaging using a spiral CT scanner for anatomical localization: Impact on diagnostic accuracy and reporter confidence in clinical practice. *Nucl Med Commun.* Dec 2006;27(12):977-987.
200. Beyer T, Townsend DW, Blodgett TM. Dual-modality PET/CT tomography for clinical oncology. *Q J Nucl Med.* Mar 2002;46(1):24-34.
201. Beyer T, Townsend DW, Brun T, et al. A combined PET/CT scanner for clinical oncology. *J Nucl Med.* Aug 2000;41(8):1369-1379.
202. Schoder H, Erdi Y, Larson S, Yeung HWD. PET/CT: a new imaging technology in nuclear medicine. *Eur J Nucl Med Mol, In Press.* 2003.
203. Sgouros G, Frey E, Wahl R, He B, Prideaux A, Hobbs R. Three-dimensional imaging-based radiobiological dosimetry. *Semin Nucl Med.* Sep 2008;38(5):321-334.
204. Abdulhathi MB, Al-Salam S, Kassis A, Ghazal-Aswad S. Unusual presentation of cervical cancer as advanced ovarian cancer. *Arch Gynecol Obstet.* Oct 2007;276(4):387-390.
205. Humm JL, Cobb LM. Nonuniformity of tumor dose in radioimmunotherapy. *J Nucl Med.* 1990;31(1):75-83.
206. Akabani G, Hawkins W, Eckblade M, Leichner P. Patient-specific dosimetry using quantitative SPECT imaging and three-dimensional discrete fourier transform convolution. *J Nucl Med.* 1997;38:308-314.
207. Bolch WE, Bouchet LG, Robertson JS, et al. MIRD pamphlet No. 17: the dosimetry of nonuniform activity distributions--radionuclide S values at the voxel level. Medical Internal Radiation Dose Committee. *J Nucl Med.* 1999;40(1):11S-36S.
208. Erdi AK, Wessels BW, DeJager R, et al. Tumor activity confirmation and isodose curve display for patients receiving iodine-131-labeled 16.88 human monoclonal antibody. *Cancer.* 1994;73(3 Suppl):932-944.
209. Erdi AK, Yorke ED, Loew MH, Erdi YE, Sarfaraz M, Wessels BW. Use of the fast Hartley transform for three-dimensional dose calculation in radionuclide therapy. *Med Phys.* 1998;25(11):2226-2233.
210. Furhang EE, Chui CS, Kolbert KS, Larson SM, Sgouros G. Implementation of a Monte Carlo dosimetry method for patient-specific internal emitter therapy. *Med Phys.* 1997;24(7):1163-1172.
211. Furhang EE, Chui CS, Sgouros G. A Monte Carlo approach to patient-specific dosimetry. *Med Phys.* 1996;23(9):1523-1529.
212. Giap HB, Macey DJ, Bayouth JE, Boyer AL. Validation of a dose-point kernel convolution technique for internal dosimetry. *Phys Med Biol.* 1995;40(3):365-381.

213. Giap HB, Macey DJ, Podoloff DA. Development of a SPECT-based three-dimensional treatment planning system for radioimmunotherapy. *J Nucl Med.* 1995;36(10):1885-1894.
214. Howell RW, Rao DV, Sastry KS. Macroscopic dosimetry for radioimmunotherapy: nonuniform activity distributions in solid tumors. *Med Phys.* 1989;16(1):66-74.
215. Humm JL. Dosimetric aspects of radiolabeled antibodies for tumor therapy. *J Nucl Med.* 1986;27(9):1490-1497.
216. Kolbert KS, Sgouros G, Scott AM, et al. Implementation and evaluation of patient-specific three-dimensional internal dosimetry. *J Nucl Med.* 1997;38(2):301-308.
217. Koral KF, Lin S, Fessler JA, Kaminski MS, Wahl RL. Preliminary results from intensity-based CT-SPECT fusion in I-131 anti- B1 monoclonal-antibody therapy of lymphoma. *Cancer.* 1997;80(12 Suppl):2538-2544.
218. Koral KF, Zasadny KR, Kessler ML, et al. CT-SPECT fusion plus conjugate views for determining dosimetry in iodine-131-monoclonal antibody therapy of lymphoma patients. *J Nucl Med.* 1994;35(10):1714-1720.
219. Kwok CS, Bialobzyski PJ, Yu SK, Prestwich WV. Effect of tissue inhomogeneity on dose distribution of point sources of low-energy electrons. *Med Phys.* 1990;17(5):786-793.
220. Kwok CS, Irfan M, Woo MK, Prestwich WV. Effect of tissue inhomogeneity on beta dose distribution of 32P. *Med Phys.* 1987;14(1):98-104.
221. Kwok CS, Prestwich WV, Wilson BC. Calculation of radiation doses for nonuniformity distributed beta and gamma radionuclides in soft tissue. *Med Phys.* 1985;12(4):405-412.
222. Leichner PK, Kwok CS. Tumor dosimetry in radioimmunotherapy: methods of calculation for beta particles. *Med Phys.* 1993;20(2 Pt 2):529-534.
223. Mird-dose estimate report no. 2. Summary of current radiation dose estimates to humans from 66Ga-, 68Ga-, and 72Ga-citrate. *J Nucl Med.* 1973;14(10):755-756.
224. Liu A, Williams LE, Lopatin G, Yamauchi DM, Wong JY, Raubitschek AA. A radionuclide therapy treatment planning and dose estimation system. *J Nucl Med.* 1999;40(7):1151-1153.
225. Ljungberg M, Strand SE. Dose planning with SPECT. *Int J Cancer Suppl.* 1988;2:67-70.
226. Mayer R, Dillehay LE, Shao Y, et al. A new method for determining dose rate distribution from radioimmuno- therapy using radiochromic media. *Int J Radiat Oncol Biol Phys.* 1994;28(2):505-513.
227. Sgouros G, Barest G, Thekkumthala J, et al. Treatment planning for internal radionuclide therapy: three-dimensional dosimetry for nonuniformly distributed radionuclides. *J Nucl Med.* 1990;31(11):1884-1891.
228. Sgouros G, Chiu S, Pentlow KS, et al. Three-dimensional dosimetry for radioimmunotherapy treatment planning. *J Nucl Med.* 1993;34(9):1595-1601.
229. Uchida I, Yamada Y, Oyamada H, Nomura E. [Calculation algorithm of three-dimensional absorbed dose distribution due to in vivo administration of nuclides for radiotherapy]. *Kaku Igaku.* 1992;29(11):1299-1306.
230. Wessels BW, Yorke ED, Bradley EW. Dosimetry of heterogeneous uptake of radiolabeled antibody for radioimmunotherapy. *Front Radiat Ther Oncol.* 1990;24:104-108.
231. Adelstein S, Kassis A, Sastry K. Cellular vs organ approaches to dose estimates. In: Schlafke-Stelson A, Watson E, eds. *Proceedings of the Fourth International Radiopharmaceutical Dosimetry Symposium (Conf-85113 (DE86010102)*. Oak Ridge, TN: US Dept of Energy and Oak Ridge Associated Universities; 1986:13-25.
232. Adelstein SJ, Kassis AI. Radiobiologic implications of the microscopic distribution of energy from radionuclides. *Int J Rad Appl Instrum B.* 1987;14(3):165-169.
233. Goddu S, Howell R, Bouchet L, et al. *MIRD Cellular S Factors: Self-Absorbed Dose per Unit Cumulated Activity for Selected Radionuclides and Monoenergetic Electrons*

and Alpha Particle Emitters Incorporated into Different Cell Compartments. Reston, VA: Society of Nuclear Medicine; 1997.

234. Goddu SM, Howell RW, Rao DV. Calculation of equivalent dose for Auger electron emitting radionuclides distributed in human organs. *Acta Oncol.* 1996;35(7):909-916.

235. Goddu SM, Rao DV, Howell RW. Multicellular dosimetry for micrometastases: dependence of self-dose versus cross-dose to cell nuclei on type and energy of radiation and subcellular distribution of radionuclides. *J Nucl Med.* 1994;35(3):521-530.

236. Griffiths GL, Govindan SV, Sgouros G, Ong GL, Goldenberg DM, Mattes MJ. Cytotoxicity with Auger electron-emitting radionuclides delivered by antibodies. *Int J Cancer.* 1999;81(6):985-992.

237. Humm JL, Howell RW, Rao DV. Dosimetry of Auger-electron-emitting radionuclides: report no. 3 of AAPM Nuclear Medicine Task Group No. 6 [published erratum appears in Med Phys 1995 Nov;22(11 Pt 1):1837]. *Med Phys.* 1994;21(12):1901-1915.

238. Humm JL, Macklis RM, Lu XQ, et al. The spatial accuracy of cellular dose estimates obtained from 3D reconstructed serial tissue autoradiographs. *Phys Med Biol.* 1995;40(1):163-180.

239. Humm JL, Roeske JC, Fisher DR, Chen GT. Microdosimetric concepts in radioimmunotherapy. *Med Phys.* 1993;20(2 Pt 2):535-541.

240. Kassis AI, Adelstein SJ. Chemotoxicity of indium-111 oxine in mammalian cells. *J Nucl Med.* Feb 1985;26(2):187-190.

241. Kassis AI, Adelstein SJ, Haydock C, Sastry KS. Radiotoxicity of 75Se and 35S: theory and application to a cellular model. *Radiat Res.* Dec 1980;84(3):407-425.

242. Kassis AI, Adelstein SJ, Haydock C, Sastry KS. Thallium-201: an experimental and a theoretical radiobiological approach to dosimetry. *J Nucl Med.* Dec 1983;24(12):1164-1175.

243. Kassis AI, Fayad F, Kinsey BM, Sastry KS, Taube RA, Adelstein SJ. Radiotoxicity of 125I in mammalian cells. *Radiat Res.* Aug 1987;111(2):305-318.

244. Macklis RM, Lin JY, Beresford B, Atcher RW, Hines JJ, Humm JL. Cellular kinetics, dosimetry, and radiobiology of alpha-particle radioimmunotherapy: induction of apoptosis. *Radiat Res.* 1992;130(2):220-226.

245. Makrigiorgos GM, Adelstein SJ, Kassis AI. Limitations of conventional internal dosimetry at the cellular level. *J Nucl Med.* 1989;30(11):1856-1864.

246. Makrigiorgos GM, Ito S, Baranowska-Kortylewicz J, et al. Inhomogeneous deposition of radiopharmaceuticals at the cellular level: experimental evidence and dosimetric implications. *J Nucl Med.* Aug 1990;31(8):1358-1363.

247. O'Donoghue JA. Strategies for selective targeting of Auger electron emitters to tumor cells. *J Nucl Med.* 1996;37(4 Suppl):3S-6S.

248. O'Donoghue JA, Wheldon TE. Targeted radiotherapy using Auger electron emitters. *Phys Med Biol.* 1996;41(10):1973-1992.

249. Wrenn ME, Howells GP, Hairr LM, Paschoa AS. Auger electron dosimetry. *Health Phys.* 1973;24(6):645-653.

250. Yorke ED, Williams LE, Demidecki AJ, Heidorn DB, Roberson PL, Wessels BW. Multicellular dosimetry for beta-emitting radionuclides: autoradiography, thermoluminescent dosimetry and three-dimensional dose calculations. *Med Phys.* 1993;20(2 Pt 2):543-550.

251. Zalutsky MR, Stabin MG, Larsen RH, Bigner DD. Tissue distribution and radiation dosimetry of astatine-211-labeled chimeric 81C6, an alpha-particle-emitting immunoconjugate. *Nucl Med Biol.* 1997;24(3):255-261.

252. Zhou X, Li B, Wang J, Yin H, Zhang Y. The feasibility of using a baculovirus vector to deliver the sodium-iodide symporter gene as a reporter. *Nucl Med Biol.* Apr;37(3):299-308.

253. Yin H, Zhou X, Wu H, Li B, Zhang Y. Baculovirus vector-mediated transfer of NIS gene into colon tumor cells for radionuclide therapy. *World J Gastroenterol.* 2010;16(42):5367-5374.
254. Spitzweg C, Baker CH, Bergert ER, O'Connor MK, Morris JC. Image-guided radioiodide therapy of medullary thyroid cancer after carcinoembryonic antigen promoter-targeted sodium iodide symporter gene expression. *Hum Gene Ther.* Oct 2007;18(10):916-924.
255. Shi YZ, Zhang J, Liu ZL, Du SY, Shen YM. Adenovirus-mediated and tumor-specific transgene expression of the sodium-iodide symporter from the human telomerase reverse transcriptase promoter enhances killing of lung cancer cell line in vitro. *Chin Med J (Engl).* Aug 5;123(15):2070-2076.
256. Huang R, Zhao Z, Ma X, Li S, Gong R, Kuang A. Targeting of tumor radioiodine therapy by expression of the sodium iodide symporter under control of the survivin promoter. *Cancer Gene Ther.* Oct 29.
257. Ahn SJ, Jeon YH, Lee YJ, et al. Enhanced anti-tumor effects of combined MDR1 RNA interference and human sodium/iodide symporter (NIS) radioiodine gene therapy using an adenoviral system in a colon cancer model. *Cancer Gene Ther.* Jul;17(7):492-500.
258. Boland A, Ricard M, Opolon P, et al. Adenovirus-mediated transfer of the thyroid sodium/iodide symporter gene into tumors for a targeted radiotherapy. *Cancer Res.* Jul 1 2000;60(13):3484-3492.
259. Shimura H, Haraguchi K, Miyazaki A, Endo T, Onaya T. Iodide uptake and experimental 131I therapy in transplanted undifferentiated thyroid cancer cells expressing the Na+/I- symporter gene. *Endocrinology.* Oct 1997;138(10):4493-4496.
260. Boland A, Magnon C, Filetti S, et al. Transposition of the thyroid iodide uptake and organification system in nonthyroid tumor cells by adenoviral vector-mediated gene transfers. *Thyroid.* Jan 2002;12(1):19-26.
261. Spitzweg C, Dietz AB, O'Connor MK, et al. In vivo sodium iodide symporter gene therapy of prostate cancer. *Gene Ther.* Oct 2001;8(20):1524-1531.
262. Chen RF, Li ZH, Pan QH, et al. In vivo radioiodide imaging and treatment of pancreatic cancer xenografts after MUC1 promoter-driven expression of the human sodium-iodide symporter. *Pancreatology.* 2007;7(5-6):505-513.
263. Merron A, Peerlinck I, Martin-Duque P, et al. SPECT/CT imaging of oncolytic adenovirus propagation in tumours in vivo using the Na/I symporter as a reporter gene. *Gene Ther.* Dec 2007;14(24):1731-1738.
264. Trujillo MA, Oneal MJ, Davydova J, Bergert E, Yamamoto M, Morris JC, 3rd. Construction of an MUC-1 promoter driven, conditionally replicating adenovirus that expresses the sodium iodide symporter for gene therapy of breast cancer. *Breast Cancer Res.* 2009;11(4):R53.
265. Hakkarainen T, Rajecki M, Sarparanta M, et al. Targeted radiotherapy for prostate cancer with an oncolytic adenovirus coding for human sodium iodide symporter. *Clin Cancer Res.* Sep 1 2009;15(17):5396-5403.
266. Peerlinck I, Merron A, Baril P, et al. Targeted radionuclide therapy using a Wnt-targeted replicating adenovirus encoding the Na/I symporter. *Clin Cancer Res.* Nov 1 2009;15(21):6595-6601.
267. Merron A, Baril P, Martin-Duque P, et al. Assessment of the Na/I symporter as a reporter gene to visualize oncolytic adenovirus propagation in peritoneal tumours. *Eur J Nucl Med Mol Imaging.* Jul;37(7):1377-1385.
268. Trujillo MA, Oneal MJ, McDonough S, Qin R, Morris JC. A probasin promoter, conditionally replicating adenovirus that expresses the sodium iodide symporter (NIS) for radiovirotherapy of prostate cancer. *Gene Ther.* Nov;17(11):1325-1332.
269. Barton KN, Stricker H, Brown SL, et al. Phase I study of noninvasive imaging of adenovirus-mediated gene expression in the human prostate. *Mol Ther.* Oct 2008;16(10):1761-1769.

270. Dingli D, Peng KW, Harvey ME, et al. Image-guided radiovirotherapy for multiple myeloma using a recombinant measles virus expressing the thyroidal sodium iodide symporter. *Blood.* Mar 1 2004;103(5):1641-1646.
271. Hasegawa K, Pham L, O'Connor MK, Federspiel MJ, Russell SJ, Peng KW. Dual therapy of ovarian cancer using measles viruses expressing carcinoembryonic antigen and sodium iodide symporter. *Clin Cancer Res.* Mar 15 2006;12(6):1868-1875.
272. Liu C, Russell SJ, Peng KW. Systemic therapy of disseminated myeloma in passively immunized mice using measles virus-infected cell carriers. *Mol Ther.* Jun;18(6):1155-1164.
273. Msaouel P, Iankov ID, Allen C, et al. Noninvasive imaging and radiovirotherapy of prostate cancer using an oncolytic measles virus expressing the sodium iodide symporter. *Mol Ther.* Dec 2009;17(12):2041-2048.
274. Blechacz B, Splinter PL, Greiner S, et al. Engineered measles virus as a novel oncolytic viral therapy system for hepatocellular carcinoma. *Hepatology.* Dec 2006;44(6):1465-1477.
275. Carlson SK, Classic KL, Hadac EM, et al. Quantitative molecular imaging of viral therapy for pancreatic cancer using an engineered measles virus expressing the sodium-iodide symporter reporter gene. *AJR Am J Roentgenol.* Jan 2009;192(1):279-287.
276. Penheiter AR, Wegman TR, Classic KL, et al. Sodium iodide symporter (NIS)-mediated radiovirotherapy for pancreatic cancer. *AJR Am J Roentgenol.* Aug;195(2):341-349.
277. Myers RM, Greiner SM, Harvey ME, et al. Preclinical pharmacology and toxicology of intravenous MV-NIS, an oncolytic measles virus administered with or without cyclophosphamide. *Clin Pharmacol Ther.* Dec 2007;82(6):700-710.
278. Goel A, Carlson SK, Classic KL, et al. Radioiodide imaging and radiovirotherapy of multiple myeloma using VSV(Delta51)-NIS, an attenuated vesicular stomatitis virus encoding the sodium iodide symporter gene. *Blood.* Oct 1 2007;110(7):2342-2350.
279. Blechacz B, Russell SJ. Measles virus as an oncolytic vector platform. *Curr Gene Ther.* Jun 2008;8(3):162-175.
280. The Clinical Trials Database. www.clinicaltrials.gov. 2011.
281. Herzog H, Zilken H, Niederbremer A, Friedrich W, Muller-Gartner HW. Calculation of residence times and radiation doses using the standard PC software Excel. *Eur J Nucl Med.* 1997;24(12):1514-1521.
282. Furhang EE, Larson SM, Buranapong P, Humm JL. Thyroid cancer dosimetry using clearance fitting. *J Nucl Med.* 1999;40(1):131-136.
283. Westfall P, Young S. *Resampling-Based Multiple Testing: Examples and Methods for p-Value Adjustment*. New York: Wiley-Interscience; 1993.
284. Garber K. China approves world's first oncolytic virus therapy for cancer treatment. *J Natl Cancer Inst.* Mar 1 2006;98(5):298-300.
285. Serganova I, Blasberg R. Reporter gene imaging: potential impact on therapy. *Nucl Med Biol.* Oct 2005;32(7):763-780.
286. Kuruppu D, Brownell AL, Zhu A, et al. Positron emission tomography of herpes simplex virus 1 oncolysis. *Cancer Res.* Apr 1 2007;67(7):3295-3300.
287. Lin SF, Yu Z, Riedl C, et al. Treatment of anaplastic thyroid carcinoma in vitro with a mutant vaccinia virus. *Surgery.* Dec 2007;142(6):976-983; discussion 976-983.
288. Thorne SH. Design and testing of novel oncolytic vaccinia strains. *Methods Mol Biol.* 2009;542:635-647.
289. Thorne SH. Oncolytic vaccinia virus: from bedside to benchtop and back. *Curr Opin Mol Ther.* Aug 2008;10(4):387-392.
290. Thorne SH, Bartlett DL, Kirn DH. The use of oncolytic vaccinia viruses in the treatment of cancer: a new role for an old ally? *Curr Gene Ther.* Aug 2005;5(4):429-443.

291. Kirn DH, Thorne SH. Targeted and armed oncolytic poxviruses: a novel multi-mechanistic therapeutic class for cancer. *Nat Rev Cancer.* Jan 2009;9(1):64-71.
292. Bruno R, Giannasio P, Ronga G, et al. Sodium iodide symporter expression and radioiodine distribution in extrathyroidal tissues. *J Endocrinol Invest.* Dec 2004;27(11):1010-1014.
293. Carrasco N. Iodide transport in the thyroid gland. *Biochim Biophys Acta.* Jun 8 1993;1154(1):65-82.
294. Bangari DS, Mittal SK. Current strategies and future directions for eluding adenoviral vector immunity. *Curr Gene Ther.* Apr 2006;6(2):215-226.
295. Baldick CJ, Jr., Moss B. Characterization and temporal regulation of mRNAs encoded by vaccinia virus intermediate-stage genes. *J Virol.* Jun 1993;67(6):3515-3527.
296. Tazebay UH, Wapnir IL, Levy O, et al. The mammary gland iodide transporter is expressed during lactation and in breast cancer. *Nat Med.* Aug 2000;6(8):871-878.
297. Dwyer RM, Bergert ER, O'Connor MK, Gendler SJ, Morris JC. Sodium iodide symporter-mediated radioiodide imaging and therapy of ovarian tumor xenografts in mice. *Gene Ther.* Jan 2006;13(1):60-66.
298. Seissler J, Wagner S, Schott M, et al. Low frequency of autoantibodies to the human Na(+)/I(-) symporter in patients with autoimmune thyroid disease. *J Clin Endocrinol Metab.* Dec 2000;85(12):4630-4634.
299. Heufelder AE, Joba W, Morgenthaler NG. Autoimmunity involving the human sodium/iodide symporter: fact or fiction? *Exp Clin Endocrinol Diabetes.* 2001;109(1):35-40.